

**HEAT/MASS TRANSFER IN SMOOTH AND RIBBED  
RECTANGULAR SERPENTINE PASSAGES OF  
DIFFERENT ASPECT RATIO'S AND ORIENTATION**

A Thesis

Submitted to the Graduate Faculty of the  
Louisiana State University and  
Agricultural and Mechanical College  
In partial fulfillment of the  
Requirements for the degree of  
Master of Science in Mechanical Engineering

In

The Department of Mechanical Engineering

by  
Peeyush Agarwal  
B.Tech., Indian Institute of Technology, 2001  
May, 2004

## **ACKNOWLEDGEMENTS**

I'll like to thank everyone who helped me to complete the MS-Thesis project. Special thanks for Mr. Fuguo Zhou, Mr. Jonathan Lagrone, and Mr. Jeremiah Oertling for their valuable support and contribution without which the project was impossible for myself to complete. I like to thank the M.E. Workshop workers, Mr. Jim and Mr. Berry who helped in manufacturing the various parts of the test-section. At last, I'll like to thank the Department of Energy (DOE-AGTSR/HEET program) for sponsoring the project.

## TABLE OF CONTENTS

ACKNOWLEDGEMENTS.....	ii
LIST OF TABLES.....	v
LIST OF FIGURES.....	vi
NOMENCLATURE.....	x
ABSTRACT.....	xii
CHAPTER 1. INTRODUCTION.....	1
1.1 INTRODUCTION.....	1
1.2 LITERATURE SURVEY.....	3
1.3 OBJECTIVE OF THE WORK.....	11
1.4 ORGANIZATION OF THE THESIS.....	12
CHAPTER 2. EXPERIMENTAL PROCEDURE.....	13
2.1 EXPERIMENTAL SET UP.....	13
2.2 PROCEDURE.....	16
2.3 DATA REDUCTION METHOD.....	18
CHAPTER 3. HEAT/MASS TRANSFER IN 1:4 RECTANGULAR SMOOTH AND RIBBED PASSAGES WITH ORIENTATION $90^0$ .....	21
3.1 INTRODUCTION .....	21
3.2 RESULTS FOR 1:4 SMOOTH CHANNEL, ORIENTATION= $90^0$ .....	21
3.3 RESULTS FOR 1:4 RIBBED CHANNEL, ORIENTATION= $90^0$ .....	27
3.4 CONCLUSION.....	33
CHAPTER 4. HEAT/MASS TRANFER IN 4:1 RECTANGULAR SMOOTH AND RIBBED PASSAGES WITH ORIENTATION= $90^0$ .....	35
4.1 INTRODUCTION.....	35
4.2 RESULTS FOR 4:1 SMOOTH CHANNEL, ORIENTATION= $90^0$ .....	35
4.3 RESULTS FOR 4:1 RIBBED CHANNEL, ORIENTATION= $90^0$ .....	43
4.4 CONCLUSION.....	49
CHAPTER 5. COMPARISON BETWEEN $90^0$ AND $45^0$ ORIENTATION FOR SMOOTH AND RIBBED CHANNEL FOR ASPECT RATIO 4:1.....	51
5.1 INTRODUCTION.....	51
5.2 RESULTS FOR 4:1 SMOOTH CHANNEL ORIENTATION= $90^0$ AND $45^0$ .....	51
5.3 RESULTS FOR 4:1 RIBBED CHANNEL ORIENTATION= $90^0$ AND $45^0$ .....	58
5.3 CONCLUSION.....	63

<b>CHAPTER 6. COMPARISON BETWEEN 90<sup>0</sup> AND 45<sup>0</sup> ORIENTATION FOR SMOOTH AND RIBBED CHANNEL FOR ASPECT RATIO 1:4.....</b>	<b>65</b>
<b>6.1 INTRODUCTION.....</b>	<b>65</b>
<b>6.2 RESULTS FOR 1:4 SMOOTH CHANNEL ORIENTATION=90° AND 45°.....</b>	<b>65</b>
<b>6.3 RESULTS FOR 1:4 RIBBED CHANNEL ORIENTATION=90° AND 45°.....</b>	<b>71</b>
 <b>BIBLIOGRAPHY.....</b>	 <b>77</b>
 <b>VITA.....</b>	 <b>80</b>

## LIST OF TABLES

Table 1: Range of parametric study .....	11
--	----

## LIST OF FIGURES

Figure 1.1.1: Variation of the maximum allowable temperature range of the gas turbine materials over the years (Courtesy: Fred Soechting).....	1
Figure 1.1.2: Different types of the cooling in the gas turbine engines (Courtesy: Saha)....	2
Figure 1.2.1: Induction of the secondary flow around the Coriolis force.....	6
Figure 1.2.2: Physics of the flow around the ribs.....	8
Figure 2.1.1: Schematic of the Rotating Experimental Facility.....	13
Figure 2.1.2: Schematic of the Test Section and Meter.....	14
Figure 2.1.3: Cross-stream section of the Test Section.....	15
Figure 2.2.1: Schematic of the Scanning procedure.....	17
Figure 3.2.1: Effect of Aspect Ratio on centerline normalized Sherwood number: $Re=5760$ , $Ro=0.12$ a) $AR=1:1$ , leading and trailing walls b) sidewalls c) $AR=1:4$ , leading and trailing walls d) sidewalls.....	23
Figure 3.2.2: Effect of Reynolds number on centerline normalized Sherwood number at $Ro=0$ a) Leading and Trailing wall average b) Sidewalls average.....	24
Figure 3.2.3: Fully developed averaged normalized Sherwood number at a) $Ro=0$ b) $Ro=0.025$ .....	24
Figure 3.2.4: Effect of Rotation on centerline normalized Sherwood number at $Re=30000$ .....	25
Figure 3.2.5: Span-wise distributions at different rotation numbers in the fully developed region at $Re=30,000$ (a) & (b) leading and trailing and (c)&(d) sidewalls.....	27
Figure 3.3.1: Centerline distribution of the Sherwood number ratio along the ribbed and sidewall (Inlet).....	28
Figure 3.3.2: Fully developed mass transfer ratio in the inlet and outlet ribbed channel a) $Ro=0$ b) $Ro=0.025$ (average of the inlet duct sidewalls and outlet duct sidewalls is plotted).....	28
Figure 3.3.3: Effect of rotation number at $Re=30000$ (fully developed averaged normalized Sherwood number).....	29

Figure 3.3.4: Centerline normalized Sherwood number distribution in the inter- rib region at $Re=30000$ , $Ro=0.045$ a) Inlet fully developed Region b) Outlet developing flow region.....	30
Figure 3.3.5: Span-wise distribution for different rotation numbers in the fully developed region at $Re=30000$ .....	33
Figure 4.2.1a) Comparison of centerline normalized sherwood number distribution for Inlet and Outlet passages at $Re=30,000$ , $Ro=0$ for $AR=1:1$ & $AR=4:1$ . b) Comparison of fully developed sherwood number ratio for $AR=4:1$ for stationary case.....	35
Figure 4.2.2: Comparison of the centerline normalized sherwood number distribution $Re=5,670$ , $Ro=0.106$ a) $AR=1:1$ , leading & trailing wall b) $AR=1:1$ sidewalls c) $AR=4:1$ , leading & trailing wall d) $AR=4:1$ sidewalls.....	36
Figure 4.2.3: Comparison of the centerline normalized Sherwood number ratio for $AR=4:1$ channel at different $Re$ numbers, $Ro=0.025$ with stationary 4:1 channel at the $Re$ number.....	37
Figure 4.2.4: Comparison of fully developed sherwood number ratio at $Ro=0.025$ at various Reynolds number at different aspect ratios.....	39
Figure 4.2.5: Fully developed sherwood number ratio at $Re=30,000$ at various rotation numbers for various aspect ratios.....	41
Figure 4.2.6: Cross-Stream normalized sherwood number distribution in the fully developed region for $AR=4:1$ channel at different $Ro$ numbers and $Re=30,000$ .....	42
Figure 4.3.1: Centerline distribution of the sherwood number ratio along the ribbed side, smooth side and the smooth sidewalls for the Inlet passage at $Re=30,000$ , $Ro=0$ , $AR=4:1$ a) developing flow b) fully developed flow.....	43
Figure 4.3.2: Comparison of fully developed normalized sherwood number ratio in different aspect ratios at different Reynolds number.....	44
Figure 4.3.3: Comparison of the effect of rotation number at $Re=30,000$ for different aspect ratios.....	45
Figure 4.3.4: Cross-stream variation at various rotation numbers at $Re=30,000$ with ribs on trailing Side.....	46
Figure 4.3.5: Cross-stream variation at various rotation numbers on side walls at $Re=30,000$ with ribs on leading Side.....	50
Figure 5.2.1: Comparison at $Re=5,760$ for various rotation numbers for two different orientations of the test-section for smooth 4:1 channel.....	52

Figure 5.2.2: Overall Effect of orientation of the test-section in the fully developed region in the smooth channel.....	53
Figure 5.2.3: Span-wise normalized Sherwood number distribution in the fully developed region for AR=4:1 channel at different Ro numbers and Re=30,000 for smooth and 90-degree orientation of the test-section.....	55
Figure 5.2.4: Span-wise normalized Sherwood number distribution in the fully developed region for AR=4:1 channel at different Ro numbers and Re=30,000 for smooth and 45-degree orientation of the test-section.....	56
Figure 5.2.5: Bend Effect in smooth channel, AR=4:1, 90-degree orientation, Re=5,760, Ro=0.12.....	56
Figure 5.3.1: Comparison at Re=5,760 for various Rotation numbers for two different orientations for ribbed 4:1 channel.....	59
Figure 5.3.2: Overall Effect of orientation of the test-section in the fully developed region in the ribbed channel.....	60
Figure 5.3.3: Span-wise normalized Sherwood number distribution in the fully developed region for AR=4:1 channel at different Ro numbers and Re=30,000 for ribbed and 90-degree orientation of the test-section.....	61
Figure 5.3.4: Span-wise normalized Sherwood number distribution in the fully developed region for AR=4:1 channel at different Ro numbers and Re=30,000 for ribbed and 45-degree orientation of the test-section.....	62
Figure 5.3.5: Contour plots in the developing and the fully developed region for 45-degree orientation of the test-section: Re=5,760, Ro=0.12.....	63
Figure 6.2.1: AR=1:4, Smooth Channel, Re=5,760, Fully developed Sherwood number ratio vs. Rotation number.....	66
Figure 6.2.2: Overall effect of the orientation in 1:4 smooth ducts.....	67
Figure 6.2.3: Span-wise distributions at different rotation numbers in the fully developed region at Re=30,000 for AR=1:4, 90-degree Smooth channel (a) & (b) leading and trailing and (c)&(d) sidewalls.....	69
Figure 6.2.4: Span-wise distributions at different rotation numbers in the fully developed region at Re=30,000 for AR=1:4, 45-degree in Smooth channel (a) & (b) leading and trailing and (c)&(d) sidewalls.....	70
Figure 6.3.1: AR=1:4, Ribbed Channel, Re=5760, Fully developed Sherwood number ratio vs. Rotation number.....	72

Figure 6.3.2: Centerline normalized Sherwood number distribution in the inter-rib region at  $Re=30000$ ,  $Ro=0.045$  a) Inlet fully developed Region, orientation= $90^0$  b) Outlet developing flow region, orientation= $90^0$  c) Inlet fully developed Region, orientation= $45^0$  d) Outlet developing flow region, orientation= $45^0$  .....73

Figure 6.3.3: Span-wise distributions at different rotation numbers in the fully developed region at  $Re=30,000$  for  $AR=1:4$ , 90-degree Ribbed channel (a) & (b) leading and trailing and (c)&(d) sidewalls.....74

Figure 6.3.4: Span-wise distributions at different rotation numbers in the fully developed region at  $Re=30,000$  for  $AR=1:4$ , 45-degree Ribbed channel (a) & (b) leading and trailing and (c)&(d) sidewalls.....76

## NOMENCLATURE

- Re -----Reynolds number ( $Re = \rho V D h / \mu$ )
- Ro ----- Rotation number ( $Ro = \omega D h / V$ )
- AR -----Aspect Ratio (W/H)
- e -----Height of the rib
- Dh -----Hydraulic diameter
- H -----Distance between leading and trailing walls
- p-----Pitch (distance between the two consecutive ribs)
- Sh -----Sherwood number
- Nu -----Nusselt number
- Sh<sub>0</sub> -----Reference Sherwood number
- Nu<sub>0</sub> -----Reference Nusselt number
- IS -----Inner sidewall
- OS----- Outer sidewall
- L ----- Leading side
- T ----- Trailing side
- IL ----- Inlet Leading
- IT ----- Inlet Trailing
- OL----- Outlet Leading
- OT----- Outlet Trailing
- OSW----- Outlet Sidewall
- ISW----- Inlet Sidewall
- SW ----- Sidewall

L-T average-- Average of Leading and Trailing side

Sc-----Schmidt number of naphthalene

$\nu$ ----- Viscosity of air

$\rho_w$ ----- Density of naphthalene

$\rho_b$  ----- Bulk density of naphthalene

$D_{n-a}$  -----Binary Diffusion coefficient of naphthalene in air

Pr----- Prandtl number (air)

$\omega$ ----- Rotation speed (RPM)

V----- Velocity of air inside the channel

W -----Distance between sidewalls

Bo----- Buoyancy parameter ( $Bo = (\Delta\rho/\rho)(R/Dh)Ro^2$ )

## ABSTRACT

An experimental study of heat/mass transfer in rectangular smooth and ribbed serpentine passages with and without rotation in two different aspect ratios (1:4 and 4:1) channel is performed for two different orientations of the test section (90-degree and 45-degree). The Reynolds number is varied in the range of 5,000 to 40,000 and rotation numbers in the range of 0-0.12. Such passages are encountered close to the mid-chord sections or towards the trailing edge of the turbine blade. Two different configurations of the normal ribs ( $e/D_h=0.3125$ ,  $P/e=8$  and  $e/D_h=0.156$ ,  $P/e=11.2$ ) are placed on the leading and the trailing sides. The experiments are conducted in a rotating two-pass coolant channel facility using the naphthalene sublimation technique. For purposes of comparison, selected measurements are also performed in a 1:1 cross-section. The local mass-transfer data in the fully developed region is averaged to study the effect of the Reynolds and the Rotation numbers. The span-wise mass transfer distributions in the smooth and the ribbed cases are also examined.

# CHAPTER 1

## INTRODUCTION

### 1.1 INTRODUCTION

Gas turbine engines provide an efficient and reliable means of power production for both aircraft propulsion and power plant applications. For maximum efficiency of a gas turbine engine, the temperature of fluid (air) entering the turbine from the combustion chamber should be as high as possible without damaging the turbine section components such as the blades.

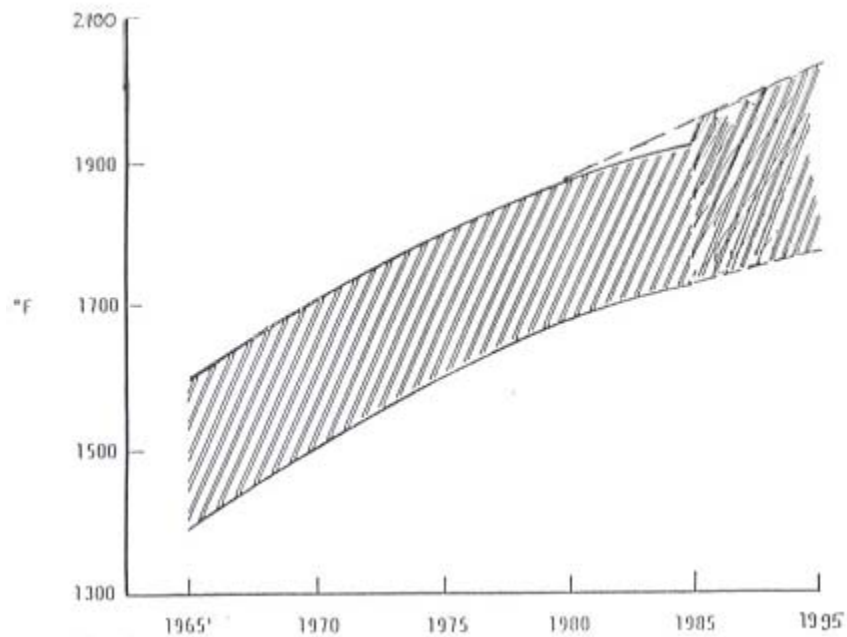


Figure 1.1.1: Variation of the maximum allowable temperature range of the gas turbine materials over the years (Courtesy: Fred Soechting)

Turbine blades are subjected to hot (2500-2600°F) gases leaving the combustion chamber. These blades must also be able to withstand the forces arising from high rates of rotation (as high as 20,000 RPM). For these reasons, extensive research of gas turbine blade design has been conducted over the past decade or so. All R&D activities are aimed at increasing the capability of turbine engines through improved blade cooling techniques

and high temperature materials with thermal barrier coating. Figure 1.1.1 shows the variation of the temperature range that the gas turbine materials can sustain over the years. It is noted that the maximum temperature the materials can withstand is around 2100°F and the turbine blades are subjected to much higher temperatures than that. Thus, the need for cooling arises for maximum efficiency of the gas turbine engines.

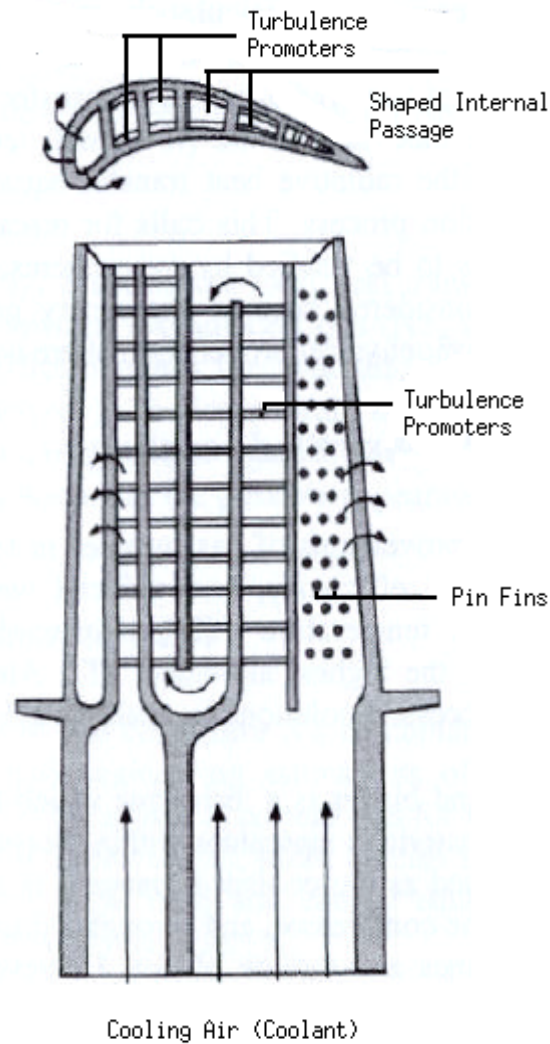


Figure 1.1.2: Different types of the cooling in the gas turbine engines.  
(Courtesy: Saha)

Figure 1.1.2 shows the two types of cooling techniques used presently in the industry. Blade cooling is accomplished through a combination of external and internal

cooling techniques. External film cooling involves blowing compressor bypass air through small holes in the surface of the blade, particularly along the leading edge. Internal cooling involves passing the compressed air through the serpentine channel inside the blade. The objective of the research is to observe and report local features of heat transfer from these internal cooling channels in great detail in different parts of the blade.

## 1.2 LITERATURE REVIEW

In recent years, efforts directed at improving internal cooling have led to concepts that include the use of inclined ribs [1], vortex generators [2, 3], profiled ribs [4, 5], dimpled surfaces [6] etc. Most of these studies have been performed with square cross section channels [1-12]. For example, Wagner et. al. [7] examined the heat transfer characteristics of turbulent flow in rotating square, smooth serpentine passages, and were among the first to quantify in detail the role of Rotation number ( $Ro = \Omega D_h / V$ ) and Buoyancy parameter ( $Bo = [\Delta\rho/\rho][R/D_h]Ro^2$ ) in square cross-sectioned channels. Detailed distributions in rotating square channels were provided through mass transfer measurements by several investigators including Park et. al. [1] and Kukreja et. al. [10]. In real gas turbine blades, practical constraints often dictate the choice of the coolant passage cross-section and orientation. Cross-sections can be modeled as having the Aspect Ratio's (AR) that span the range from 1:4 (near the thickest portion of the blade) to 10:1 or higher (near the trailing edge), while the channel orientation can deviate significantly from the orthogonal orientation (90-degrees to the rotational axis). However, the literature dealing with low or high AR channels is quite limited compared to the square-aspect ratio channel. Han [11] and Han et. al. [12] reported heat transfer, pressure drop and the friction factor for ribbed rectangular channels of low aspect ratios (=1:4)

under stationary conditions. Park et. al. [13] investigated the effect of various rib configurations angled to the main flow direction in stationary channels with different AR's (1:4,1:2,1:1,2:1,4:1). However, the majority of the data published for low AR coolant channels are for stationary conditions, and there is little or no experimental data available under rotating conditions.

Sparrow et. al. [14] investigated local mass transfer behavior in a high aspect ratio, rectangular channel with a sharp edged inlet. He concluded symmetric, constant wall temperature heating indicate the sharp edged inlet results in flow separation and reattachment within the first hydraulic diameter downstream of the inlet. In addition to stream-wise heat transfer distributions, he also investigated cross-stream heat transfer distributions, particularly in the first hydraulic diameter from the entrance where flow separation and reattachment occur. It is concluded that the heat transfer is essentially uniform for the duct width along the entire length, with the exception of local regions of decreased heat transfer near the corners. Furthermore, these regions of decreased heat transfer become smaller as the flow becomes fully developed.

Hart [15] investigated the effect of rotation on flow in rectangular channels. Through flow visualization, he observed the formation of secondary flow arising from Coriolis force. The secondary flow occurs in the form of complementary, longitudinal vortices that direct fluid from the leading wall towards the trailing wall. He found this secondary flow circulation to be stable at low rotation rates, but becomes unstable as rotation increases. This instability was observed to begin where the mean flow is slightly influenced by the circulation and spreads throughout the channel, like a perturbation, to the double roll structure. Further increase in rotation was found to result in a stable flow field.

Figure 1.2.1 shows the pictorial view of how the Coriolis force induces the secondary flow structures. It is shown that the secondary circulation is the result of Coriolis force and that slight rotation will induce a weak circulation without significantly affecting the mean flow. Johnston et. al. [16] in an experimental investigation of turbulent flow through a rotating channel, found that Coriolis force affects both the local and global stability of the mean flow. The examination of the governing equations revealed that Coriolis force, in general, acts to stabilize the leading wall boundary layer while destabilizing that on the trailing wall. Flow visualization experiments revealed both stabilized and destabilized regions that are clearly defined. Coriolis force, thus maintaining stability, rapidly damps disturbances originating in the destabilized region that propagate into the stabilized region. Additional experiments indirectly revealed that rates of Reynolds stress and kinetic energy production are reduced in the stabilized region.

Hwang et. Al. [17] performed numerical simulations of heat transfer in a rotating, smooth-walled rectangular duct of different Aspect Ratio's. He observed the influence of rotation on both the velocity and temperature fields and concluded that Coriolis force is stronger near the centerline, thus creating hydrodynamic instability.

Morris et. al. [18] studied the local heat transfer distributions along the leading and trailing walls of a rectangular duct with smooth walls. He presented the results from five different experiments that differed only in heat generation rate. In addition to the familiar trailing wall enhancement and leading wall degradation, he found noticeable variation between experimental trials. This is attributed to the variation of buoyancy effects. By scaling local heat transfer results with the Reynolds number dependence predicted by theoretical correlations, he isolated the effect of Reynolds and Rotation

numbers. The Rayleigh number effectively quantifies the relative influence of buoyancy force using the well-known Boussinesq approximation.

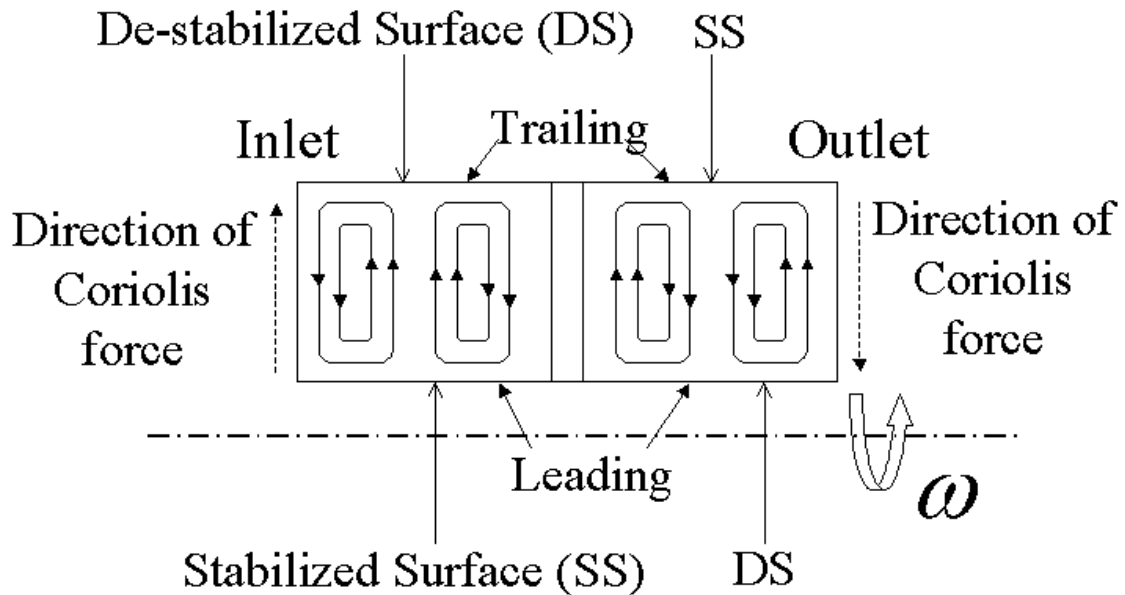


Figure 1.2.1: Induction of the secondary flow around the Coriolis force.

Harasgama et. al. [19] studied the effects of rotation and centripetal buoyancy on heat transfer in ducts of different cross sections. He concluded that heat transfer correlations for a rotating circular duct are valid for ducts with triangular and square cross sections using the appropriate length scale (hydraulic diameter).

Metzger et. al. [20] studied the effect of a  $180^\circ$  bend on heat transfer in rectangular channels. Within the bend, sidewall heat transfer is found to be considerably lower than that along the top and bottom walls due to flow separation at the entrance to the bend. Heat transfer is reported to steadily increase through the bend, with nearly uniform transfer from all surfaces occurring near the middle of the bend. Highest heat transfer rates were observed just after the bend and sharper bends were found to promote heat transfer.

Yang et. al. [21] conducted heat transfer experiments in a rotating, four-pass, square-sectioned channel for high Reynolds number and low rotation number flow. His findings of heat transfer enhancement and reduction on opposite leading and trailing surfaces were consistent with previous results though, because of the low rotation numbers investigated, the effects of rotation were not as pronounced.

Han et. al. [22] investigated the effects of wall temperature condition on heat transfer from rotating, two-pass, square-sectioned channels. Three temperature conditions: constant temperature, constant heat flux, and asymmetric constant temperature were used because the actual temperature boundary condition for an internal coolant channel cannot be known. Their findings indicate that constant wall heat flux resulted in an overall increase in heat transfer compared to constant wall temperature. Furthermore, asymmetric wall heating resulted in moderate increase along the higher temperature wall and greater increase along the opposing, cooler wall. Differences between heat transfer from opposing surfaces were found to be greater in the radially outward flow inlet duct than in the radially inward flow outlet duct. This behavior was reported to result from the concurrent effects of Coriolis and buoyancy forces in the inlet duct and the counter-acting effects of these forces in the outlet duct.

Durst et. al. [23] performed experiments in a rectangular channel that contains a large ( $1/2$  channel height) square-sectioned rib against one wall. Although no direct heat transfer measurements were made, velocity measurements and flow visualization techniques were used to investigate the behavior of separated shear flows. He found that a large separation region downstream of the rib is formed, as expected. From a heat transfer perspective, this region of separation is expected to result in decreased heat

transfer, but the subsequent reattachment and development of the boundary layer will result in increased heat transfer.

Acharya et. al. [24,25] reported a detailed investigation of turbulent flow and heat transfer in a channel containing a single rib. The experimental technique involved the use of a non-intrusive, laser-Doppler-based measurement system. Both fluid and wall surface temperature was used in the evaluation of the effect of the rib on local heat transfer. Flow measurement results were reported to indicate a peak in stream-wise turbulence intensity that occurred directly above the rib. Cross-stream turbulence intensity profiles, however, were reported to reach a maximum downstream of the rib. Local heat transfer results indicated a peak in stream-wise heat transfer upstream of the point of flow reattachment. Figure 1.2.2 shows the pictorial view of the flow physics over and between the ribs.

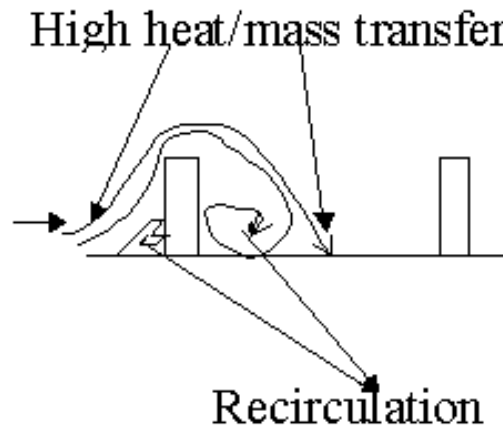


Figure 1.2.2: Physics of the flow around the ribs.

Humphrey et. al. [26] conducted experiments in a channel with one ribbed wall. Their velocity measurements indicated that the ribs generated longitudinal Reynolds stress, which is convected by, cross-stream flow and was found to result in a high degree of anisotropy near the ribbed surface. These Reynolds stresses were found to be about four times greater than those near the opposing smooth walls, which resulted in an

increased generation of turbulent kinetic energy. Increased turbulent kinetic energy is expected to promote turbulent mixing and, consequently, heat transfer.

Liou et. al. [27] investigated the periodic nature of ribbed wall channels. They found that periodic fully developed conditions exist after 2-3 ribs from the entrance. Heat transfers and pressure loss results showed a periodic behavior between consecutive ribs. Additionally, both friction factor and heat transfer were reported to increase with decreasing rib spacing. Similar observations were made by Han et. al. [11,12] for high Aspect Ratio channels. He attributed the decrease in heat transfer with increased rib spacing to the thicker boundary layer that forms for the larger spacing.

Hirota et. al. [28] made cross-stream measurements of velocity and heat transfer in a square channel with one ribbed wall. He concluded that momentum transport near the ribs is greater than heat transfer. The results support earlier reports of increased pressure loss resulting from smaller rib spacing. Additional observations indicated that the ribs caused a production of turbulent heat flux, which results in increased heat transfer.

Zhang et. al. [29] performed heat transfer experiments in a serpentine channel with ribbed walls to observe the effects of relatively low rotation. Johnson, et. al. [30] found that a twisting of the channel resulted in a reduction of rotation effects on heat transfer, particularly the effect of Coriolis force.

Hong et. al. [31] conducted experiments to report the effects of rib alignment and channel aspect ratio on heat transfer and friction factor in a ribbed duct. Specifically, the two rib alignments tested were for aligned ribs on opposite walls and for ribs staggered on opposing walls. In general, an increase in heat transfer was reported for the staggered rib configuration.

Taslim et. al. [32] used the staggered rib configuration in a rotating channel with radially outward flow. In addition to reporting the effects of the staggered configuration, he also investigated the effects of rib size on heat transfer. In general, it was reported that the staggered rib configuration increases the heat transfer along the trailing wall of the channel.

The brief survey of literature performed above gives a summary of the state of current available knowledge in the area of heat transfer in ducts modeled for internal turbine blade coolant channels. Preliminary results from non-rotating channels with smooth walls indicate the effect of hydrodynamically developing flow on heat transfer. The effect of rotation, specifically the effect of Coriolis force, has been studied for the smooth-walled and the ribbed channel. As expected from theory, rotation induces secondary flow that acts to stabilize the leading wall boundary layer while destabilizing that on the trailing wall for radially outward flow. This trend is reversed for radially inward flow. Investigations into heat transfer augmentation methods have revealed that roughness elements, such as ribs, result in substantial increases in heat transfer. Results presented for channels with repeated rib roughness elements placed on opposite walls have shown the formation of a periodically fully developed profile after only a few rib spaces. Additional experiments for rotating ribbed channels have revealed trends similar to those observed for channels with smooth walls.

The majority of the results discussed in the literature are from direct heat transfer measurement experiments. Because heat transfer data is typically obtained through temperature measurement, resolution is rather limited, especially for rotating channels. A few of the investigations discussed have employed mass transfer measurements to report heat transfer behavior. These mass transfer results reported in the thesis are in great detail

than the previous heat transfer results and are thus better suited for investigations of local heat transfer behavior. Agreement between heat and mass transfer experiments has been reported to be excellent which confirms the validity of the heat and mass transfer analogy used to relate them.

### 1.3 OBJECTIVE OF THE WORK

The objectives of the present work are as follows:

1. To study the aspect ratio effect (1:4 and 4:1) on the mass transfer ratio for smooth and ribbed walls for different Reynolds and Rotation numbers. The Reynolds number is in the range of 5000-40000 and the Rotation number in the range of 0-0.12.
2. To study the channel orientation effect (90° and 45°) for the above two Aspect Ratio's.

The ranges of the parameters are as follows:

Table 1: Range of parametric study

E: Experiments	Tests	Re >	Re <	Ro <
E1: 1:1, 90 degree Rib & Smooth, 2 pass, 90 degree Orientation	Mass transfer	5000	45000	0.2
E2: 1:4, 90 degree Inline Rib & Smooth, 2 pass, 90 degree Orientation	Mass transfer	5000	45000	0.12
E3: 4:1, 90 degree Inline Rib & Smooth, 2 pass, 90 degree Orientation	Mass transfer	5000	45000	0.12
E4: 1:4, 90 degree Inline Rib & Smooth, 2 pass, 45 degree Orientation	Mass transfer	5000	45000	0.12
E5: 4:1, 90 degree Inline Rib & Smooth, 2 pass, 45 degree Orientation	Mass transfer	5000	45000	0.12

## 1.4 ORGANIZATION OF THE THESIS

The thesis consists of six chapters.

In Chapter one, a brief introduction of the problem and the objectives of the work are given and the significant contributions of the eminent researchers are critically reviewed. In Chapter two, the experimental apparatus is described, along with the procedure of the experiment and the data reduction procedure. Note that for data reduction, the suitable code is written in C/C++ and FORTRAN.

In Chapter three, the results for mass/heat transfer ratio in 1:4 rectangular smooth and ribbed channels for 90-degree orientation are discussed. The ribs are placed on the leading and the trailing edge. Chapter four deals with the mass/heat transfer ratio in 4:1 case for smooth and ribbed channels for 90-degree orientation. Ribs are placed on either the leading or the trailing side. Chapter 5 compares the mass/heat transfer ratio in 90-degree and 45-degree orientation of the test section for Aspect ratio 4:1 for smooth and ribbed passages. In this case, the ribs are placed on both the leading and the trailing edges and the ribs are of the different dimensions (rib-height and rib spacing) than the studies in Chapter 3,4 and 6. Chapter 6 compares the mass/heat transfer ratio in 90-degree and 45-degree orientation channels for Aspect ratio 1:4 for smooth and ribbed passages.

## CHAPTER 2

### EXPERIMENTAL PROCEDURE

#### 2.1 EXPERIMENTAL SET UP

The results presented are obtained by using mass transfer measurement techniques and are related to the heat transfer observations through the heat and mass transfer analogy. This process eliminates the complexity of heat losses from the test section, which is present in direct heat transfer measurements.

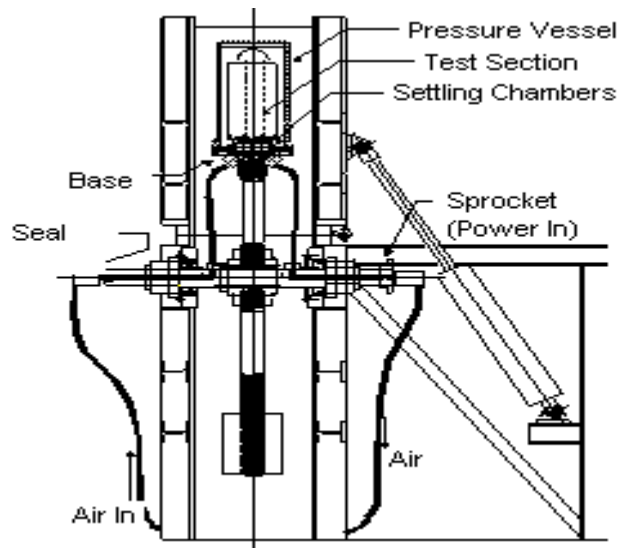


Figure 2.1.1: Schematic of the Rotating Experimental Facility

Figure 2.1.1 shows a schematic diagram of the rotating rig facility. The test section is mounted on a rotating arm driven by hydraulic motor. A dummy counterweight on the opposite end of the arm is used for balancing. The rotating arm is housed inside a pressure vessel for safety purposes. Compressed air is used as the working fluid for all experiments. The air is taken from large, exterior reservoirs in order to minimize flow disturbances caused by the compressor. A concentric bore orifice plate is used to

measure the mass flow rate in the meter run. Naphthalene laden exhaust air is directed through flexible tubing to a fume hood.

Figure 2.1.2 shows the schematic of the two-pass test section and Figure 2.1.3 shows the corresponding cross sectional view. The aluminum alloy test section consists of a 69.85 mm tapered settling chamber; a frame that supports eight removable, wall frames; and a removable 180-degree bend. These major components are secured in a flange-like manner, using O-rings between all parts to prevent air leakage. The ribs are placed using double-sided tape to prevent leaks and to prevent them from rattling. For Aspect Ratio 1:4, when assembled, the test section forms 6.35 x 25.4 x 304.8 mm long inlet and outlet sections 38.1 mm apart that are connected by the 180-degree, 6.35 x 25.4 mm square cross-section bend. For Aspect Ratio 4:1, when assembled, the test section forms 25.4 x 6.35 x 304.8 mm long inlet and outlet sections 38.1 mm apart that are connected by the 180-degree, 25.4 x 6.35 mm square cross-section bend.

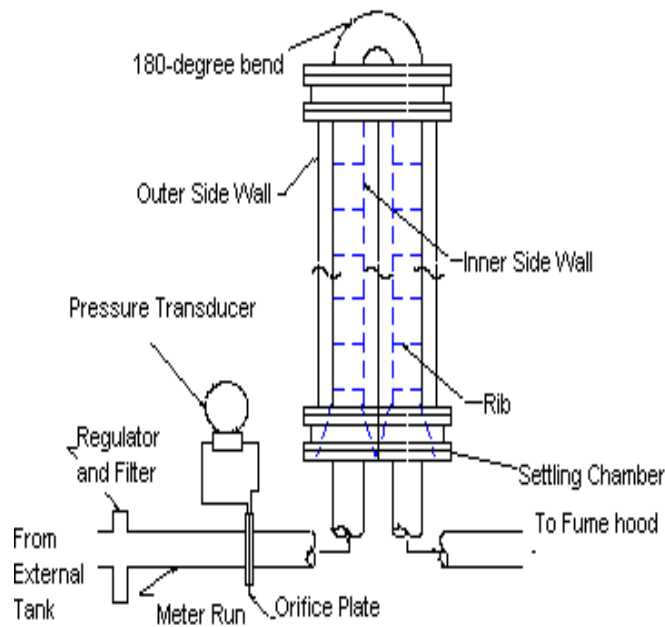


Figure 2.1.2: Schematic of the Test Section and Meter

Two configurations of the ribs are used in the present study to obtain different blockage ratios and pitch to rib height ratio. For the ribbed duct (ribs on Leading and Trailing sides) for Aspect ratio 1:4, the aluminum ribs are used of the dimensions 3.175 x 3.175 x 6.35 mm long and have holes on either end for mounting. Steel, 0.635-mm diameter music wire is inserted into these holes to secure them to the sidewalls of the test section. For the ribbed duct (ribs on Leading and Trailing sides) for Aspect ratio 4:1, the aluminum ribs of the dimensions 1.5875 x 1.5875 x 25.4 mm are used. For ribs on one side (ribs on Leading or Trailing side) for Aspect ratio 4:1, the aluminum ribs are used of the dimensions 3.175 x 3.175 x 25.4 mm long and have holes on either end for mounting. The ribs are mounted only on opposite walls. All exposed surfaces except the ribs are coated with naphthalene.

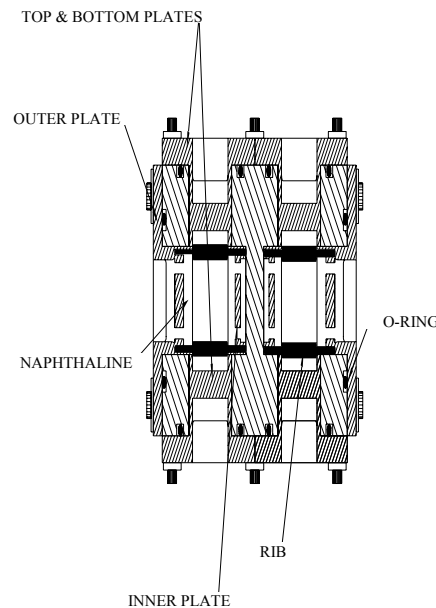


Figure 2.1.3: Cross-stream section of the Test Section

Fresh, 99% pure naphthalene crystals are melted in a heavy-walled glass beaker and the molten naphthalene is quickly poured into the hollow cavity of the plate frame to

completely fill the region between the walls. The cast plates stand for at least eight hours in a fume hood to attain thermal equilibrium with the laboratory. The assembly is started by first inserting the two inner sidewalls and then attaching the bend. For ribbed surfaces, ribs are then attached to these walls and the two outer sidewalls are mounted. Further, the leading and trailing walls are inserted.

Detailed surface profiles of the cast surfaces are required for the local mass transfer results. These profiles are obtained by moving the walls under a fixed, linear variable differential transducer (LVDT) type profilometer. A bi-directional traversing table is securely mounted to the platform on the milling machine. The plates are secured to a 15.875-mm thick tooling aluminum plate, which is fixed to the traversing table. This mounting plate has been machined with an assortment of pin supports and machine screw taps to ensure the walls not only lie flat on the plate, but are also mounted in the same locations for all scans. A custom written program run on the personal computer is used to control the motion of the traversing table through micro-step drive motors with a 0.00127-mm step size.

## **2.2 PROCEDURE**

The first step in performing these experiments is casting of the test section walls. Pouring the molten naphthalene into the walls of the test section that have been secured to the casting plates performs casting. These cast walls stand for about 10-12 hours to harden and then are separated from the casting plates and placed in a sealed container saturated with naphthalene vapor to hinder natural sublimation. Measurement of local sublimation depth is accomplished by comparing surface profiles of the walls before and after the experiment. After the walls have been separated from the casting plates, an

initial reference scan of each wall is performed on the acquisition system. A reference plane for the wall is calculated from three measurement points taken on the edge of the walls.

Following the initial scan of the walls, the test section is assembled. The inner walls are slid and the bend is secured to hold them in place. For ribbed wall experiments, the ribs are placed in support tubes of the inner walls. The outer walls are then placed on the test section and secure the other end of the ribs. The leading and trailing walls are then placed in their respective locations, completing the assembly. The pressure vessel is then placed over the test section and secured to the platform.

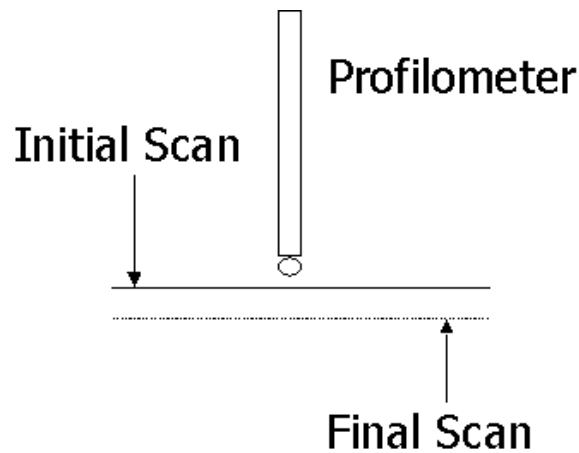


Figure 2.2.1: Schematic of the Scanning procedure.

For rotating experiments, the enclosure lid is closed and the shaft is rotated to warm the hydraulic fluid from the room temperature to 40-degree Centigrade. When the shaft attains a uniform speed (which approximately takes 45 minutes), the airflow is started. During the experiment, meter run pressure, differential pressure across the orifice plate, outlet pressure, and the temperature along with the rotation speed are recorded. At the end of the of the desired test duration (usually 120 minutes), rotation is stopped and the test section is disassembled. Each wall is placed in the sealed container until it is

scanned again with the acquisition system. After the final scanning, the plates are melted and thoroughly cleaned before next casting. A schematic diagram shown in Figure 2.2.1 illustrates the scanning procedure.

### 2.3 DATA REDUCTION METHOD

Naphthalene sublimation depth is calculated from the two surface profiles for each wall. Each profile is normalized with respect to a reference plane computed from three points scanned on the aluminum surface of the walls. The difference between the normalized profiles gives the local sublimation depth. The local mass flux  $\dot{m}''$  and the local mass transfer convection coefficient  $h_m$  at each location are then calculated from the following expressions:

$$\dot{m}'' = \rho_s \delta / \Delta t ; h_m = \dot{m}'' / (\rho_w - \rho_b(x)) \quad (1)$$

where  $\rho_s$  is the density of solid naphthalene,  $\delta$  is the local sublimation depth,  $\Delta t$  is the duration of the experiment, and  $\rho_w$  and  $\rho_b(x)$  are the vapor density of the naphthalene at the wall (obtained from equation of state) and the bulk density at each location on the centerline (obtained by mass balance). The local Sherwood number  $Sh$  is then calculated by:

$$Sh = h_m D_h / D_{n-a} = h_m D_h Sc / \nu \quad (2)$$

where the binary diffusion coefficient  $D_{n-a}$  for naphthalene sublimation in air is taken as the ratio of the kinematic viscosity of air  $\nu$  to the Schmidt number for naphthalene-air ( $Sc = 2.5$ ). Sherwood number results presented in this study have been scaled with a correlation adapted from for fully developed smooth wall pipe flow.

$$Sh_o = 0.023 Re^{0.8} Sc^{0.4} \quad (3)$$

where  $Re$  is the duct Reynolds number. Comparison of heat transfer and mass transfer results can be done through the use of the heat-mass transfer analogy [36]:

$$Nu = Sh(Pr/Sc)^{0.4} \quad (4)$$

where  $Nu$  is the Nusselt number and  $Pr$  is the Prandtl number of air. Both local and area-averaged results are reported in this paper. Area averaging is performed as a simple arithmetic average of the 30x28 data points scanned over the region between consecutive ribs.

Uncertainties for all computed values are estimated using the second-power equation method. Volume flow rate and duct Reynolds number ( $Re$ ) uncertainties are estimated to be less than 10% for  $Re > 6,000$ . The uncertainty is higher for low Reynolds numbers due to the combined uncertainty in the gas expansion factor, and the generic calibration equation used for the orifice flow meter, which is not very accurate at low flow rates. The uncertainty is much less at higher Reynolds numbers.

For the stationary experiments, a thermocouple is embedded in the naphthalene filled plate to measure wall temperature for the calculation of vapor density of naphthalene, whereas in the rotating experiments the measured temperature of the incoming air is used. Since the temperature difference between inlet and exit temperature of the facility has been measured to be substantially less than a degree the effect is not significant and has been included in the uncertainty estimates. Viscous heating of the test section due to rotation-induced relative motion is insignificant because the test section is inside the small pressure and exposed only to stagnant air.

The reported resolution of the LVDT is 0.00127 mm while the analog-to-digital (A/D) board is reported to have an accuracy of 0.002 mm in a 12 kHz acquisition rate,

16-bit resolution mode. Experimental tests of accuracy and repeatability for the entire acquisition system indicate a sublimation depth uncertainty of 0.0038 mm. Maximum sublimation depths are maintained at about 0.152 mm by varying the duration of the experiment. This target depth was selected to minimize uncertainties in both depth measurement and changes in duct cross-section area. These uncertainties were found to be 1% and 3%, respectively. The resulting experimental duration was between 120 minutes for  $Re=30,000$  and 180 minutes for  $Re=5,000$ . Overall uncertainty in Sherwood number calculation is about 8 % and varies slightly with Reynolds number (<1 %).

## CHAPTER 3

### HEAT/MASS TRANSFER IN 1:4 RECTANGULAR SMOOTH AND RIBBED PASSAGES WITH ORIENTATION $90^\circ$

#### 3.1 INTRODUCTION

The experiments are conducted in 1:4 rectangular channel for 90-degree orientation for smooth and ribbed passages. The ribs have the configuration of  $e/D_h = 0.3125$  and  $P/e = 8$ . The rib angle of attack is 90-degree. The value of  $e/H = 0.125$  and  $e/W = 0.5$ .

#### 3.2 RESULTS FOR 1:4 SMOOTH CHANNEL, ORIENTATION= $90^\circ$

Experiments have been conducted at  $Re=5,760$  and  $Ro=0.12$  for both 1:1 and 1:4 aspect ratio channels in order to examine the effect of the aspect ratio. The comparison of the centerline normalized Sherwood number ratios are shown in Figure 3.2.1, and the same qualitative trend is observed for the two aspect ratios. In the inlet duct (radially outward flow), the trailing walls experience increased mass transfer while the leading-wall mass transfer is reduced because of the rotation-induced secondary flows. The opposite is true for the outlet duct where the flow is towards the axis of rotation. While the qualitative features are the same, quantitative differences are observed between the 1:1 and 1:4 aspect ratios, with the 1:4 case having lower values in the developing region. In the fully developed region of the 1:4 aspect ratio inlet-channel, the rotation-induced increase in the mass transfer ratio is 17.5% on the trailing wall compared to 29% in the 1:1 channel. The rotation-induced decrease in the mass transfer ratio on the inlet leading side is 40% for the 1:4 case compared to 30% in the 1:1 channel. Thus, with rotation the 1:4 channel shows a net degradation in the heat transfer on the leading and trailing

surfaces combined, while the 1:1 channel does not exhibit a net change with rotation. In the outlet channel, the increase in mass transfer ratio on the leading side is 24% and the decrease on the trailing side is 20% for the 1:4 aspect ratio case. For the 1:1 channel the enhancement on the leading side is 30% while the degradation on the trailing side is only 12%. Thus, for both aspect ratios the level of rotation-induced degradation is lower in the outlet channel relative to the inlet channel, and is presumably linked to the bend induced secondary flows increasing the mixing and heat transfer in the outlet channel. However, as in the inlet channel, the 1:4 aspect ratio channel still has lower net heat transfer enhancement relative to the 1:1 aspect ratio channel. On the sidewalls, the mass transfer ratio evolution is nearly identical for both aspect ratios, except for the lower values in the developing region for the 1:4 case.

To examine the effect of Reynolds number, experiments were conducted at three different Reynolds numbers under stationary conditions for both 1:1 and 1:4 channels. The comparison of the centerline normalized Sherwood number ratio is shown in Figure 3.2.2 for the 1:4 aspect ratio only. The fully-developed normalized values for the 1:4 channel are slightly lower than 1, and are typically 9-12% lower than those of the 1:1 aspect ratio case (not shown in the interest of brevity). Figure 3.2.2 shows that as the Reynolds number is increased from 20,000 to 30,000, the fully developed mass transfer ratio decreases slightly along the leading and trailing surfaces. No further decrease is observed when the Reynolds number is increased to 40,000. This is consistent with the expected asymptotic behavior in the fully developed region at high Reynolds numbers. In the developing region, the mass transfer ratio increases slightly with Reynolds number, with values in the range of 1.5 to 1.7 for the leading/trailing walls (Figure 3.2.2a) and 1.62 to 1.92 for the sidewalls (Figure 3.2.2b). The slightly higher values in the above-

mentioned ranges correspond to the developing regions of the outlet duct and are presumably due to the secondary flows induced by the bend.

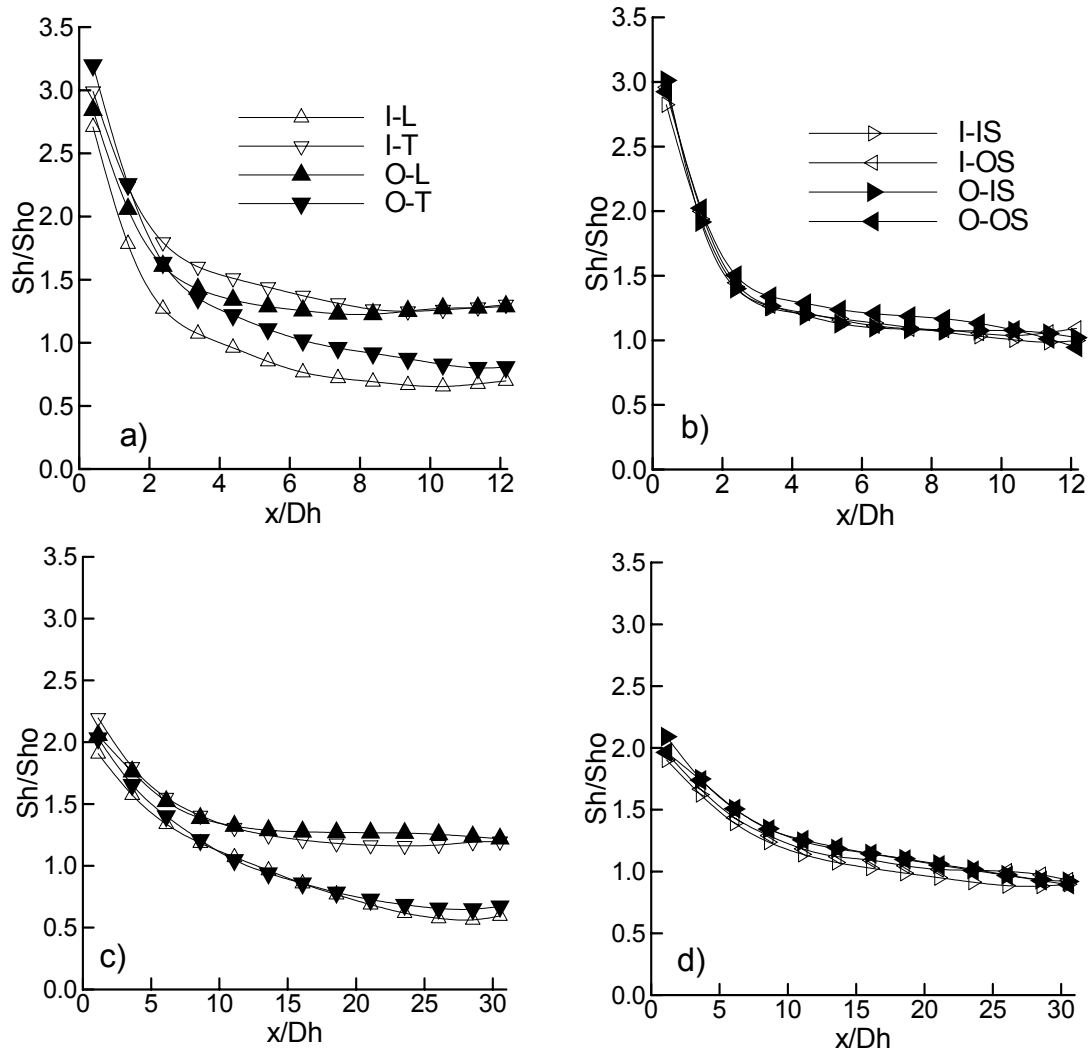


Figure 3.2.1: Effect of Aspect Ratio on centerline normalized Sherwood number:  $Re=5,760$ ,  $Ro=0.12$  a) AR=1:1, leading and trailing walls b) sidewalls c) AR=1:4, leading and trailing walls d) sidewalls

Figure 3.2.3 shows the average value of the fully developed mass transfer ratio with increasing Reynolds number at  $Ro=0$  and  $Ro=0.025$ . In Figure 3.2.3(a), for  $Ro=0$ , the dependence on Reynolds number appears to be relatively weak. In Figure 3.2.3(b) the differences between the stabilized and de-stabilized surfaces are of the order of 10% for both the outward-flow and inward-flow passages, and this difference appears to increase

marginally with Reynolds number. In fact, the heat transfer on the stabilized surface remains insensitive to Reynolds number while the heat transfer on the stabilized surface appears to decrease slightly with Reynolds number.

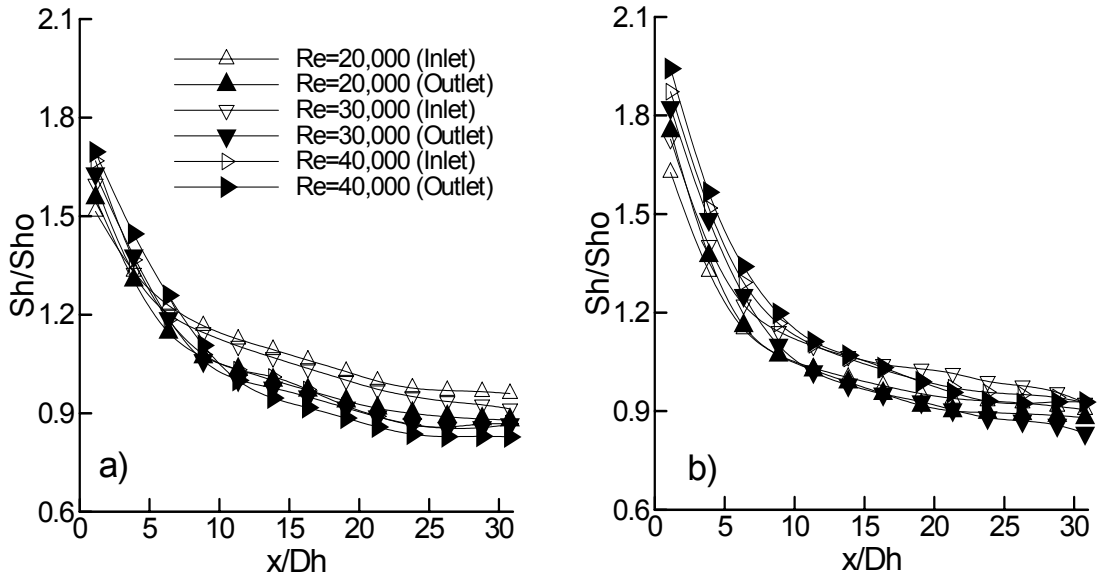


Figure 3.2.2: Effect of Reynolds number on centerline normalized Sherwood number at  $Ro=0$  a) Leading and Trailing wall average b) Sidewalls average

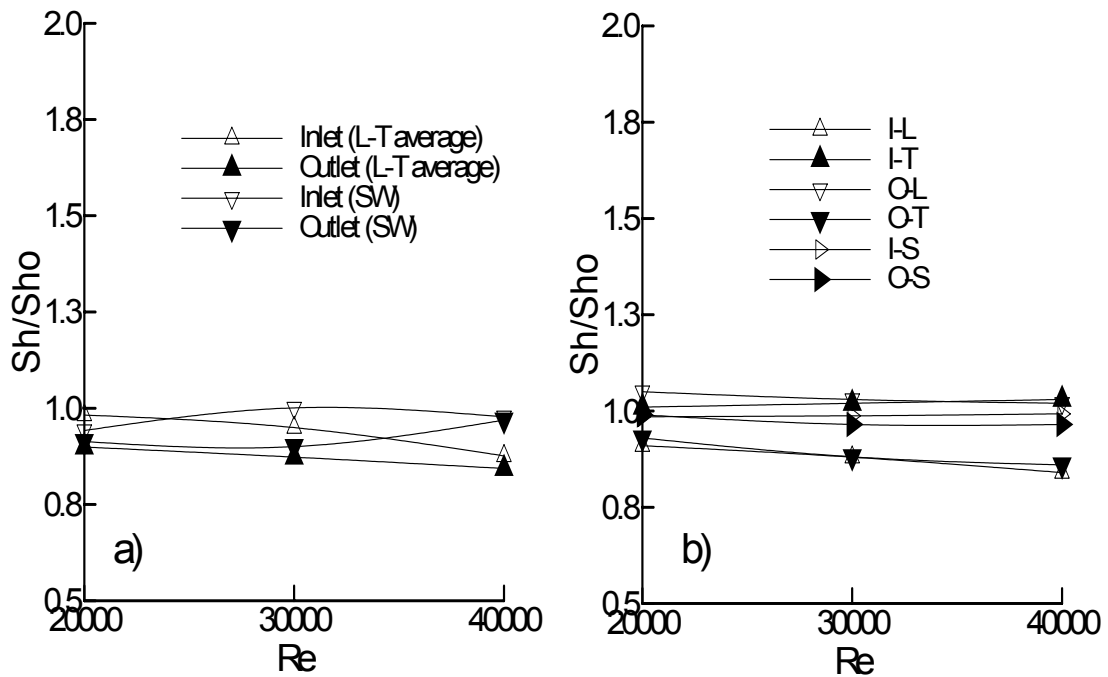


Figure 3.2.3: Fully developed averaged normalized Sherwood number at a)  $Ro=0$  b)  $Ro=0.025$

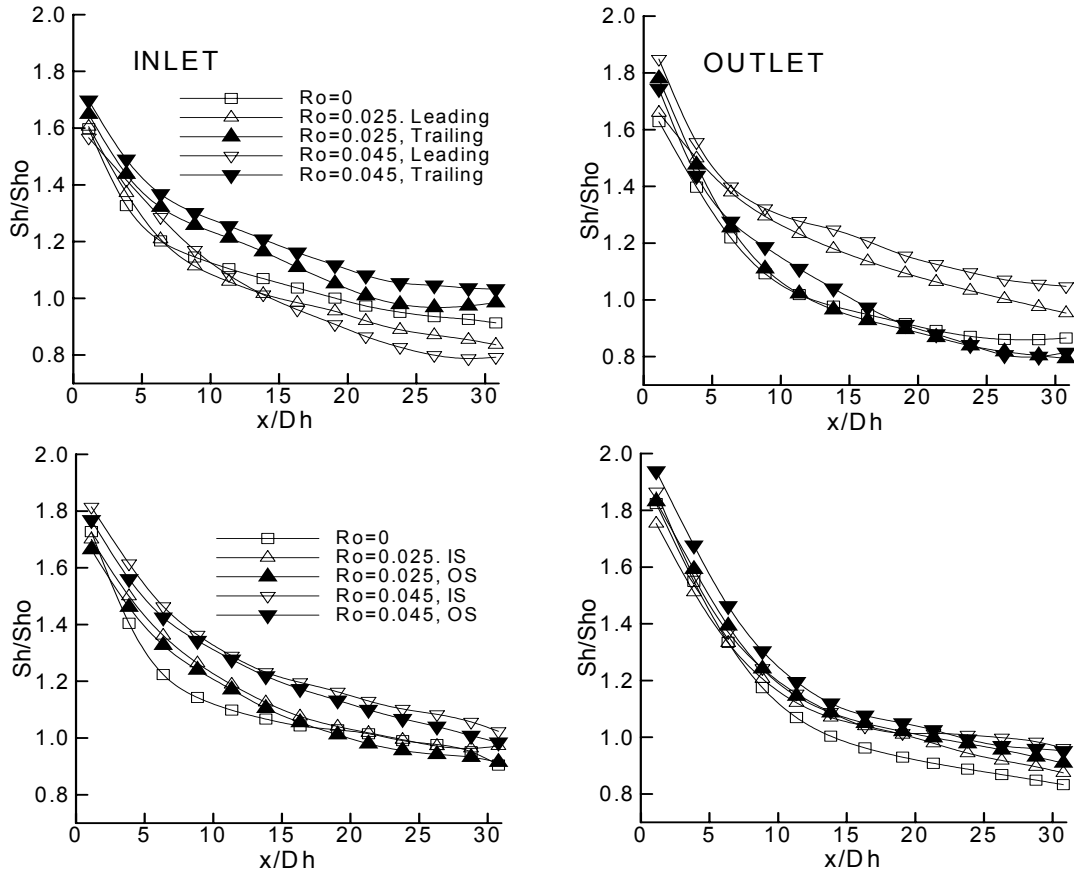


Figure 3.2.4: Effect of Rotation on centerline normalized Sherwood number at  $Re=30,000$

A set of experiments has been conducted at three different Rotation numbers at  $Re=30,000$  for 1:4 channel. The results are shown in Figure 3.2.4 for both inlet (flow radially outward) and outlet (flow radially inward) channels. The Sherwood number ratio on the leading wall is reduced by 10% relative to the stationary case by increasing the rotation number from 0 to 0.045, while on the trailing wall the Sherwood number ratio is increased by 12%. The Sherwood number ratio along the sidewall also generally exhibits an increase with rotation, with an increase of about 8% for  $Ro=0.045$  relative to the stationary case ( $Ro=0$ ). In the outlet channel the reverse behavior is expected on the leading and trailing walls relative to the inlet channel. However, only the destabilized

wall is entirely consistent with expectations. It is observed that the rotation-induced mass transfer enhancement (20% relative to the stationary case) on the leading (destabilized) wall is much more pronounced than the degradation (6%) observed on the leading (stabilized) wall, which does not appear to change from  $Ro=0.025$  to  $0.045$ . A strong bend effect is a possible explanation for this behavior. The sidewall mass transfer displays a modest monotonic increase with rotation, which is as high as 10% relative to the stationary case for the highest Rotation number examined.

Figure 3.2.5 shows the span-wise distributions for different rotation numbers in the fully developed region at  $Re=30,000$ . Some level of asymmetry can be seen in the profiles and is indicative of the asymmetry in the flow induced by the bend and the asymmetry in the incoming flow. In smooth channels, these asymmetries do not wash out quickly, and persist well downstream. In general, the cross-stream profiles follow the expected patterns of reduction and enhancement of mass transfer along leading and trailing walls. For the destabilized surface, the peak heat transfer occurs close to the centerline where the Coriolis-induced secondary flows impinge, and decay outwards along the lateral direction. Along the stabilized surface, the minimum heat transfer occurs in the middle where the secondary flow lifts off the surface, and the peak heat transfer occurs close to the corners where the secondary flow moving down the sidewall impinges. Thus close to the corners, there is a cross-over of the profiles along the stabilized and destabilized surfaces, with heat transfer along the stabilized surface actually being greater than the heat transfer along the destabilized surface. Note that close to the centerline, the differences in the Sherwood number ratio between the stabilized and destabilized surface can be a factor of 1.5 different at  $Ro=0.045$ . This is in contrast to the average Sherwood number ratio where the differences are much smaller and in the range

of 10% to 20%. Along the sidewalls, enhancement is consistently noted with rotation, with the span-wise variation being relatively flat except close to the corners.

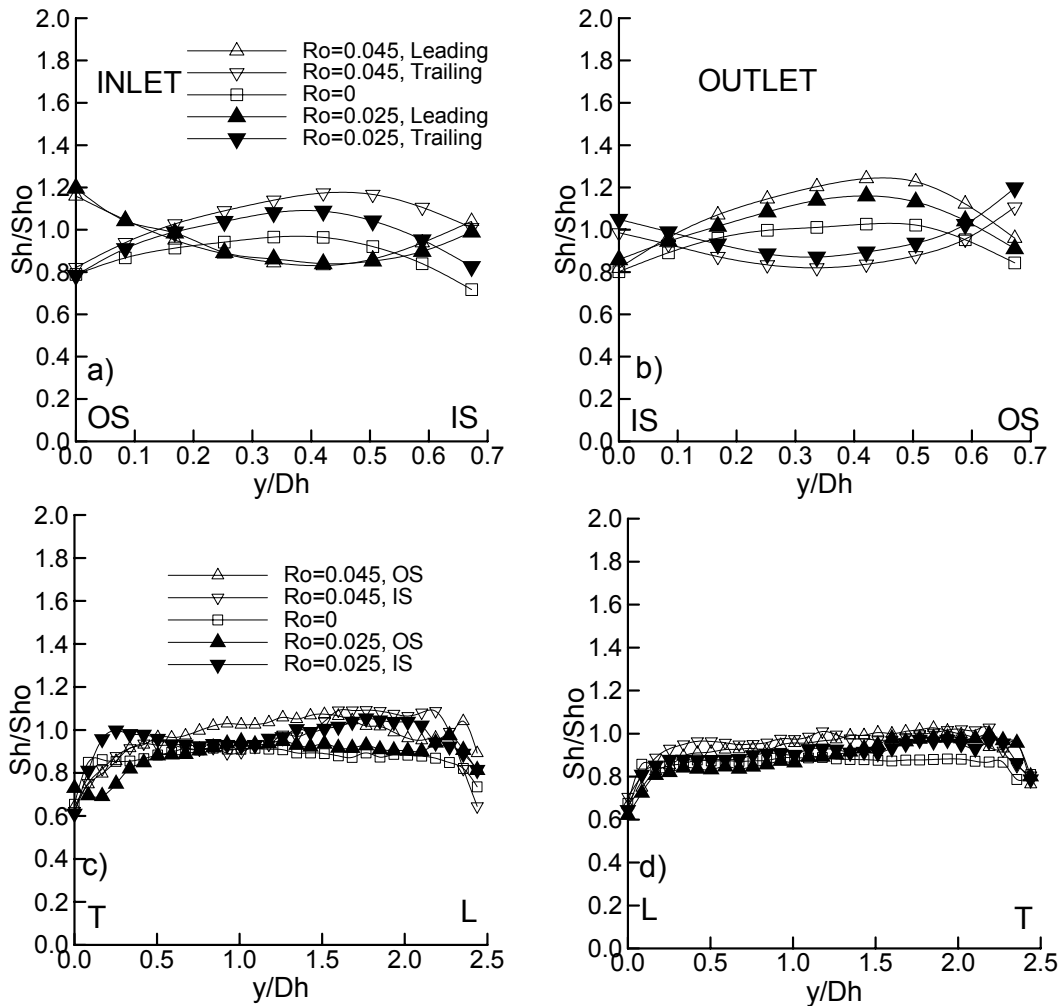


Figure 3.2.5: Span-wise distributions at different rotation numbers in the fully developed region at  $Re=30,000$  (a) & (b) leading and trailing and (c)&(d) sidewalls.

### 3.3 RESULTS FOR 1:4 RIBBED CHANNEL, ORIENTATION= $90^\circ$

For the ribbed channel, measurements are made with thermally inactive square cross-sectioned ribs, mounted on the leading and trailing surfaces in an in-line arrangement and  $90^\circ$  angle of attack ( $e/D_h=0.3125$  and  $P/e=8$ ). Figure 3.3.1 shows the centerline distribution of the Sherwood number along the leading surface and the average

of the Sherwood number ratio along the sidewalls in the inlet channel for a non-rotating case. An obvious feature of the ribbed wall mass transfer profile is its periodic behavior.

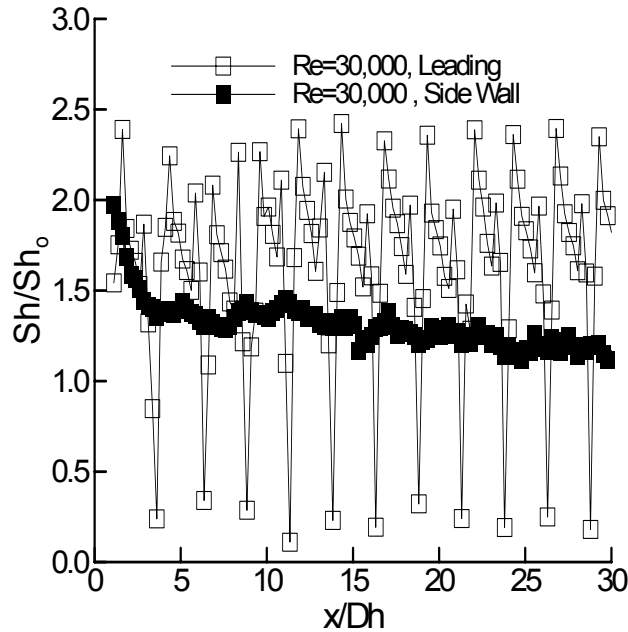


Figure 3.3.1: Centerline distribution of the Sherwood number ratio along the ribbed and sidewall (Inlet) for AR=1:4

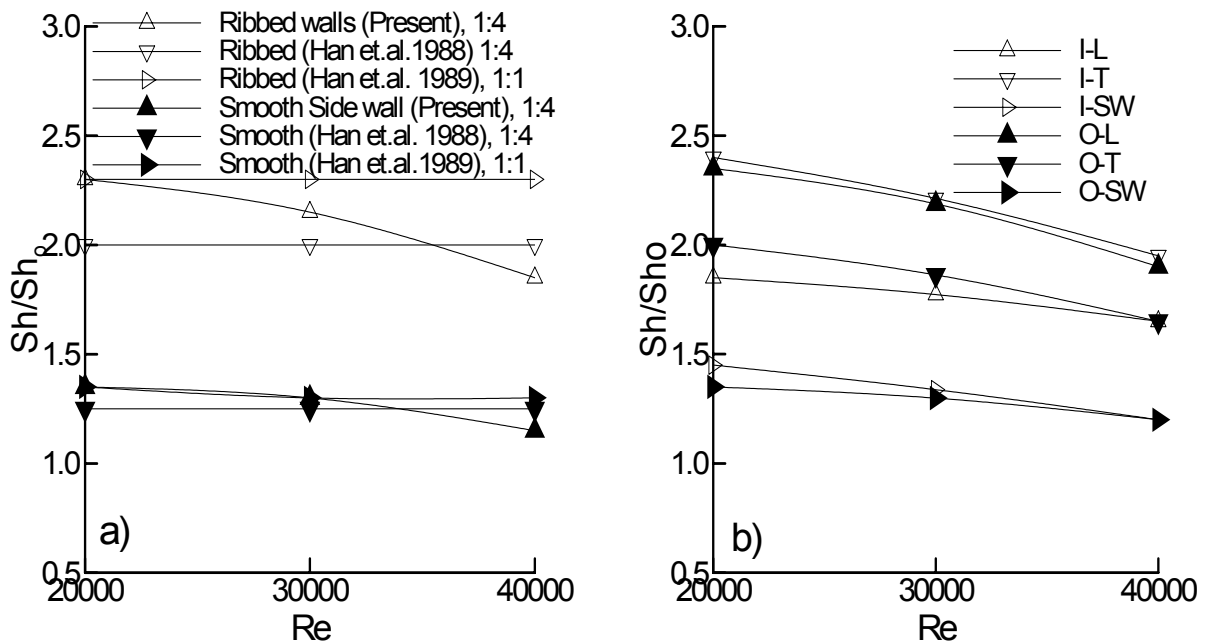


Figure 3.3.2: Fully developed mass transfer ratio in the inlet and outlet ribbed channel a)  $Ro=0$  b)  $AR=1:4$ ,  $Ro=0.025$  (average of the inlet duct sidewalls and outlet duct sidewalls is plotted).

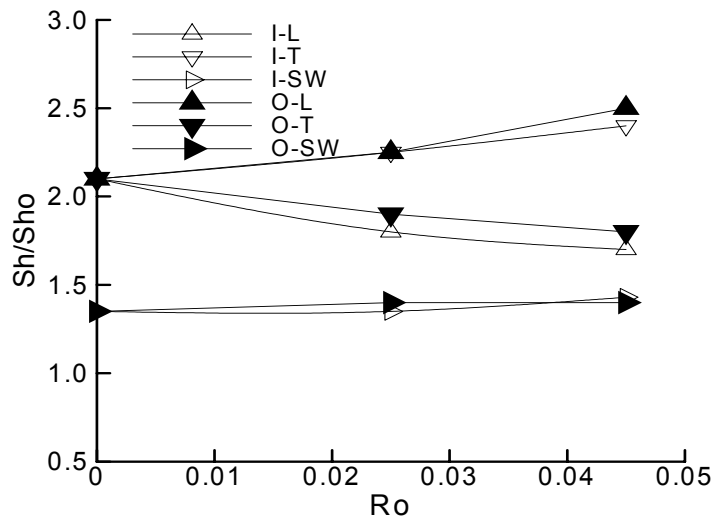


Figure 3.3.3: Effect of rotation number at  $Re=30,000$  (fully developed averaged normalized Sherwood number)

Unlike the smooth channel, which did not attain truly fully developed conditions, the ribbed channel reaches periodically fully developed conditions shortly after the entrance (in the inlet channel) or after the bend (in the outlet channel). Inspection of the centerline mass transfer profiles (Figure 3.3.1) indicates that there is a peak behind the rib where the flow reattaches and a peak immediately upstream of the rib due to a corner vortex. The lowest heat transfer occurs directly at the rib location, and this is a consequence of the rib being thermally inactive in the present study. The ribs also significantly enhance the mass transfer along the smooth sidewalls. This increase in mass transfer is believed to result from the acceleration of fluid between the ribs and an associated increase in turbulent kinetic energy.

Figure 3.3.2 shows the average fully developed mass transfer ratio in the inlet and outlet channels for the ribbed leading and trailing walls and for the smooth sidewalls at different Reynolds numbers. The results for the stationary case are compared with Han et. al. [11] and Han et. al. [12] for aspect ratio 1:4 and 1:1 channel respectively. The present

results for the stationary 1:4 aspect ratio case generally agree with those of Han et. al. [11, 12]. However, in the present results, a consistent Reynolds number effect is observed, with  $Sh/Sh_0$  decreasing with  $Re$  (by nearly 20% on the ribbed surface and 13% on the smooth sidewall). With rotation (Figure 3.3.2(b)) it is observed that for all the walls, the mass transfer ratio also decreases (in the range of 10%-20%) with increasing Reynolds number. This dependence on  $Re$  for the rotational case is comparable to that observed for the non-rotating case.

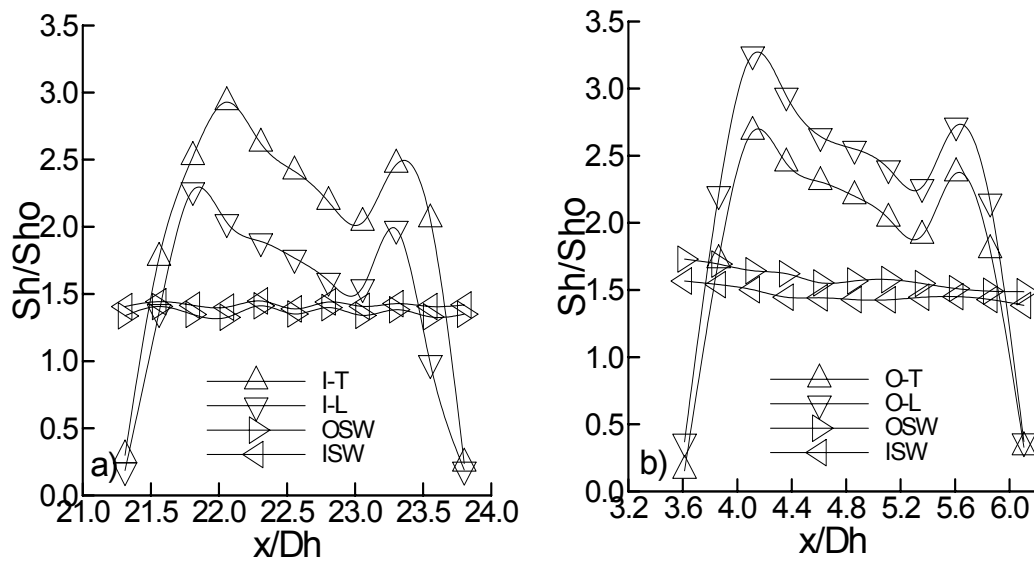


Figure 3.3.4: Centerline normalized Sherwood number distribution in the inter-rib region at  $Re=30,000$ ,  $Ro=0.045$  a) Inlet fully developed Region b) Outlet developing flow region.

Figure 3.3.3 shows the effect of the rotation number at  $Re=30,000$ . In the inlet (radially outward flow) passage, the trailing wall shows an increase of 18% and leading wall decreases by 18% when the rotation number is increased to 0.045. Correspondingly, in the outlet (radially inward flow) passage, the mass transfer ratio on the leading edge increases by 20% and decreases by 14% on the trailing edge. The sidewalls show a rather modest increase with  $Ro$  (within the experimental error range). For a 1:1 case at  $Re=25,000$ ,  $Ro=0.05$  (Wagner et. al. [9]), the enhancements on the destabilized surfaces

were observed to be nearly 10% and the degradation on the stabilized surfaces were nearly 20%. Therefore, it is concluded that for 1:4 case, the rotation effects are stronger and the enhancement is higher than the 1:1 rotating case. This is believed due to the effect of the stronger secondary flow formation in a 1:4 channel.

Figure 3.3.4(a) shows the centerline distribution of the normalized Sherwood number in a single periodically developed region between successive ribs in the inlet duct. The first peak corresponds to flow reattachment while the second peak corresponds to the corner vortex upstream of the rib. At  $Ro=0.045$ , the trailing surface shows roughly a 20% enhancement over the leading surface over most of the inter-rib module. Figure 3.3.4(b) shows the corresponding profiles for developing flow in the first inter-rib module following the bend in the outlet channel. Even in the first inter-rib module following the bend, there is an increase in the Sherwood number ratio (15-20%) on the leading surface relative to the trailing side. This indicates that in a 1:4 channel, the bend induced secondary flows are not strong enough to counter the rotation-induced secondary flows. The outer sidewall in the outlet channel has a slightly higher (less than 10%) Sherwood number ratio than inner sidewall. This is due to the bend effects and is associated with the accelerating flow on the outer sidewall. Note that unlike a 1:1 duct where a separation on the inner sidewall leads to low heat transfer values in this region, no such separation or region of significantly reduced heat transfer is along the inner sidewall immediately following the bend. This is to be expected, based on the fact that for the 1:1 channel the bend is effectively of a “shorter radius” compared to the 1:4 channel. This is also evidenced by the fact that for the 1:1 channel the Ito [33] curved-pipe similarity parameter ( $Re\{D_h/[2r]\}^2$ , where  $r$  is the bend radius) is larger by a factor of 3 compared to that of the 1:4 channel.

Figure 3.3.5 shows the span-wise distribution along the ribbed trailing and leading surfaces (Figures 3.3.5a and 3.3.5b) and smooth inner and outer side walls (Figures 3.3.5c and 3.3.5d) for different rotation numbers in the fully developed region at  $Re=30,000$ . The profiles along the leading and trailing surfaces indicate a relatively uniform mass transfer distribution in the mid-span regions of the ribbed walls followed by a sharp drop-off toward the corners. Note that this behavior is distinctly different than the smooth channel (Figure 3.2.5) where an increase in the Sherwood number was observed toward the corners. Along the smooth sidewalls (Figure 3.3.5c and 3.3.5d), no significant variation is observed with rotation in the inlet duct (Figure 3.3.5c). Slightly higher values (relative to the stationary case) are obtained close to the destabilized trailing-surface side where the rotation-induced secondary flows impinge, and correspondingly slightly lower values are obtained at the opposite end adjacent to the stabilized surface. In the outlet duct, larger differences are observed (Figure 3.3.5d). Values are again higher closer to the destabilized surface (leading surface) and lower closer to the stabilized surface, but surprisingly this is only true along the inner wall. A plausible explanation for this is that the bend-induced acceleration along the outer wall skews the rotation induced secondary flow pattern toward the inner wall. Along the outer wall, a relatively uniform distribution is obtained with a mild increase toward the stabilized surface. With span-wise averaging however, the high and lows in the profiles average out, and the averaged values do not show a strong  $Ro$  number dependence as seen in Figure 3.3.3.

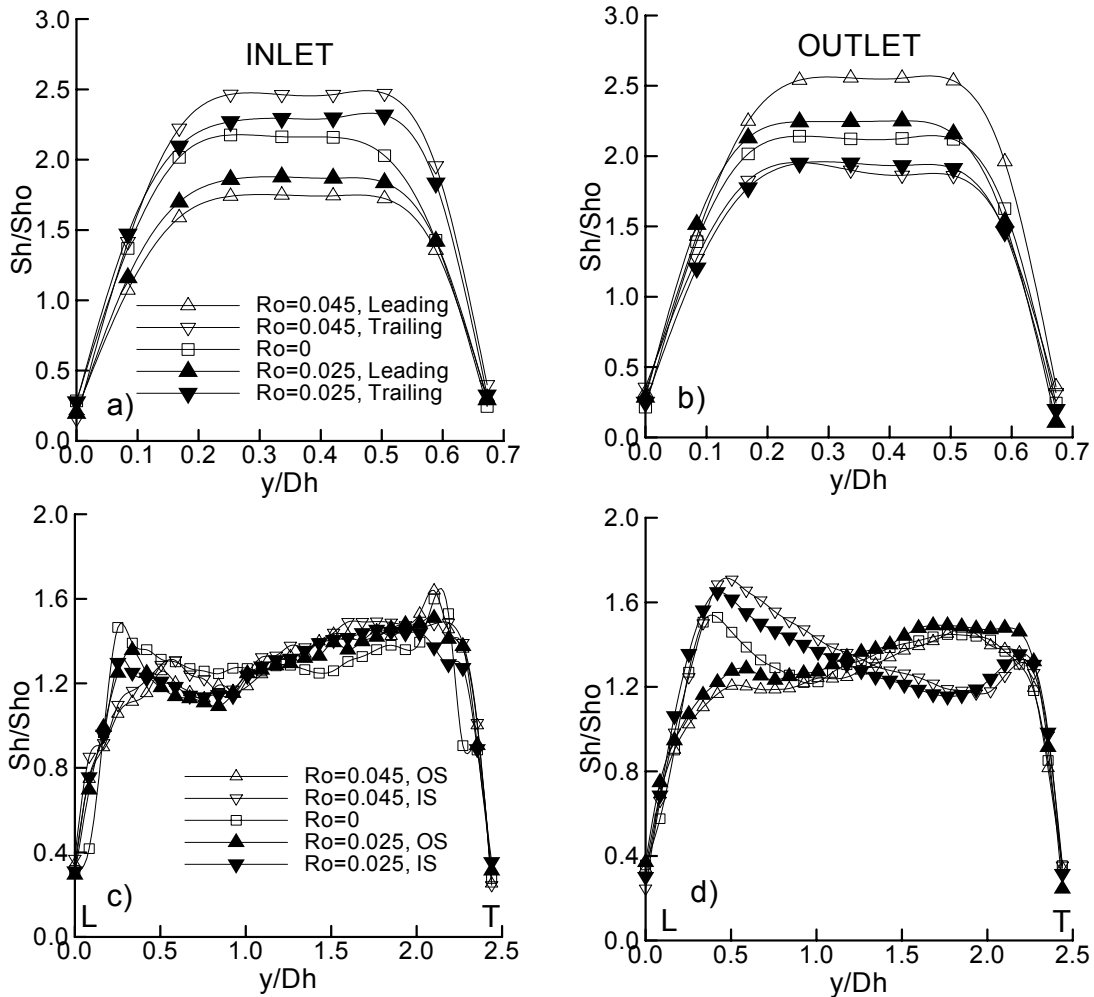


Figure 3.3.5: Span-wise distribution for different rotation numbers in the fully developed region at  $Re=30,000$ .

### 3.4 CONCLUSION

Mass/heat transfer distributions have been obtained in a 1:4 smooth and ribbed channel under stationary and rotating conditions. The naphthalene sublimation technique has been used to obtain these measurements. These results have been compared with results for a 1:1 square cross-section channel. The following conclusions can be drawn:

1. For a smooth channel, the 1:4 cross-section shows lower levels of enhancement along the destabilized surface, and higher levels of degradation along the stabilized surface compared to the 1:1 cross-section channel. Thus, for a specific

- parameter value, the 1:4 cross-section channel has lower heat transfer rates compared to the 1:1 channel.
2. For a smooth channel, the span-wise distributions along the destabilized surface show a peak at the center and decrease toward the corner. Along the stabilized surface, the center has the lowest heat transfer value and the values increase toward the corners. A crossover point is observed near the corners where the stabilized surface has higher heat transfer than the destabilized surface.
  3. For the smooth duct, the Sherwood numbers are relatively insensitive to  $Re$ . For the ribbed duct, the Sherwood number ratios show a weak  $Re$  number dependence under stationary and rotating conditions, with Sherwood number ratios decreasing with  $Re$ .
  4. At  $Re=30,000$ , as  $Ro$  is increased from 0 to 0.045, the 1:4 cross-section smooth duct shows roughly a 10-12% change in the inlet duct relative to the stationary case. For the ribbed duct, the corresponding change is about 18%. This observation is consistent with the square-aspect ratio results of Johnson et al. [30] who also show that 90-degree trips show a greater sensitivity to  $Ro$  compared to the smooth channel.
  5. The span-wise distribution for the ribbed cases show fairly uniform distributions in the mid-span regions, and unlike the smooth channel case, the peak heat transfer rate on the stabilized surface is highest in the middle.

## CHAPTER 4

### HEAT/MASS TRANSFER IN 4:1 RECTANGULAR SMOOTH AND RIBBED PASSAGES WITH ORIENTATION = 90°

#### 4.1 INTRODUCTION

The experiments are conducted in 4:1  $\left[\left(\frac{W}{H}\right) = 4:1\right]$  rectangular channel for 90-degree orientation for smooth and ribbed passages. The ribs have the configuration of  $\frac{e}{D_h} = 0.3125$  and  $\frac{P}{e} = 8$ . The rib angle of attack is 90-degree. The value of  $\frac{e}{H} = 0.5$  and  $\frac{e}{W} = 0.125$ . In this case, the ribs are placed on one side only i.e. the ribs are on leading side or the ribs are on the trailing side.

#### 4.2 RESULTS FOR 4:1 SMOOTH CHANNEL, ORIENTATION=90°

Firstly, the experiments are conducted in the stationary rectangular channel at different Reynolds number.

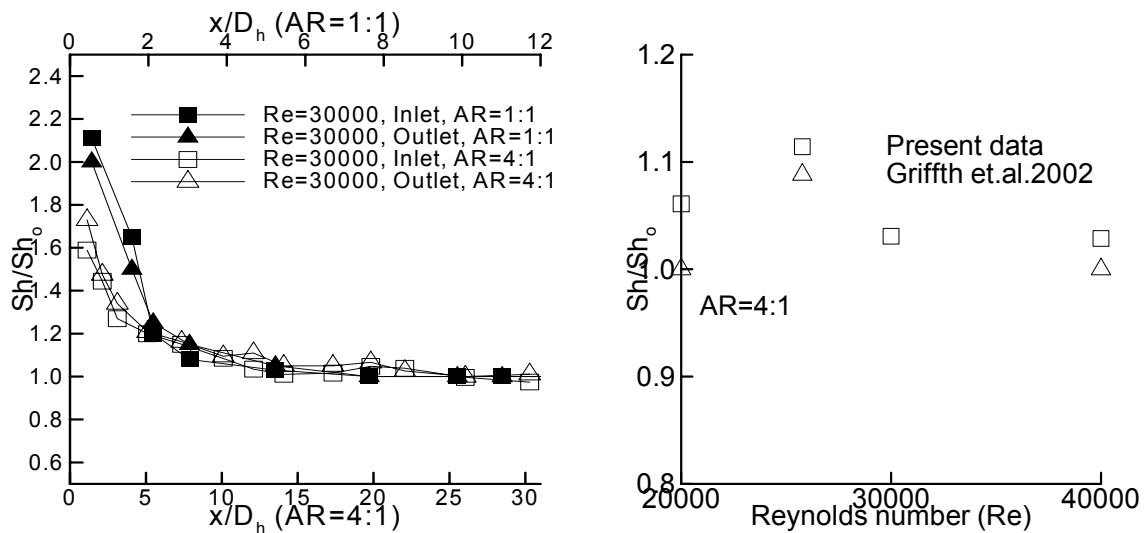


Figure 4.2.1a) Comparison of centerline normalized sherwood number distribution for inlet and outlet passages at  $Re=30000$ ,  $Ro=0$  for  $AR=1:1$  &  $AR=4:1$ . b) Comparison of fully developed sherwood number ratio for  $AR=4:1$  for stationary case.

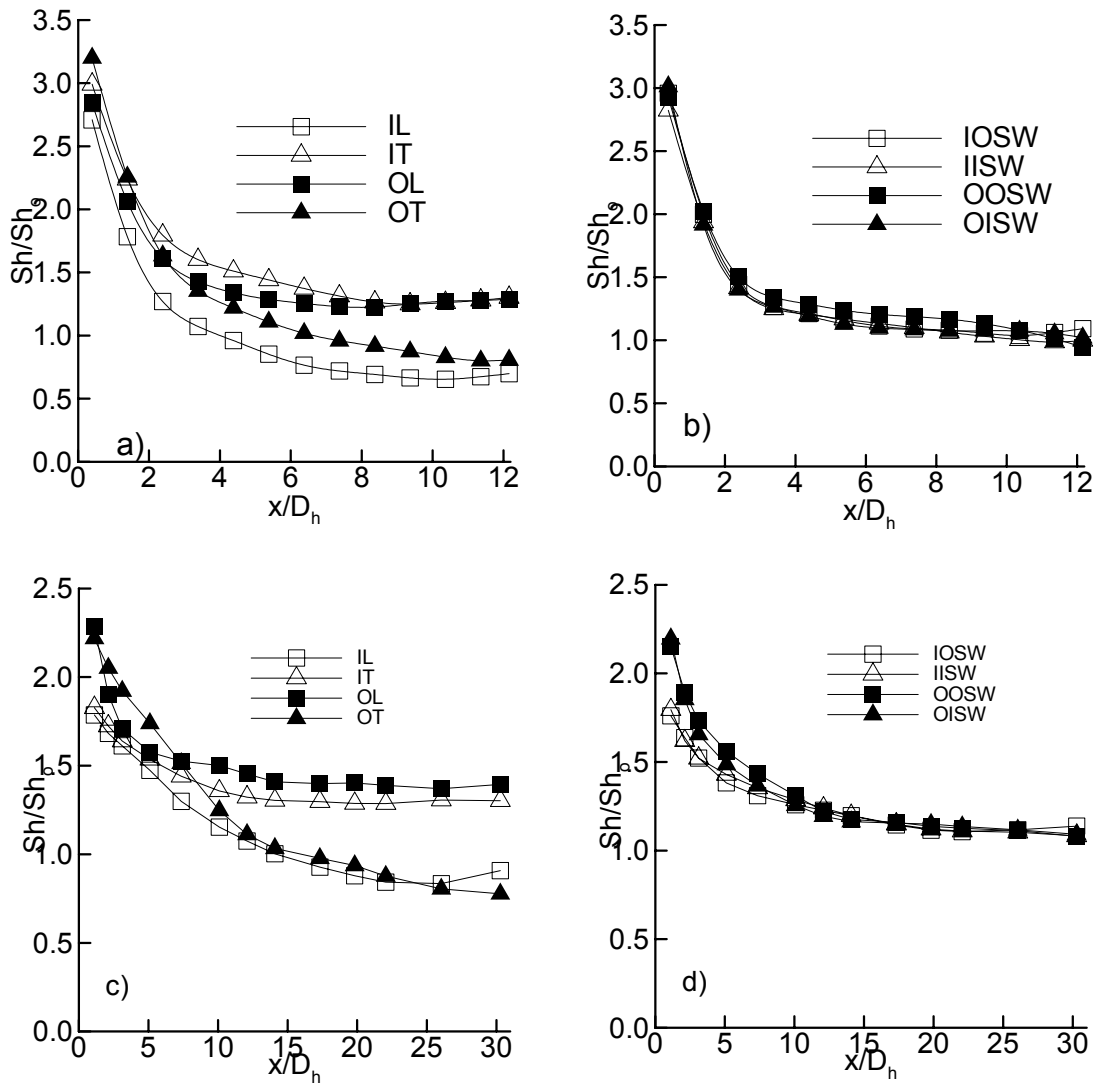


Figure 4.2.2: Comparison of the centerline normalized Sherwood number distribution  $Re=5,670$ ,  $Ro=0.12$  a)  $AR=1:1$ , leading & trailing wall b)  $AR=1:1$  sidewalls c)  $AR=4:1$ , leading & trailing wall d)  $AR=4:1$  sidewalls.

All the walls have asymptotes tend to 1 for no rotation at both the aspect ratios. It is observed that the mass transfer ratio is higher in the developing range for aspect ratio 1:1 than with respect to 4:1. This may be attributed to the decrease in the cross sectional area of the channel in 4:1 channel. Figure 4.2.1(b) shows the comparison of the fully developed Sherwood number ratio. An excellent agreement is observed with the values

reported in the literature. It is observed that the increase in the Reynolds number does not affect the mass transfer ratio in a stationary duct.

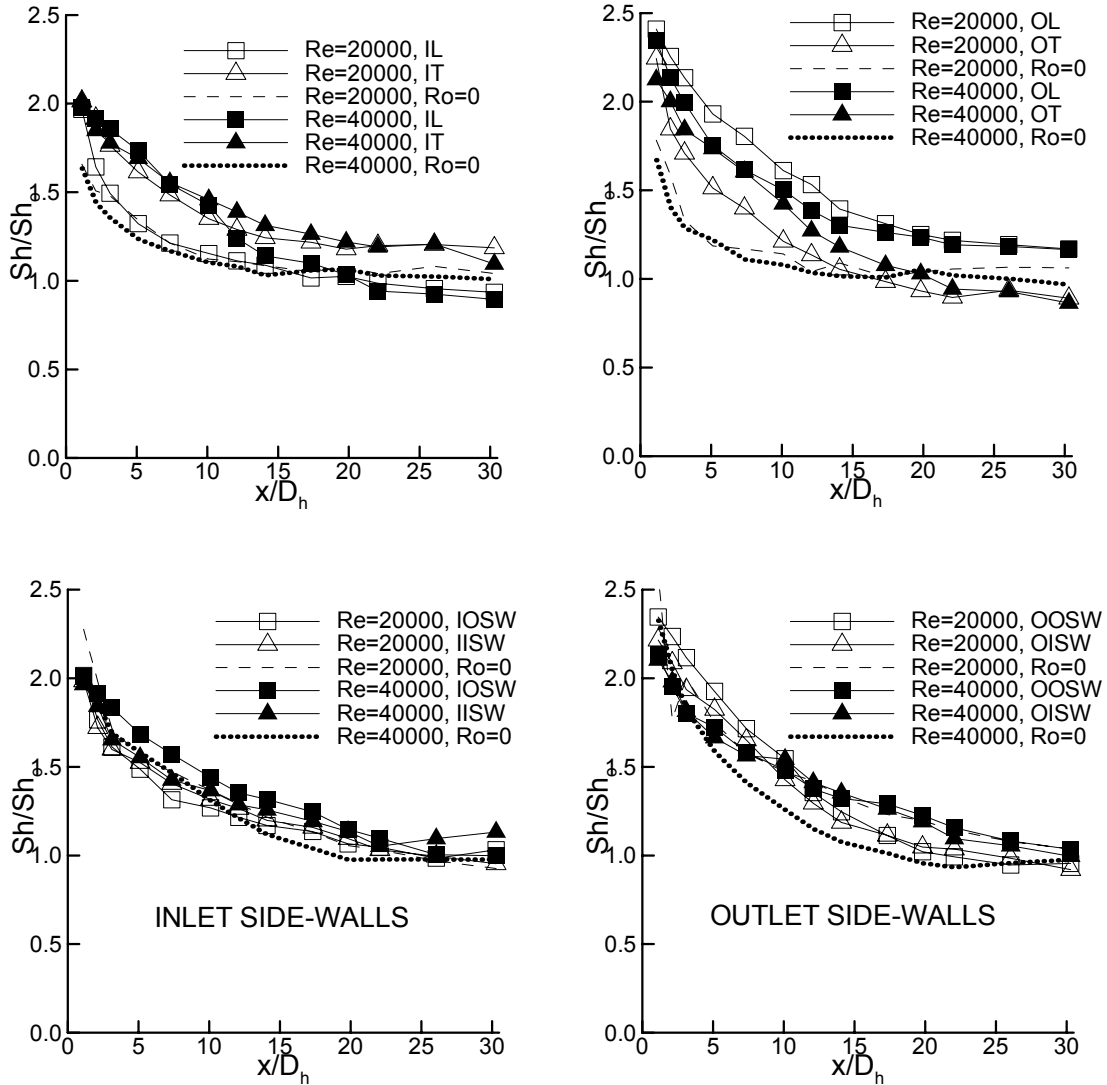


Figure 4.2.3: Comparison of the centerline normalized Sherwood number ratio for AR=4:1 channel at different Re numbers,  $Ro=0.025$  with stationary 4:1 channel at the Re number.

Figure 4.2.2 shows the comparison in two different aspect ratios at low Reynolds number  $Re=5,670$  and a high rotation number of 0.12. The comparison of the centerline normalized Sherwood number ratios are shown and the same qualitative trend are observed for the two aspect ratios. The scale on the x-axis is different due to the

difference in hydraulic diameter between AR=1:1 (=1 inch) and AR=4:1 (=0.4 inches). In the inlet duct (radially outward flow), the trailing walls experience increased mass transfer while the leading-wall mass transfer is reduced because of the rotation-induced secondary flows. The opposite is true for the outlet duct where the flow is towards the axis of rotation. While the qualitative features are the same, quantitative differences are observed between the 1:1 and 4:1 aspect ratios, with the 4:1 having lower values in the developing region. In the fully developed region of the 4:1 aspect ratio, a decrease of about 9% is observed on the inlet leading wall and there is an increase of 30% on the trailing wall. In the outlet passage, leading side shows an increase of 39.6% as compared to the trailing side, which shows only a decrease of 8%. The inlet and the outlet sidewalls show an increase of 13%. For both aspect ratios the level of rotation-induced degradation is lower in the outlet channel relative to the inlet channel, and is presumably linked to the bend induced secondary flows increasing the mixing and heat transfer in the outlet channel.

Figure 4.2.3 shows the comparison of the centerline normalized Sherwood number ratio for AR=4:1 channel at different Reynolds numbers,  $Ro=0.025$  with stationary 4:1 channel at the same Reynolds number. It is observed that the Inlet trailing and outlet leading edge have increased while Inlet leading and outlet trailing edge have decreased mass transfer ratio distribution with respect to the stationary case. The sidewalls also show the enhancement. This may be attributed to the Coriolis pressure gradient set up by the primary flow (stream wise flow) influences the leading and trailing wall boundary layers. The boundary layer fluid is convected towards the suction surface while retaining its axial momentum, and then starts the secondary flow circulations. In fully developed flow, there is a corresponding imbalance between the Coriolis and pressure forces acting

on the “slow-moving fluid” near the leading and trailing walls of the channel that cause secondary flows. It is observed that there is an increase in the mass transfer ratio of approximately 19%-24% on the destabilized surfaces and decrease of approximately 6%-10% on the stabilized surfaces in the radially outward and inward flow in AR=4:1 channel with respect to the stationary case. Also, no significant effect of increasing the Reynolds number is observed.

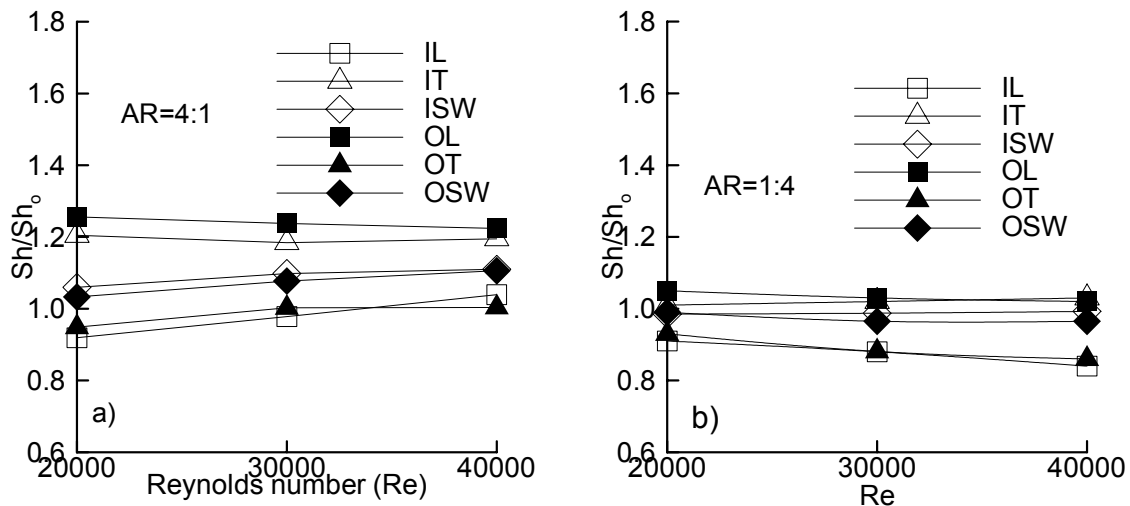


Figure 4.2.4: Comparison of fully developed Sherwood number ratio at  $Ro=0.025$  at various Reynolds number at different aspect ratios.

Figure 4.2.4 shows the quantitative picture of the enhancement and decrease on each wall at a Rotation number of 0.025 for Aspect ratio 1:4 and 4:1. For Aspect ratio 4:1, at a Reynolds number of 20,000, the decrease of the Sherwood number ratio in the leading edge of the inlet passage is about 9%, and as the Reynolds number is increased to 30,000 and 40,000, the corresponding decrease is in the experimental error range. Along the trailing edge of the inlet passage, the increase in the Sherwood number ratio is about 19.5% at  $Re=20000$  and does not change ( $\approx 20\%$ ) significantly when the Reynolds number is increased to 40000. Along the sidewalls of the inlet passage, the average

between the outer sidewall and the inner sidewall shows an increase of 7% at a Reynolds number of 20,000 and increases to 11% as the Reynolds number is increased to 40,000.

In the radially inward passage (outlet duct), the increase in Sherwood number ratio due to rotation is greater but it is little affected by the increase in the Reynolds number. At  $Re=20,000$ , the increase is about 25.6% along the leading edge and at  $Re=40,000$ , it is about 22%. Along the trailing edge, the decrease at  $Re=20,000$  is about 6% and falls in the experimental error range as the Reynolds number is increased to 40,000. The sidewalls show an increase that is significant (=10%) only at the highest Reynolds number of 40,000. Thus, we note that there is an increase in the mass transfer ratio with respect to the stationary case for every Reynolds number investigated. The increase is about 15-17% as the Reynolds number is varied and is significant than with respect to the 1:4 channel investigated earlier.

Figure 4.2.5 shows the fully developed Sherwood number ratio at  $Re=30,000$  and different Rotation numbers. It is seen that as the rotation number is increased, there is an increase in the overall mass transfer ratio coefficient. Along the inlet leading edge, at  $Ro=0.045$ , the decrease is 9% whereas on the trailing edge, it increases by 24.6%. The inlet sidewalls show a smaller increase with Rotation and at  $Ro=0.045$ , show a consistent increase of 11%. In the radially inward flow passage, at  $Ro=0.045$ , the increase along the leading edge is about 30% while it is 24% at  $Ro=0.025$ . The decrease along the trailing edge is within the experimental error range. The sidewalls at  $Ro=0.045$  and at 0.025 shows an increase of about 12% and 9% respectively. Thus, it is observed that the increase in rotation number significantly increases the mass/heat transfer in the high aspect ratio channel.

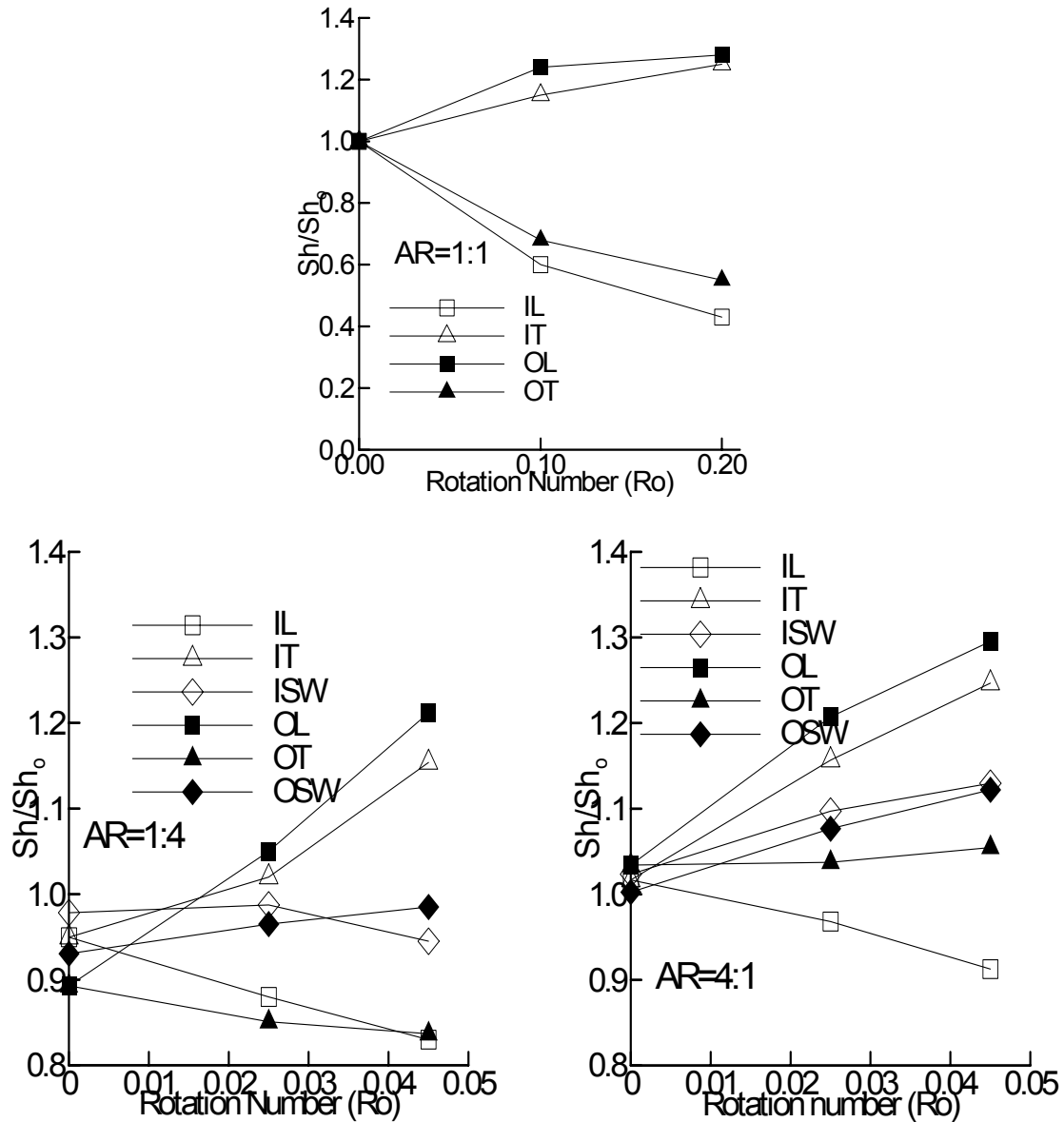


Figure 4.2.5: Fully developed Sherwood number ratio at  $Re=30,000$  at various rotation numbers for various aspect ratios

Figure 4.2.6 shows the span wise distribution for different rotation numbers at  $Re=30,000$ . It is observed that the asymmetry is enhanced due to the rotation in the outlet passage. Centerline increase due to the rotation is clearly shown by the cross-streams. The cross over of the mass transfer profiles is explained in the same manner as above. Also the increase in the sidewalls is observed.

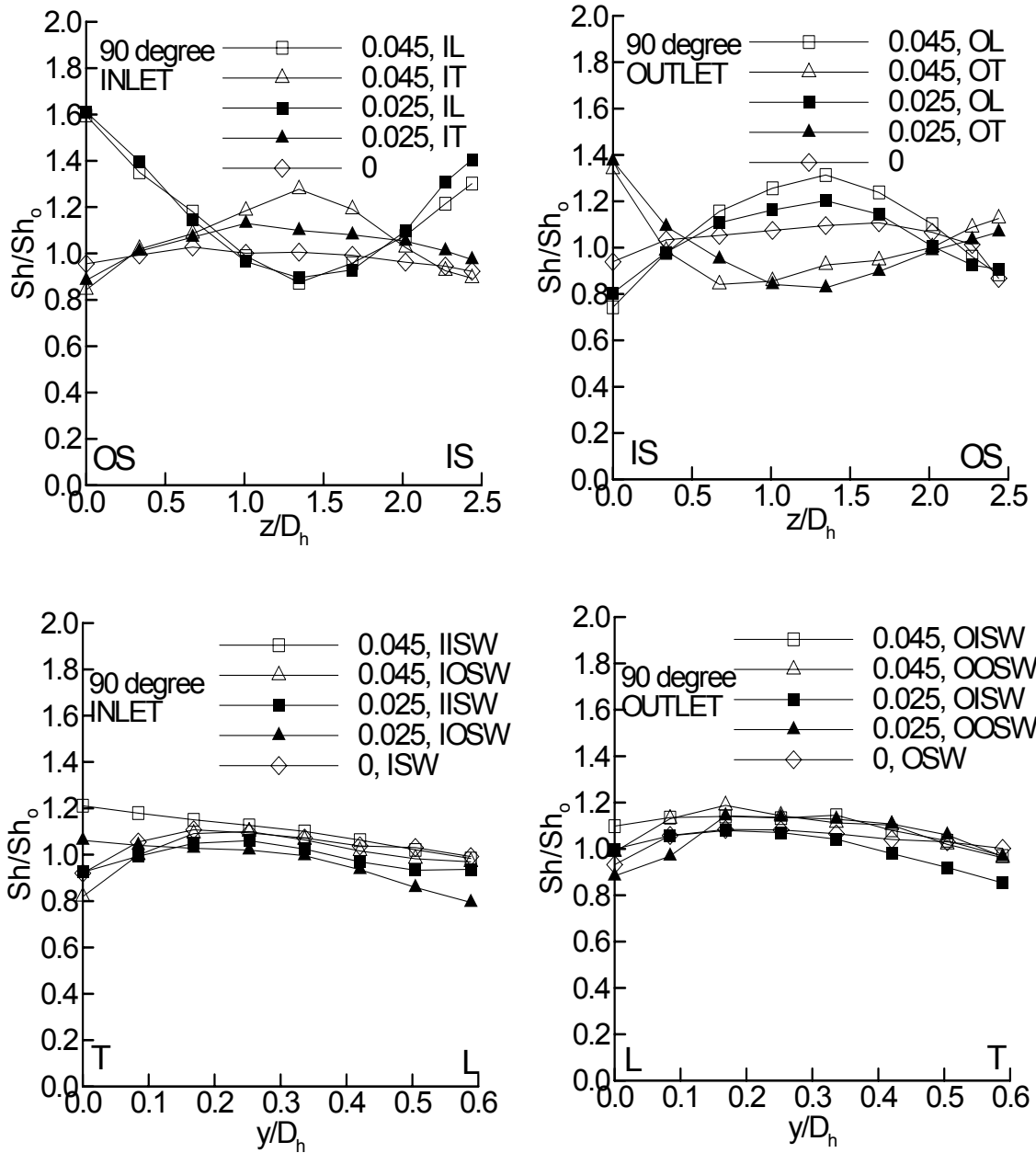


Figure 4.2.6: Cross-Stream normalized Sherwood number distribution in the fully developed region for AR=4:1 channel at different Ro numbers and Re=30,000.

Thus it is observed that rotational effects can be large and significant on the development of a turbulent boundary layer in a rotating rectangular channel. This is also attributed to the fact that wall shear stress on the pressure surface is higher than for a zero pressure gradient boundary layer; while on the suction side it is lower.

### 4.3 RESULTS FOR 4:1 RIBBED CHANNEL, ORIENTATION=90°

Figure 4.3.1 represents the centerline distribution of the Sherwood number along the various surfaces in the inlet channel for non-rotating case at  $Re=30,000$ . The square ribs of the above-described cross-section are placed on one side of the channel. An obvious feature of the ribbed wall mass transfer profile is its periodic behavior. The ribbed channel reaches periodically fully developed conditions shortly after the entrance in the inlet channel or after the bend in the outlet channel. The enhancement of the mass transfer coefficient is observed on all the walls and is due to the blockage of the channel, which in turns increases the surface area, and thus higher the mass transfers. We also observe that the flow separates very close to the upstream corner. Introduction of ribs raises overall turbulence levels. It causes the formation of large separation along the outer wall, as the flow encounters the first outer wall rib, after the bend exit. The flow is 3-dimensional in the U-bend used since there are strong variations from the symmetry plane to the leading wall.

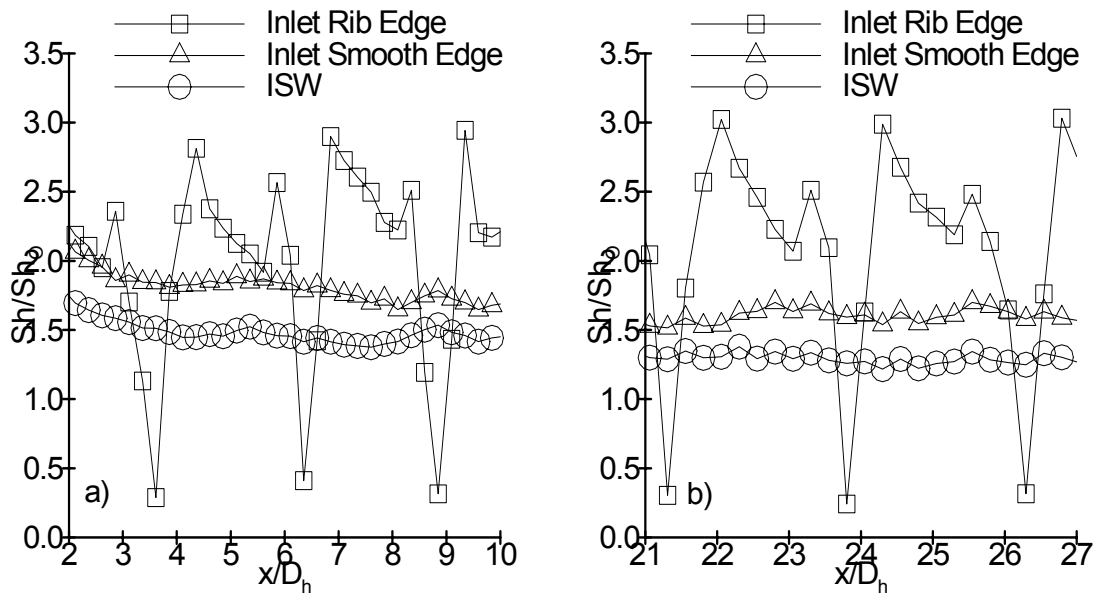


Figure 4.3.1: Centerline distribution of the sherwood number ratio along the ribbed side, smooth side and the smooth sidewalls for the inlet passage at  $Re=30,000$ ,  $Ro=0$ ,  $AR=4:1$   
 a) developing flow b) fully developed flow.

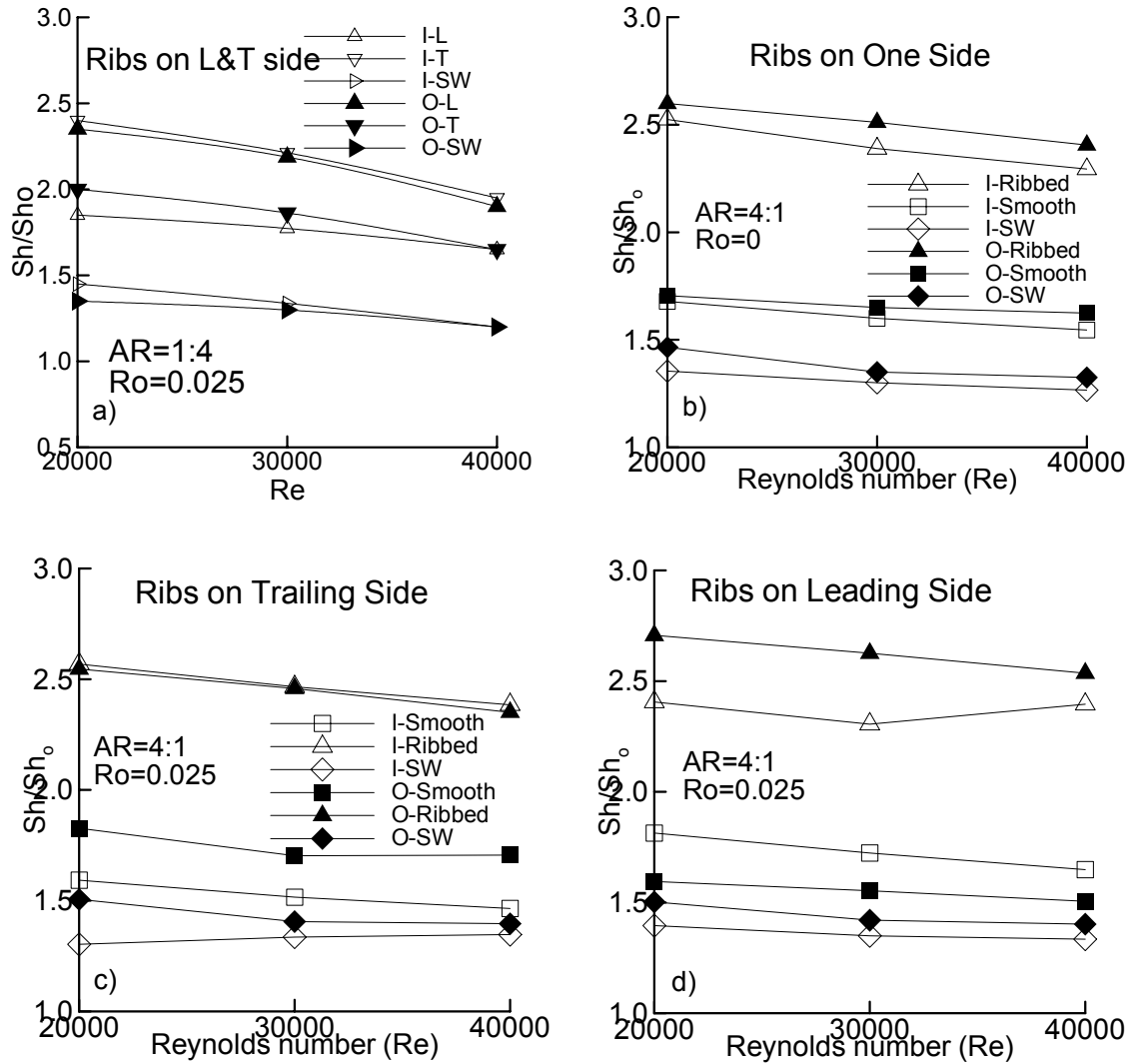


Figure 4.3.2: Comparison of fully developed normalized sherwood number ratio in different aspect ratios at different Reynolds number.

Figure 4.3.2(a) shows the effect of the Reynolds number for aspect ratio 1:4 when the ribs are placed on both leading and trailing sides at  $Ro=0.025$ . It is observed that for all the walls, the mass transfer ratio decreases in the range of 10%-20% with increasing Reynolds number.

Figure 4.3.2(b) shows the effect of Reynolds number for aspect ratio 4:1 for the non-rotating case when the ribs are placed on one side (leading or trailing side). Figure 4.3.2(c) and (d) shows the effect when the ribs are placed on trailing and leading edge

respectively. A consistent Reynolds number effect is observed for both the aspect ratios. The behavior is surprising considering the flow appears to be fully developed with consistently periodic modules. The trend is verified through repeated experiments. One possibility is that the exponent of the Reynolds number ( $=0.8$ ) with which it is normalized is different. The correct value of the Reynolds number cannot be estimated due to the limited number of Reynolds number values studied.

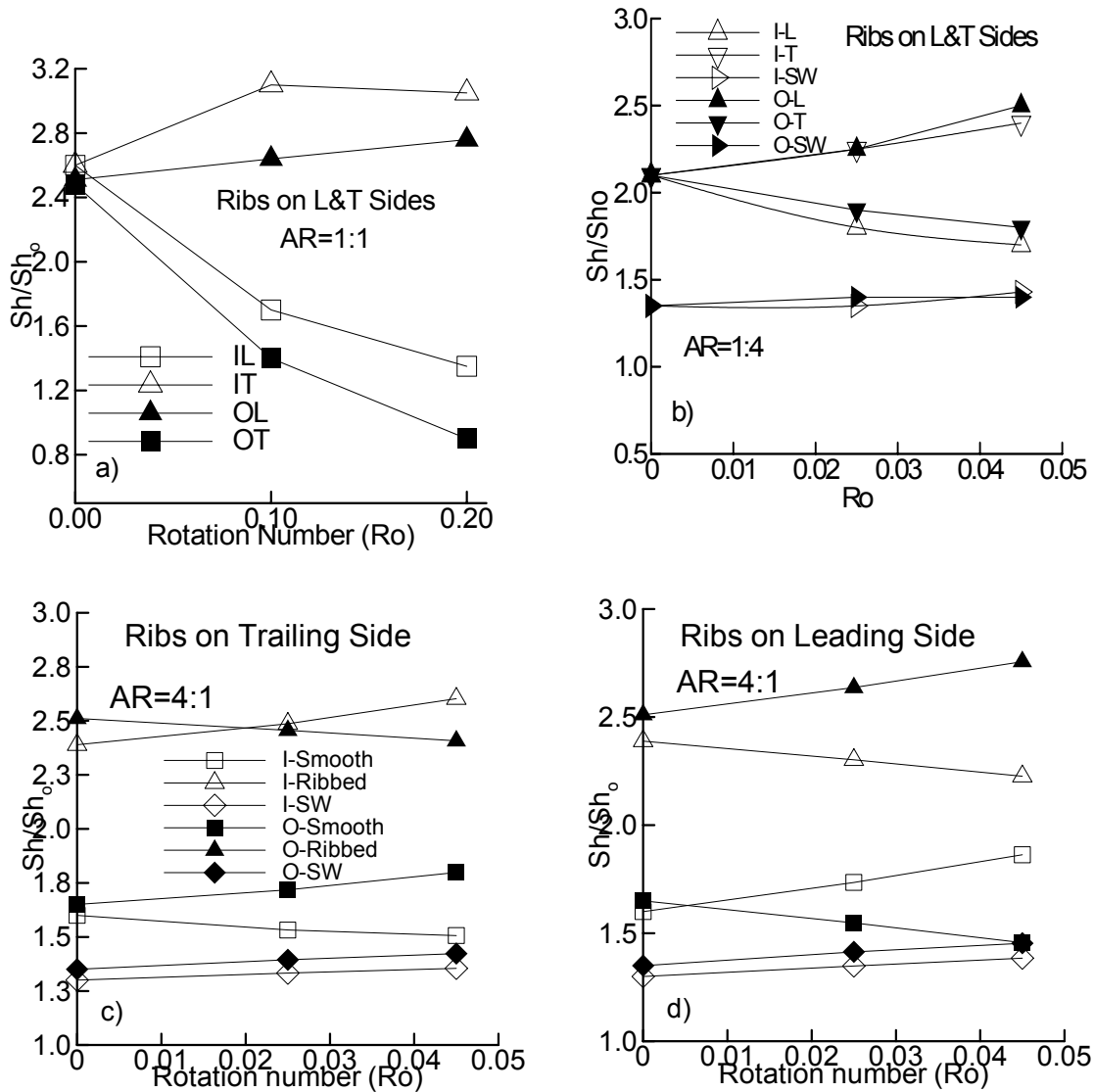


Figure 4.3.3: Comparison of the effect of rotation number at  $Re=30,000$  for different aspect ratios.

Figure 4.3.2(b) shows an increase of 150%-130% on the ribbed wall, 68%-58 % on the smooth side (not sidewalls) and around 40% on the sidewalls in the radially outward flow stationary channel as the Reynolds number is increased from 20,000 to 40,000 with respect to the smooth channel (AR=4:1) for the non-rotating case. In the radially inward flow stationary channel, there is an increase of 160%-140 % on the ribbed wall, 70%-64% on the smooth side (not side walls) and around 48%-40% on the side walls as the Reynolds number is increased from 20,000 to 40,000 with respect to the smooth channel (AR=4:1) for the non-rotating case.

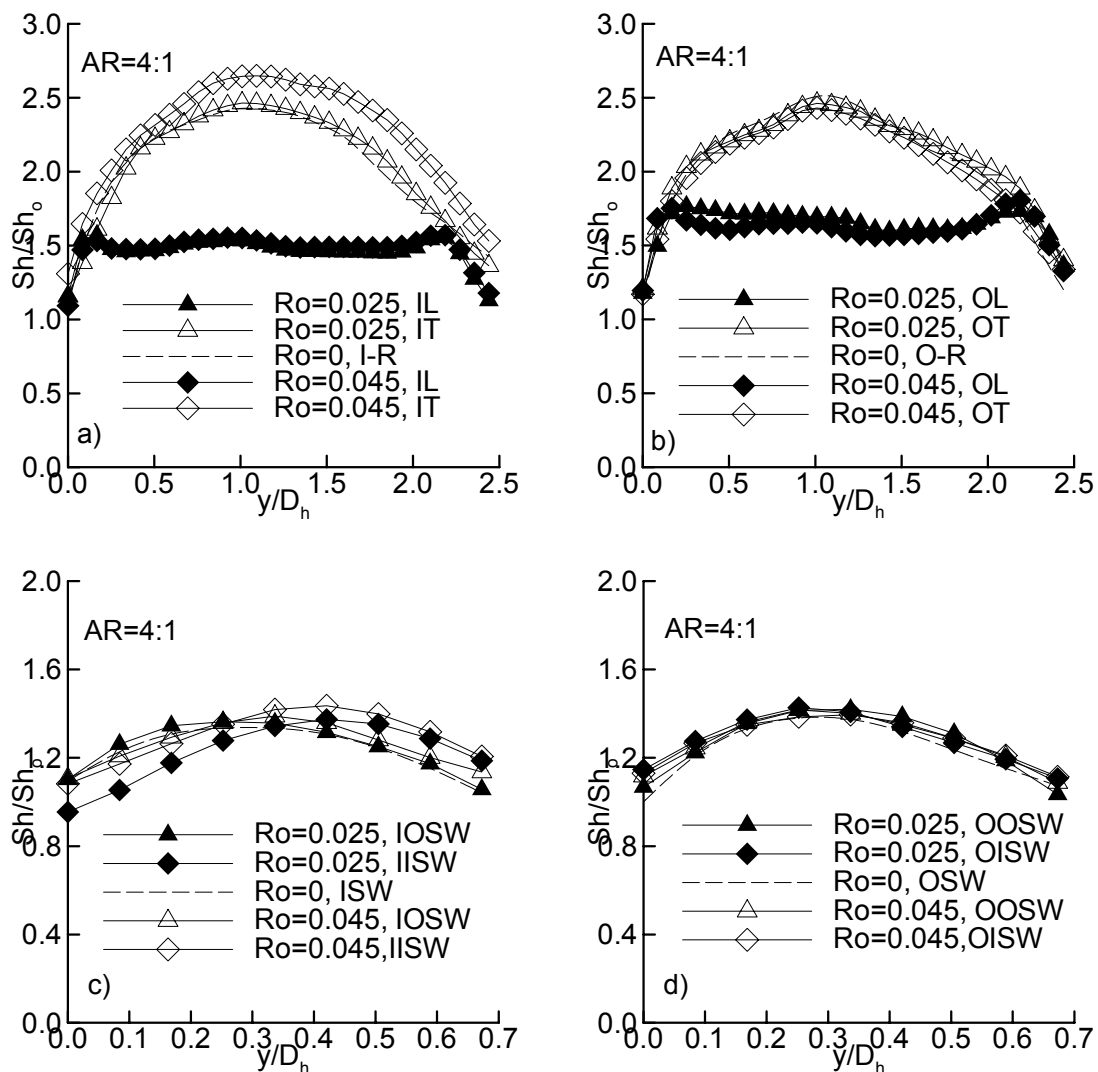


Figure 4.3.4: Cross-stream variation at various rotation numbers at  $Re=30,000$  with ribs on trailing Side.

Figure 4.3.2(c) shows the Reynolds number effect at  $Ro=0.025$  when the ribs are placed on the destabilized and the stabilized surface in the radially outward and radially inward flow passage respectively. The surfaces with ribs consistently decrease with increase in the Reynolds number from 6%-10%. The surface labeled as I-Smooth or O-Smooth is the Stabilized and the destabilized surface (SS and DS) in the inlet and the outlet passage respectively. In comparison with the non-rotating case, the SS decreases by 8% and DS increases by 8%-10% and does not change appreciably with the increase in Reynolds number. The sidewall does not change appreciably with the increase in Reynolds number.

Figure 4.3.2(d) shows the Reynolds number effect at  $Ro=0.025$  when the ribs are placed on the stabilized and the destabilized surface in the radially outward and radially inward flow passage respectively. The DS in the outlet and the inlet passage increases with the rotation number by approximately 8% and does not change appreciably with the increase in Reynolds number. The SS in the inlet and the outlet passages decreases in the error range.

Figure 4.3.3(a) shows the effect of rotation number at Reynolds number 30000 for aspect ratio 1:1 when the ribs are placed on both the leading and the trailing sides. The DS in the inlet passage shows an increase of 30% when the rotation number is increased to 0.1. When the rotation number is further increased to 0.2, there is appreciably no change. This may be due to the difference in the buoyancy parameter at  $Ro=0.1$  and  $Ro=0.2$ . The experiment was repeated to conclude that the buoyancy parameter does not affect the mass transfer ratio at low rotation numbers and thus the experiment with the  $AR=1:4$  or  $4:1$  were carried out at low Rotation numbers only. The SS in the inlet and the

outlet passage shows a decrease of 30% and 34% respectively when the rotation number is increased to 0.1.

Figure 4.3.3(c) shows the effect of rotation number at Reynolds number 30000 for aspect ratio 4:1 when the ribs are placed on both the destabilized surface in the inlet passage and stabilized surface in the outlet passages. The ribbed surface in the inlet passage (DS) shows an increase of 13% when the rotation number is increased to 0.045 where as the ribbed surface in the outlet passage (SS) shows decreasing curve but the decrease is within the experimental error range ( $\approx 4\%$ ). The inlet smooth side, which is the SS, shows a decrease of 8% as the rotation number is increased to 0.045 and the outlet smooth side, which is the DS, shows an increase from 10%-15% as the rotation number is increased from 0.025-0.045. The sidewalls also show an increase of about 6% when the rotation number is increased to 0.045.

Figure 4.3.3(d) shows the effect of rotation number at Reynolds number 30000 for aspect ratio 4:1 when the ribs are placed on both the stabilized surface in the inlet passage and destabilized surface in the outlet passages. The SS surface in the inlet passage shows a decrease of 12% and the DS in the outlet passage shows an increase of approximately 10% as the rotation number is increased to 0.045. The inlet smooth side, which is the DS, shows an increase of approximately 16% while the SS in the outlet passage shows a decrease of 12% at  $Ro=0.045$ . The sidewalls show an increase of around 7% at a  $Ro=0.045$ .

Figure 4.3.4 shows the span-wise variation of increasing the Rotation number at Reynolds number 30,000 with turbulators on the DS in the inlet passage and on the SS in the outlet passage. It is observed that the most important effects of rotation are due to secondary flows, and not Coriolis instability or force. Also a loss of momentum in the

integrated centerline distributions profiles agrees with the transfer of axial momentum due to secondary circulations. Fully developed turbulent flow in rectangular channels, shows a decrease in integrated centerline momentum.

Figure 4.3.5 shows the span-wise variation of increasing the Rotation number at Reynolds number 30,000 with turbulators on the SS in the inlet passage and on the DS in the outlet passage. The distributions are a result of averaging in the stream-wise direction between successive ribs. It should be noted that the secondary flow effects after the bend are different with and without ribs. This is expected since the ribs induce secondary flows that are confined near the walls. The interactions of rib induced and bend induced secondary flow result in a different pattern generating multiple rolls to cause greater turbulence and thus high mass transfer.

#### **4.4 CONCLUSION**

The Sherwood number shows the same trend for both the ribbed side and the smooth sidewalls show the same trend for larger aspect ratio channel 4:1. The mass transfer ratio gradually increases with increasing channel aspect ratio. This is because that, for the same rib geometry and flow condition, the high aspect ratio channels have wider ribbed side surfaces (i.e. narrower smooth side walls) to produce higher heat transfer coefficient, while the low aspect ratio channels have narrower ribbed side surface (i.e. wider smooth side walls) to produce lower heat transfer coefficients. The Sherwood number ratio decreases with increasing Reynolds number. The centerline effect of rotation on the mass transfer ratio is strongly dependent on aspect ratio and thus the wall shear stress and the velocity distributions are also strongly dependent on aspect ratio.

This study provides data for the study of the internal cooling of turbine blades and to validate the computational data. It also provides insight into the nature of flow and heat transfer in internal cooling passages as a function of design.

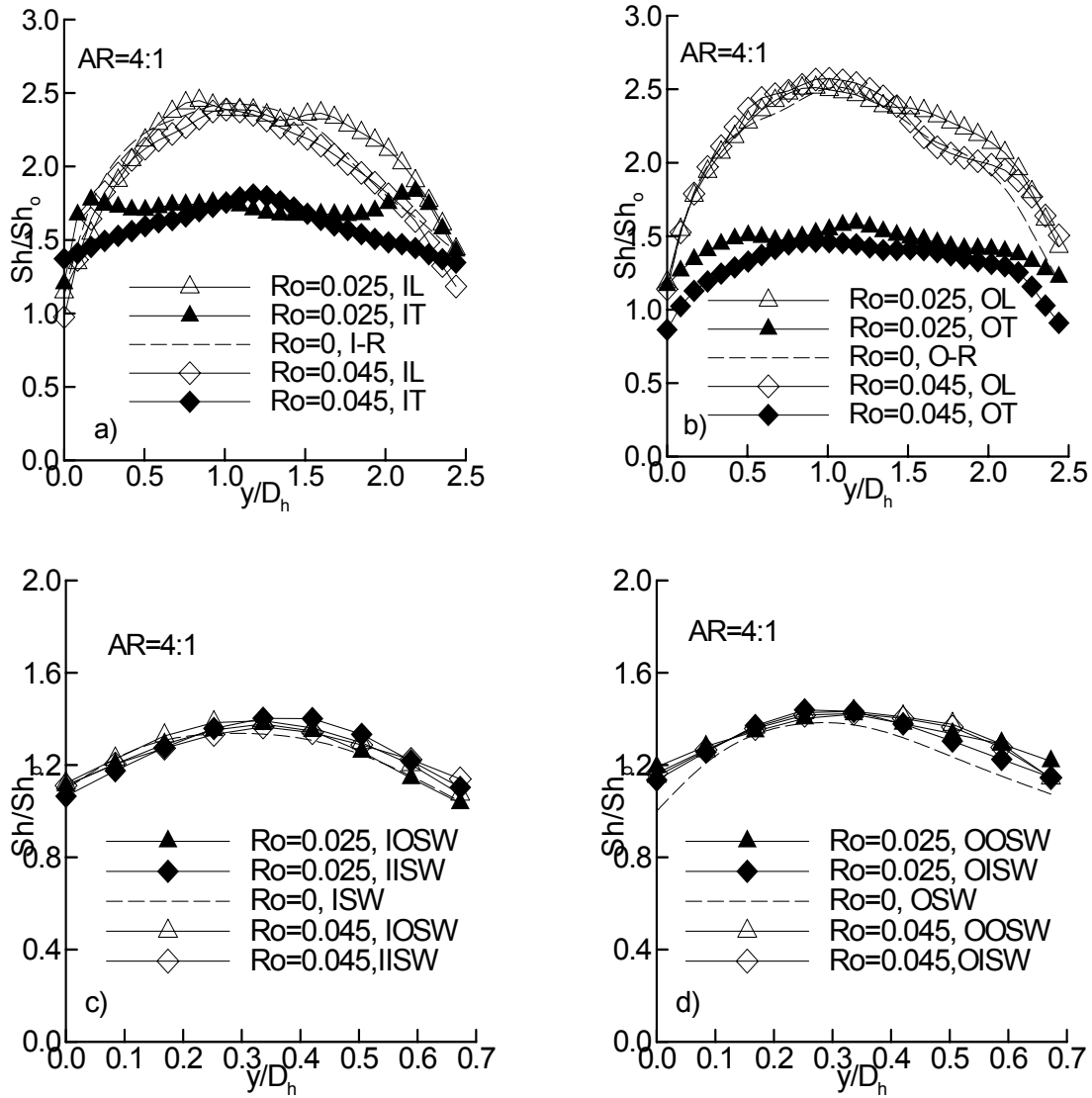


Figure 4.3.5: Cross-stream variation at various Rotation numbers on sidewalls at  $Re=30,000$  with ribs on leading Side.

## CHAPTER 5

### COMPARISON BETWEEN 90° AND 45° ORIENTATION FOR SMOOTH AND RIBBED CHANNEL FOR ASPECT RATIO 4:1

#### 5.1 INTRODUCTION

A comparison study of two different orientations of the test section 90-degree and 45-degree channel for smooth and ribbed case for aspect ratio 4:1  $\left[\left(\frac{W}{H}\right)=4:1\right]$  is presented in this chapter. The ribs have the configuration of  $\frac{e}{D_h}=0.15625$  and  $\frac{P}{e}=11.2$ . The rib angle of attack is 90-degree. The value of  $\frac{e}{H}=0.25$  and  $\frac{e}{W}=0.0625$ .

#### 5.2 RESULTS FOR 4:1 SMOOTH CHANNEL, ORIENTATION=90° AND 45°

Figure 5.2.1 shows the spanwise-averaged Sherwood number ratio in the fully developed region of a 4:1 AR smooth duct at a Reynolds number of 5,760. Results are shown at various rotation numbers for both the 90-degree and 45-degree orientations, and along all four walls (leading-L, trailing-T, inner side wall-ISW, and outer side wall-OSW) in both the inlet (radially-outward flow) channel and the outlet (radially-inward flow) channel.

In the 90-degree orientation, due to Coriolis forces, the cooler fluid moves from the leading to trailing surface in the radially outward flow passage, and thus at a  $Ro=0.12$ , the leading surface experiences a 10% degradation in Sherwood number (relative to stationary conditions) while a 27% enhancement is obtained along the trailing wall and the side walls. It is shown later that the lower degradation on the leading surface is linked to the behavior in the corner regions where no reduction in heat transfer rate is observed.

The greater enhancement on the trailing wall may also be due to greater unsteadiness (or Reynolds stresses) in the secondary flow structures near the surface that accentuates the heat transfer enhancement. Both the corner effect along the leading surface and greater unsteadiness along the trailing surface have been confirmed by unsteady numerical calculations in a 4:1 AR geometry.

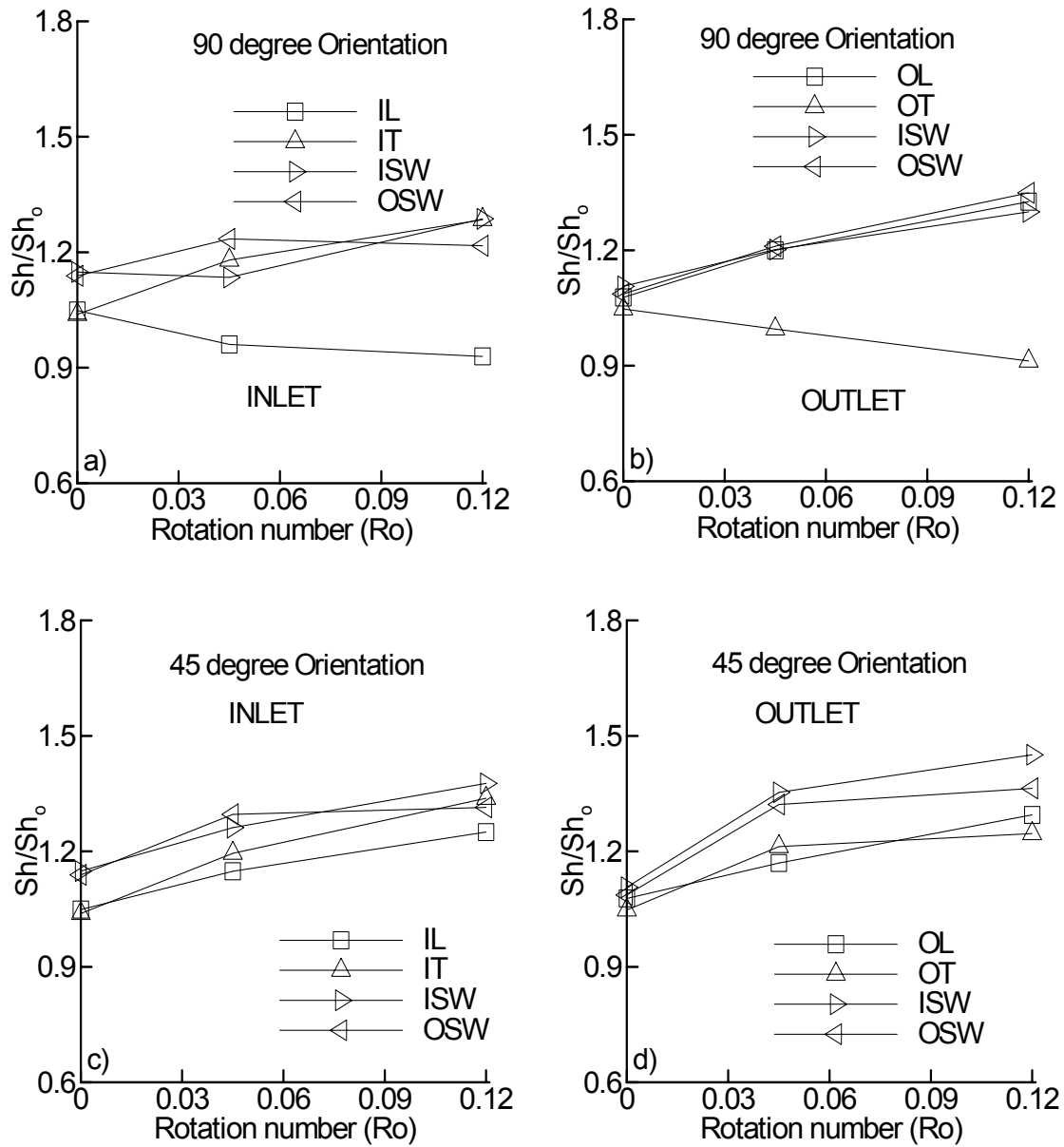


Figure 5.2.1: Comparison at  $Re=5,760$  for various Rotation numbers for two different orientations of the test-section for smooth 4:1 channel.

In the outlet duct the direction of the Coriolis force is opposite to that in the inlet duct. The leading surface is now the destabilized wall, and both the leading surface and the sidewalls show an enhancement of 31%, which is greater than the corresponding enhancement in the inlet duct. The greater enhancement in the outlet duct may be due to residual bend-induced secondary flows and/or turbulence enhancement due to the bend. The stabilized/trailing wall shows a reduction in Sherwood number ratio of 11%, which is comparable to the degradation obtained in the inlet duct.

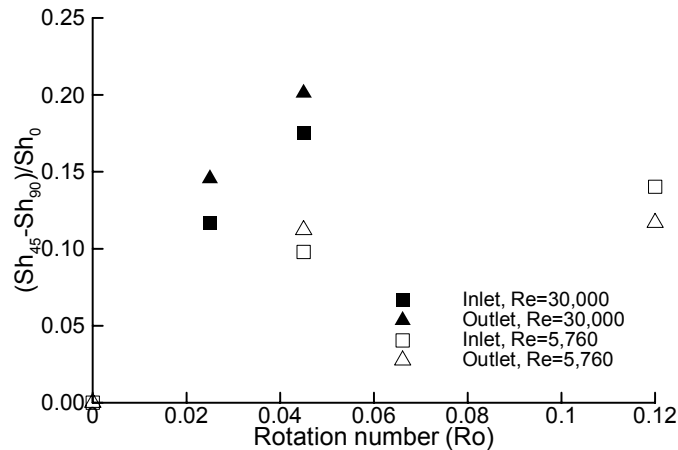


Figure 5.2.2: Overall Effect of orientation of the test-section in the fully developed region in the smooth channel.

For the 45-degree orientation of the test-section, it is observed that with rotation the mass transfer ratio increases on all walls with respect to the stationary duct value, and while there is greater enhancement along the destabilized surfaces, the fully developed heat/mass transfer ratio along the stabilized surface is also enhanced and greater than 1. This is because with the 45-degree orientation, the Coriolis driven secondary flow are no longer directed from the center of the destabilized surface to the center of the stabilized surface as in the 90-degree orientation. Rather, the flow is directed in a roughly diagonal-direction, impinges in the vicinity of the corner formed by the trailing surface and the

outer wall, and re-circulates down along the leading and trailing surfaces. Thus both surfaces see enhanced heat transfer. This explains the higher heat/mass transfer coefficient along the stabilized surface when the test-section is at an orientation of 45-degree relative to the 90-degree orientation. In the inlet duct, at a  $Ro=0.12$ , the mass transfer ratio increases along the trailing surface by nearly 25%, and along the leading wall an enhancement of 15% is noted. Thus the primary difference relative to the 90-degree orientation is the enhancement along the leading surface with rotation. In the outlet duct, the direction of the Coriolis force is reversed with respect to the inlet duct. The leading and trailing wall Sherwood number ratios are nearly the same, and exhibit enhancement levels of nearly 20% at a  $Ro=0.12$ . The enhancement level on the leading surface are lower than those noted earlier for the 90-degree orientation while the trailing surface exhibits enhancement instead of the degradation observed for the 90-degree orientation. The sidewalls show enhancement levels in the range of 25-30%.

The orientation effect is summarized in Figure 5.2.2, which shows the overall channel averaged Sherwood number ratio difference between the 45-degree and 90-degree orientation plotted as a function of rotation number. The average mass transfer coefficient increases when the test-section is oriented at an angle of 45-degree. The increase in the inlet and the outlet ducts are approximately the same and is nearly 20% at  $Ro=0.045$  for a  $Re=30,000$ . At a lower  $Re$ , the orientation effect is lower with a 10-15% enhancement at  $Ro=0.12$ ).

Figure 5.2.3 and Figure 5.2.4 show the span-wise distributions in the fully developed regions of the 4:1 smooth duct at  $Re=30,000$  and at various rotation numbers, for both the 90-degree and 45-degree orientations, respectively. Figure 5.2.3 shows that the expected trends of enhancement and degradation on the destabilized and stabilized

surfaces occur primarily along the central regions of the surfaces, and that along the corners, the trend actually reverses. Thus, in the corner regions, higher heat transfer is observed on the stabilized surfaces and lower heat transfer is observed on the destabilized surface, with the enhancement along the stabilized surface greater than the reduction along the destabilized surface. This observation regarding the reversal in the trend is somewhat surprising, but is consistent in all the results obtained with rotation. In recent numerical simulations performed by Saha and Acharya in a 4:1 AR duct, it was observed that the enhancements in the corner region are linked to a multi-cellular secondary flow pattern, where corner vortices formed near the leading wall corners resulting in high heat transfer rates in the corner regions.

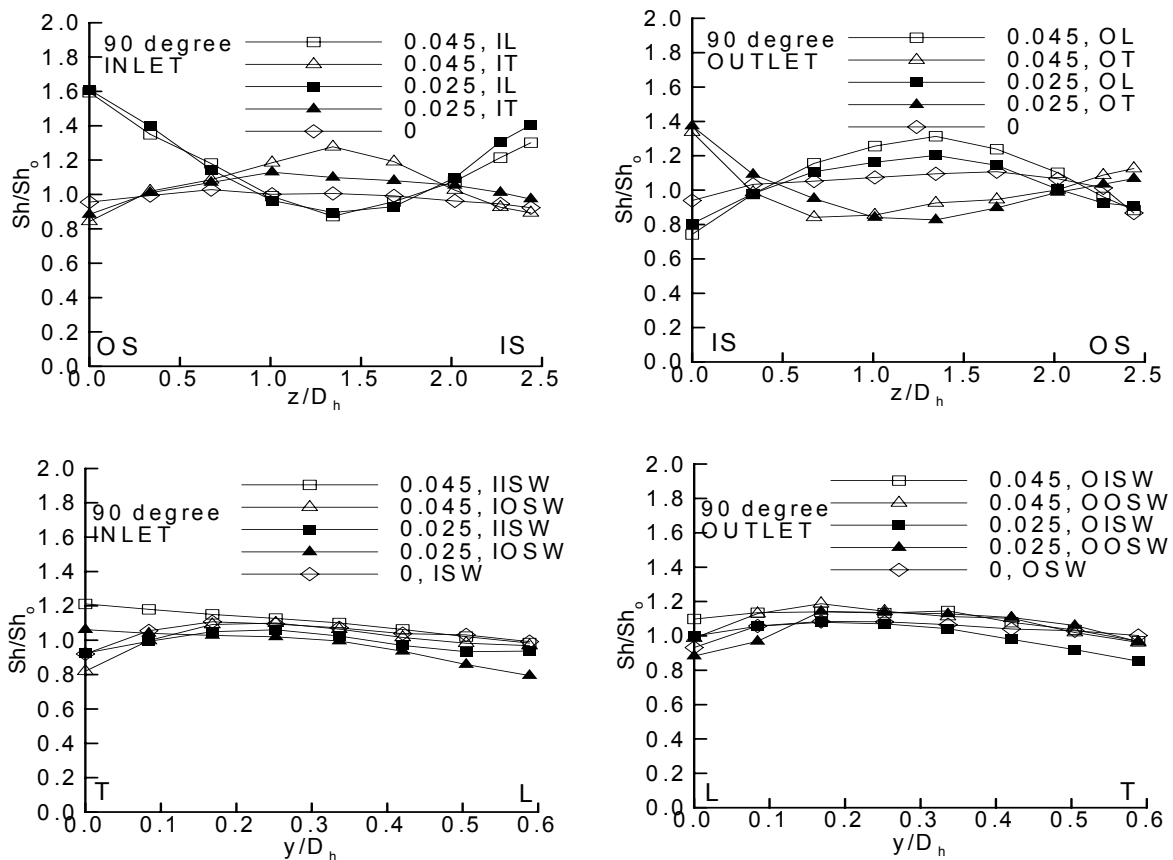


Figure 5.2.3: Span-wise normalized Sherwood number distribution in the fully developed region for AR=4:1 channel at different Ro numbers and Re=30,000 for smooth and 90-degree orientation of the test-section.

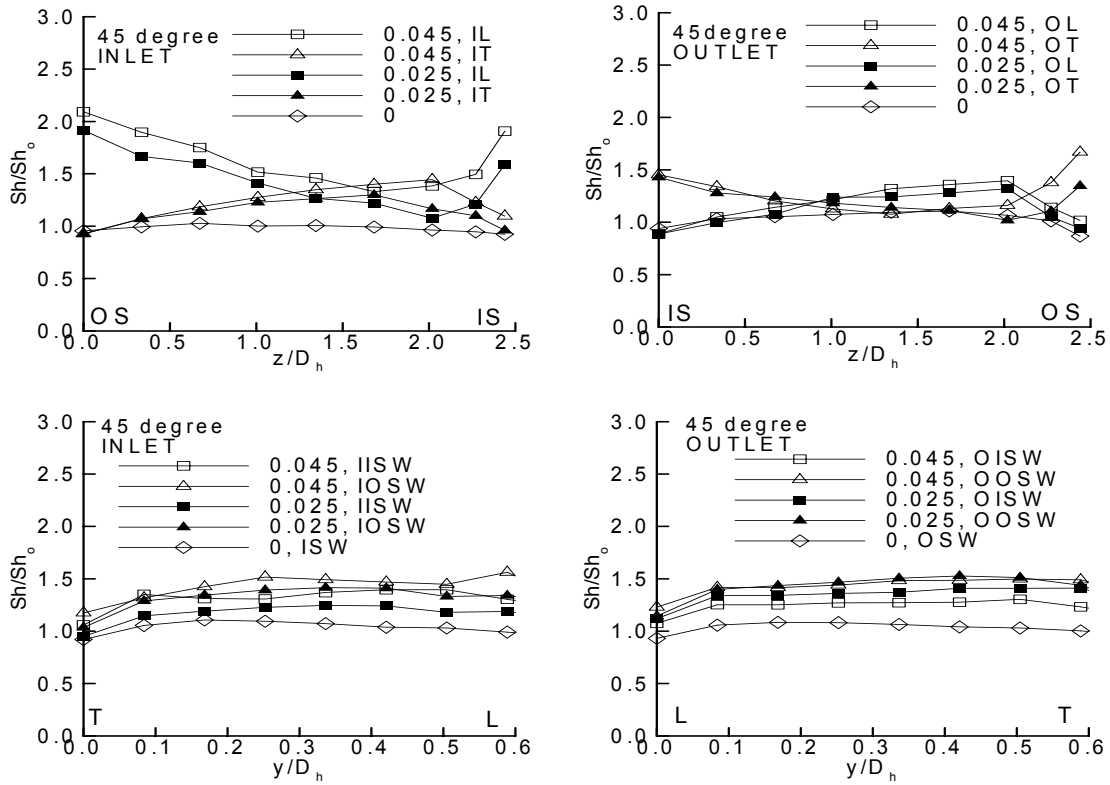


Figure 5.2.4: Span-wise normalized Sherwood number distribution in the fully developed region for AR=4:1 channel at different Ro numbers and  $Re=30,000$  for smooth and 45-degree orientation of the test-section.

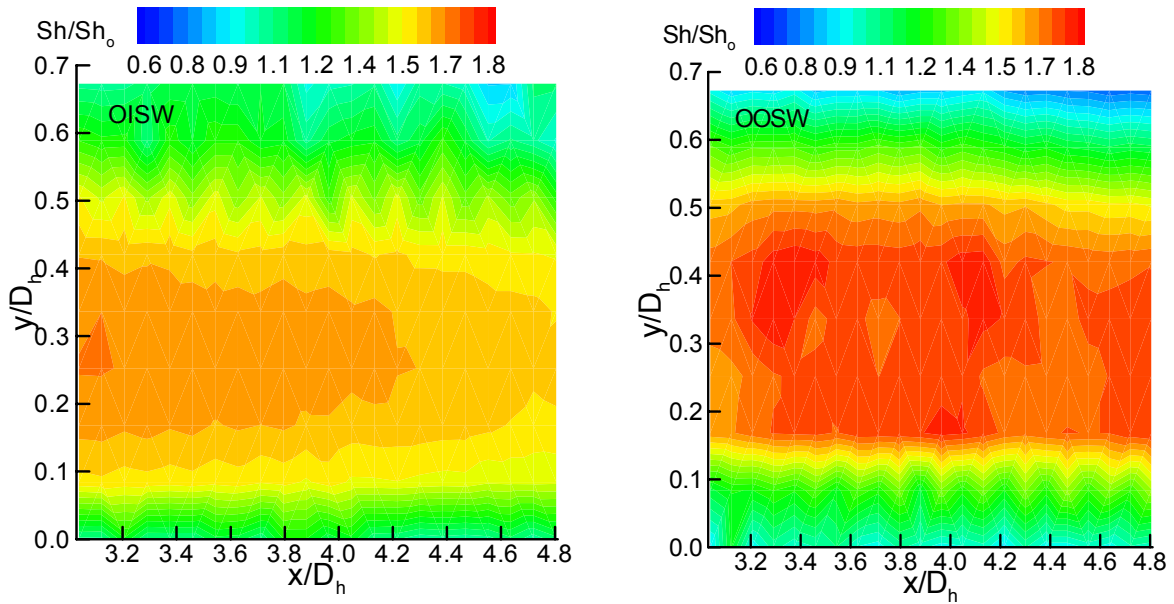


Figure 5.2.5: Bend Effect in smooth channel, AR=4:1, 90-degree orientation,  $Re=5,760$ ,  $Ro=0.12$ .

The average Sherwood number ratios reported earlier represents an area-average, and these averages conformed to the expected trend. However, in the averages, it was noted that the averaged enhancement on the destabilized surface was generally greater than the degradation on the stabilized surface. The lower reduction along the stabilized surface is linked to the behavior in the corner regions where enhancement is observed and balances the degradation in the mid-span regions. Thus the span-wise averaged degradation on the stabilized surface is smaller in magnitude compared to the average enhancement on the destabilized surface.

For the 45-degree orientation, the span-wise profiles show enhancement along all walls due to the diagonal orientation of the secondary flows, and the span-wise variations are asymmetric. Since the flow is directed from corner to corner, one can expect higher heat transfer along the outer trailing corner in the inlet duct and inner leading corner along the outlet duct. This observation is confirmed in the results of Figure 5.2.4.

In the outlet 90-degree orientation duct, the differences between the stabilized and destabilized surfaces seem to differ by 1.5 times as compared to the 45-degree orientation duct where the differences are of the order of 1.1 to 1.2 times. The sidewalls show a flat trend in the span-wise direction both in the inlet and the outlet channel. With the 45-degree orientation of the duct, higher increase is observed on the sidewalls also (peak values of 1.5 compared to 1.2 for the 90-degree orientation) but the profiles are relatively flat.

Figure 5.2.5 shows the effect of the bend by presenting the developing mass transfer ratio in the outlet duct immediately downstream of the bend. It is observed that as the flow passes through the bend, the mass transfer coefficient on the inner sidewall decreases whereas near the outer sidewall it increases. The bend induces a secondary

flow directed from the inner sidewall to the outer sidewall; this secondary flow is responsible for the higher mass transfer along the outer sidewall.

### **5.3 RESULTS FOR 4:1 RIBBED CHANNEL, ORIENTATION=90° AND 45°**

For both the 90-degree and 45-degree orientation of the test-section for AR 4:1, periodic behavior is observed approximately at the same stream-wise distance in the fully developed region as in 1:1 duct. For both orientations, two peaks are observed, one upstream of the rib corresponding to a corner vortex, and one downstream of the rib corresponding to flow reattachment. The rib is inactive in the present study, and therefore corresponds to the lowest heat transfer. Depending on the channel orientation, the rib-induced separated flow may combine differently with the rotation-induced secondary flows. At 90-degree orientation of the channel, the rotation-induced secondary flow pattern is nearly orthogonal to the separated shear layer. In the 45-degree orientation, the secondary flow pattern due to rotation is directed nearly in a diagonal direction, and therefore the flow is at an angle to the separated shear layer. Thus, the resulting flow pattern is different in the 45-degree orientation leading to differences in magnitude of the rotation-induced changes on the mass transfer coefficient. For the 45-degree orientation, higher enhancement levels are generally noted.

Figure 5.3.1 represents the distributions of Sherwood number ratio at various rotation numbers and for both the 90-degree and 45-degree orientations in a 4:1 ribbed duct. As for the smooth case, the 45-degree orientation shows rotation-induced enhancements along all four walls. When the smooth and the ribbed cases are compared, the rotation-induced percentage changes in the ribbed duct heat transfer are lower by a factor of 2 or greater than in the smooth duct. For instance, in both the 90-degree and 45-degree orientations, the inlet-trailing increases by about 11%, while the outlet-leading

increases by about 15% at a  $Ro=0.12$ . Note that along the smooth sidewalls, the heat transfer ratios are much lower, and show only a small increase (about 10%) with  $Ro$  in both orientations. This implies that for the high blockage ratios considered here ( $\frac{e}{H} = 0.25$ ), rotation effects are lower than those in a smooth channel.

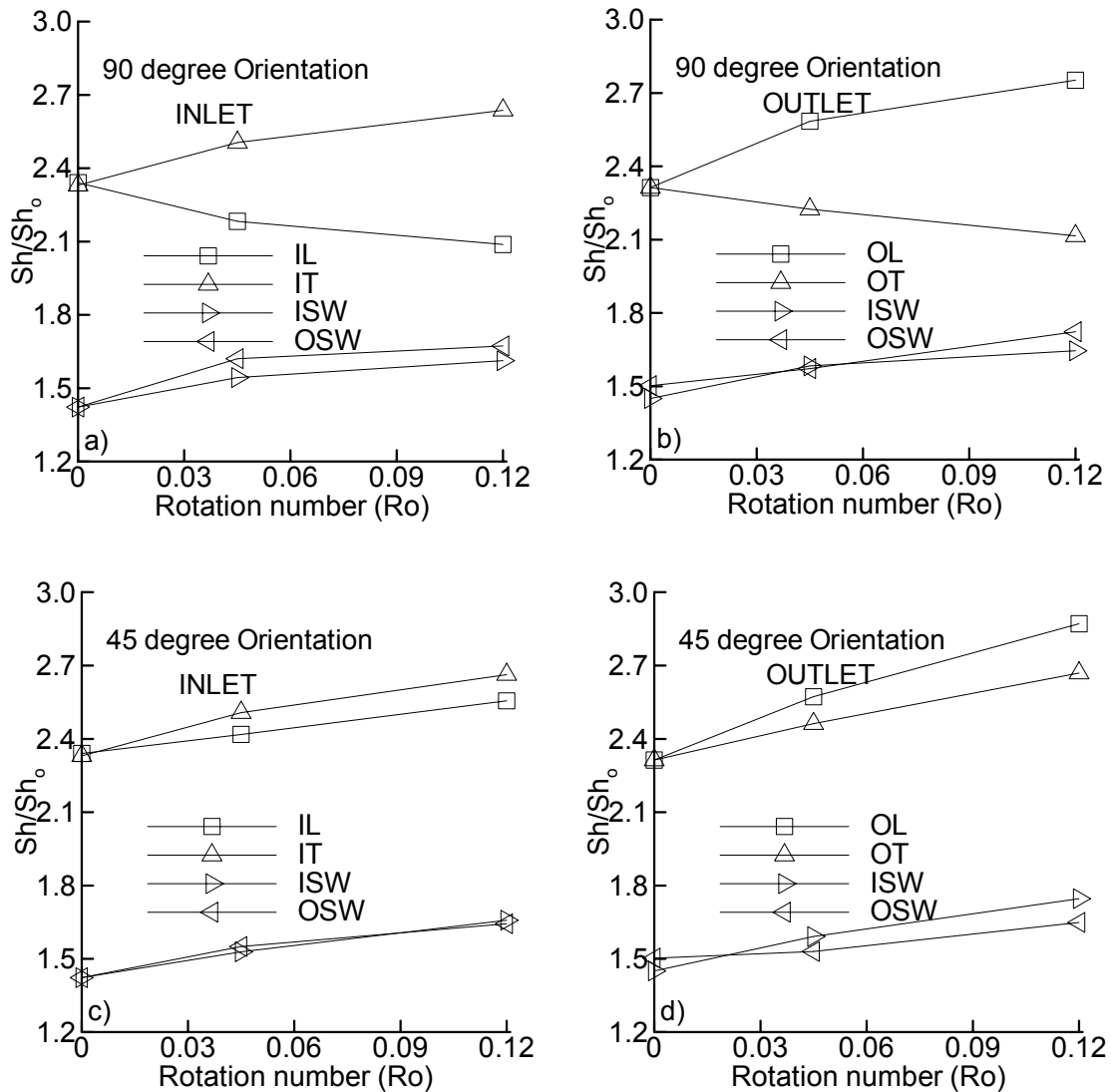


Figure 5.3.1: Comparison at  $Re=5,760$  for various Rotation numbers for two different orientations for ribbed 4:1 channel.

Figure 5.3.2 shows the overall effect of the orientation of the test-section in the ribbed channel. It shows that the mass transfer coefficient increases when the test-section

is oriented at an angle of 45-degree. It is observed that at a Reynolds number 5,760 and  $Ro=0.12$ , the radially-inward flow (outlet duct) is more sensitive to the orientation since it observes higher mass transfer coefficient than the radially-outward flow (inlet duct). Note that at the higher  $Re$ , the orientation effects are much lower for the ribbed duct compared to the smooth duct.

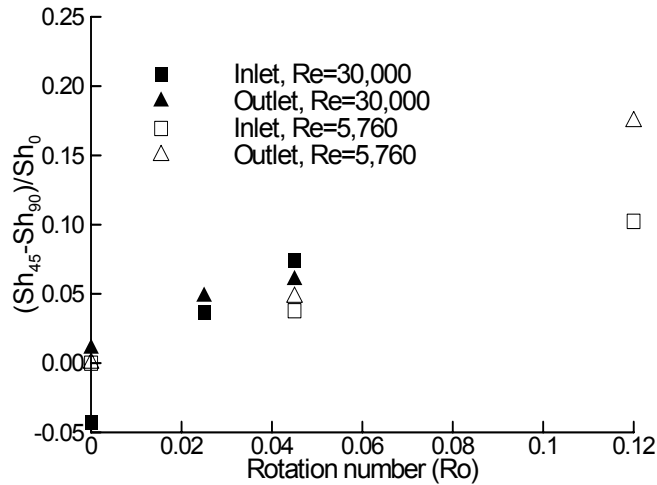


Figure 5.3.2: Overall Effect of orientation of the test-section in the fully developed region in the ribbed channel.

Figure 5.3.3 and Figure 5.3.4 shows the span-wise distributions in the fully developed region for 4:1 AR ribbed duct at  $Re=30,000$  and at various rotation numbers for both 90-degree and 45-degree orientation, respectively. These distributions are a result of averaging in the stream-wise direction between successive ribs in the fully developed region. The profiles along the leading and trailing surfaces indicate a relatively uniform mass transfer distribution in the mid-span regions of the ribbed walls followed by a sharp drop-off toward the corners. In general, the mid-span regions show the expected behavior- enhancement on the stabilized and degradation on the destabilized surface. In the corner regions crossover effects are also seen, but these occur in the low

Sherwood number corner regions. Note that this behavior is distinctly different than in the smooth channel (Figure 5.2.3 and Figure 5.2.4) where an increase in the Sherwood number was observed toward the corners.

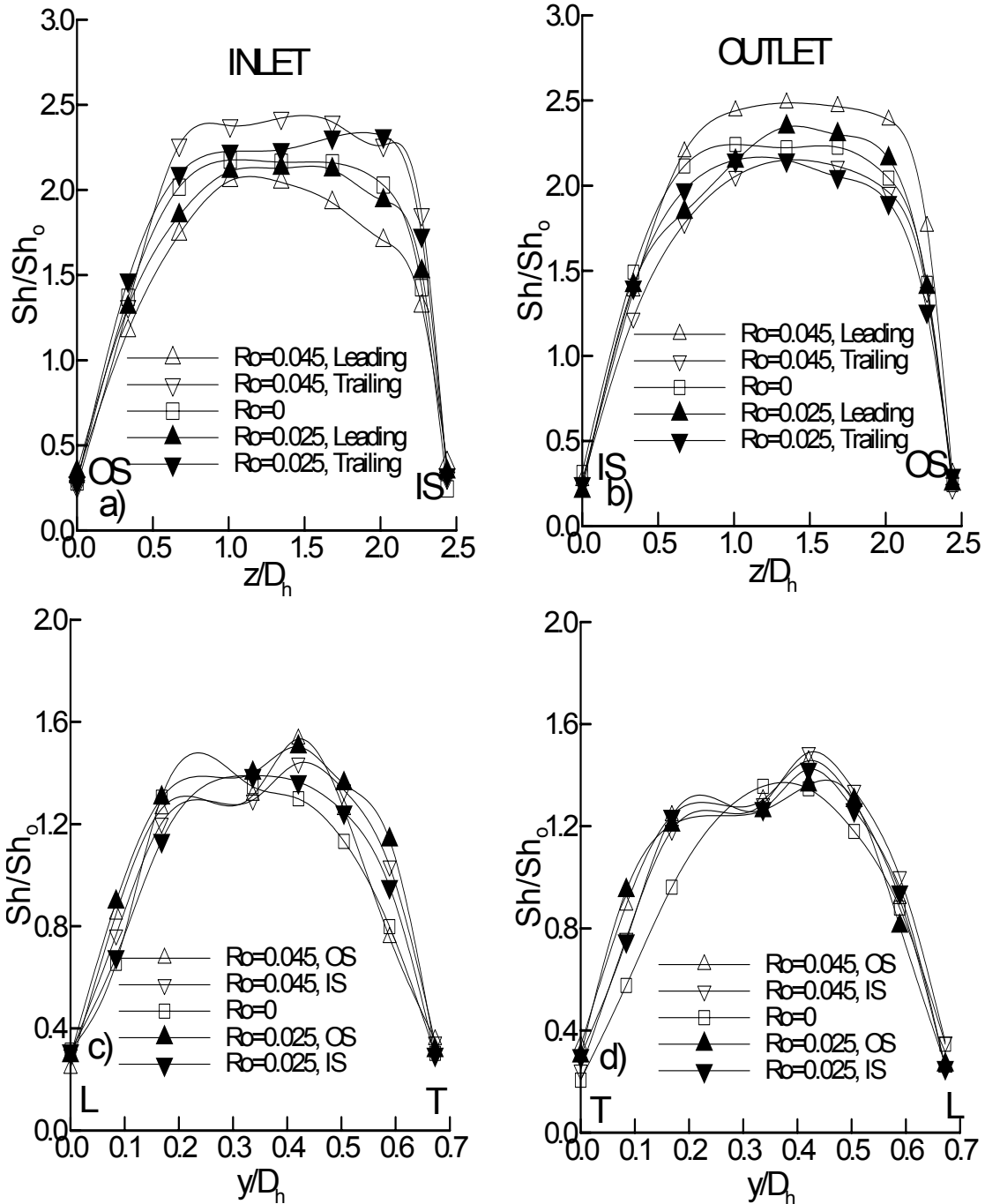


Figure 5.3.3: Span-wise normalized Sherwood number distribution in the fully developed region for AR=4:1 channel at different  $Ro$  numbers and  $Re=30,000$  for ribbed and 90-degree orientation of the test-section.

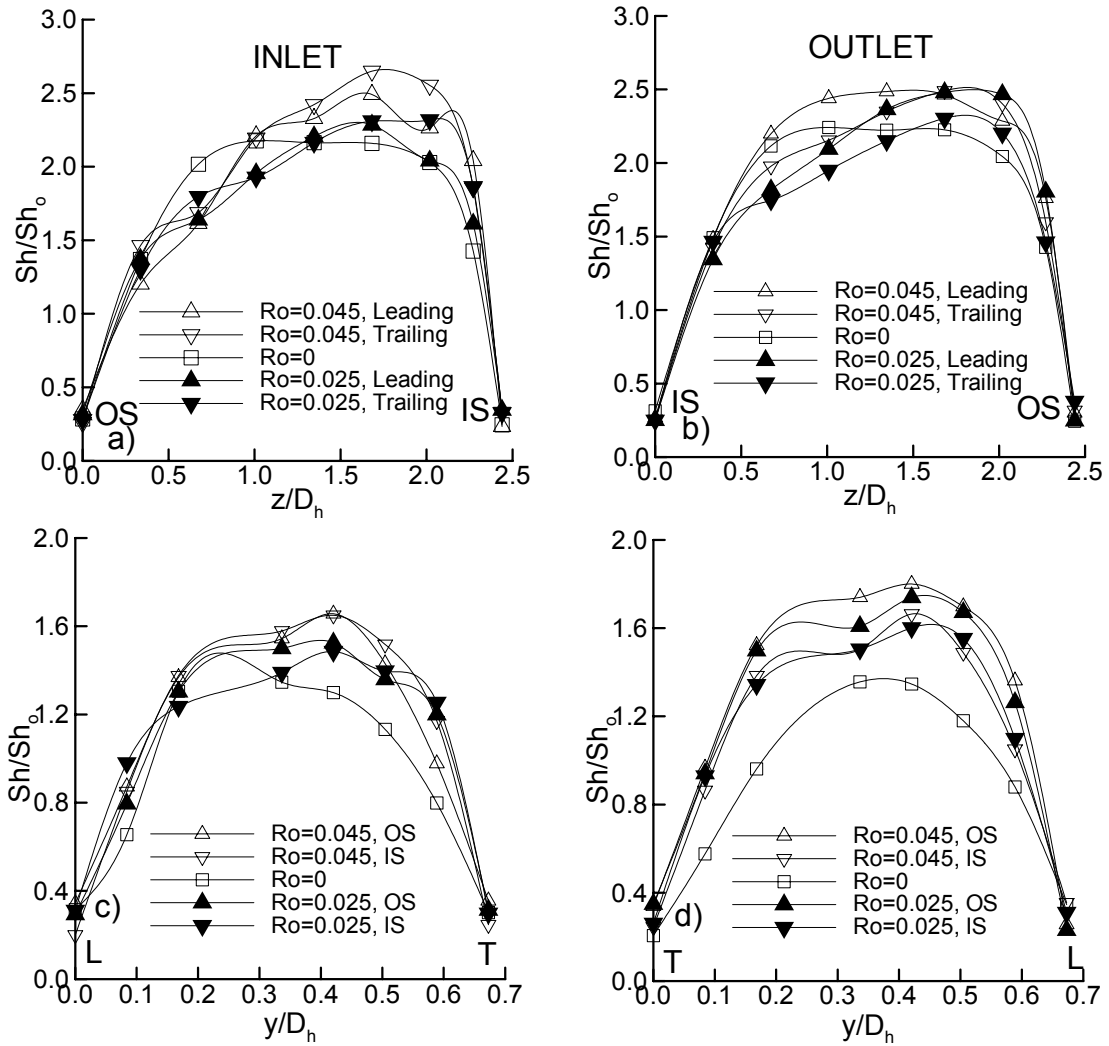


Figure 5.3.4: Span-wise normalized Sherwood number distribution in the fully developed region for AR=4:1 channel at different Ro numbers and  $Re=30,000$  for ribbed and 45-degree orientation of the test-section.

In the 45-degree orientation duct, the Sherwood number ratio distribution on the stabilized and the destabilized surfaces are skewed towards the inner sidewall in the radially outward inlet flow channel and towards the outer sidewalls in the radially inward outlet channel. This is due to the direction of the secondary flows relative to the leading and trailing walls. For the 90-degree orientation the secondary flow impinges normally in the vicinity of the mid-span, while in the 45-degree orientation the secondary flow impinges at an angle closer to the corner of the destabilized surface. Local differences of

the order of 30% or greater can be seen between the  $Ro=0$  and  $Ro=0.045$  profiles. However, with span-wise averaging, the high and lows in the profiles average out, and the fully developed averaged values do not show a strong rotation number dependence as seen earlier in Figure 9.

Figure 5.3.5 shows the Sherwood number ratio contours on the leading surface in the developing region after the bend and in the fully developed region of the outlet channel. It is observed that in the developing region two patches of high Sherwood numbers are obtained reflecting a pair of counter-rotating vortex pair. This flow structure is a reflection of the bend-induced secondary flows. Further downstream, as the bend-induced secondary flows diminish, the contours show a single region of high Sherwood number, where the Coriolis-induced secondary flows impinge on the leading surface.

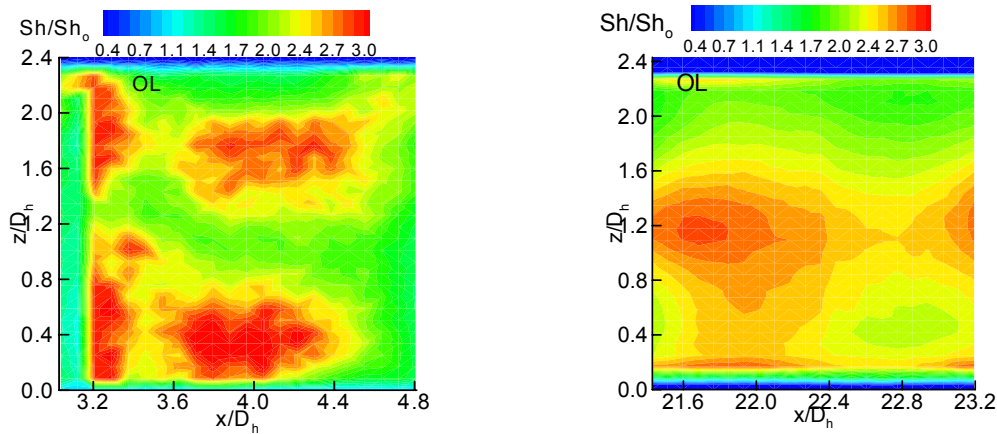


Figure 5.3.5: Contour plots in the developing and the fully developed region for 45-degree orientation of the test-section:  $Re=5,760$ ,  $Ro=0.12$

## 5.4 CONCLUSION

Mass transfer experiments were performed in a rotating two-pass coolant channel with a 4:1 AR. Both smooth and ribbed channels were considered in 90-degree and 45-degree channel orientation relative to the rotational axis. Results presented include spanwise-averaged fully developed values, span-wise distributions, and Sherwood

number contours past the bend. The following are the major observations of the present study:

1. For the 90-degree orientation, the destabilized surfaces show enhancement in the range of 25-31% and the stabilized surfaces show a degradation of about 10% at a  $Ro=0.12$ . For the 45-degree orientation, both leading and trailing surfaces experience enhancement in Sherwood number with rotation. The enhancement along the destabilized surface is of the order of 20-25% at a  $Ro=0.12$ , which is lower than that for the 90-degree orientation. Along the stabilized surface a 15-20% enhancement is noted, in contrast to the degradation observed for the 90-degree orientation.
2. For the smooth channel, with rotation, the stabilized surfaces exhibit high Sherwood numbers along the corner regions in contrast to the degradation in the mid-span regions. Thus the averaged Sherwood numbers do not exhibit significant degradation with rotation.
3. For 45-degree orientation of the ribbed duct, the span-wise distributions are skewed towards the corners whereas in 90-degree orientation, they are more symmetric.
4. Orientation effects are more significant for the smooth channel.
5. For the ribbed channel, oriented at 45-degrees to the rotational axis, bend induces a pair of counter-rotating vortex pair.

## CHAPTER 6

### COMPARISON BETWEEN 90° AND 45° ORIENTATION FOR SMOOTH AND RIBBED CHANNEL FOR ASPECT RATIO 1:4

#### 6.1 INTRODUCTION

The experiments are conducted for the two different orientations of the test section 90-degree and 45-degree channel for smooth and ribbed case for aspect ratio 1:4.

The ribs have the configuration of  $\frac{e}{D_h} = 0.3125$  and  $\frac{P}{e} = 8$ . The rib angle of attack is

90-degree. The value of  $\frac{e}{H} = 0.125$  and  $\frac{e}{W} = 0.5$ .

#### 6.2 RESULTS FOR 1:4 SMOOTH CHANNEL, ORIENTATION=90° AND 45°

A set of experiments has been conducted at three different Rotation numbers at  $Re=5,760$  for the 1:4 channel cross-section at 90-degree and 45-degree orientations. In 90-degree orientation, Figure 6.2.1 (a&b), the Sherwood number ratio on the leading wall is reduced by 30% relative to the stationary case by increasing the rotation number from 0 to 0.12, while on the trailing wall the Sherwood number ratio is increased by 20%. The mass transfer ratio along the inner sidewall also exhibits an increase with rotation, with an increase of about 8% for  $Ro=0.12$  relative to the stationary case ( $Ro=0$ ) while the change on the outer sidewall does not change appreciably. In the outlet channel the reverse behavior is expected on the leading and trailing walls relative to the inlet channel. It is observed that the rotation-induced mass transfer enhancement (26% relative to the stationary case) on the leading (destabilized) wall is more pronounced than the degradation (16%) observed on the trailing (stabilized) wall, which does not appear to change from  $Ro=0$  to 0.12. The sidewall mass transfer ratio remains insensitive to the increase.

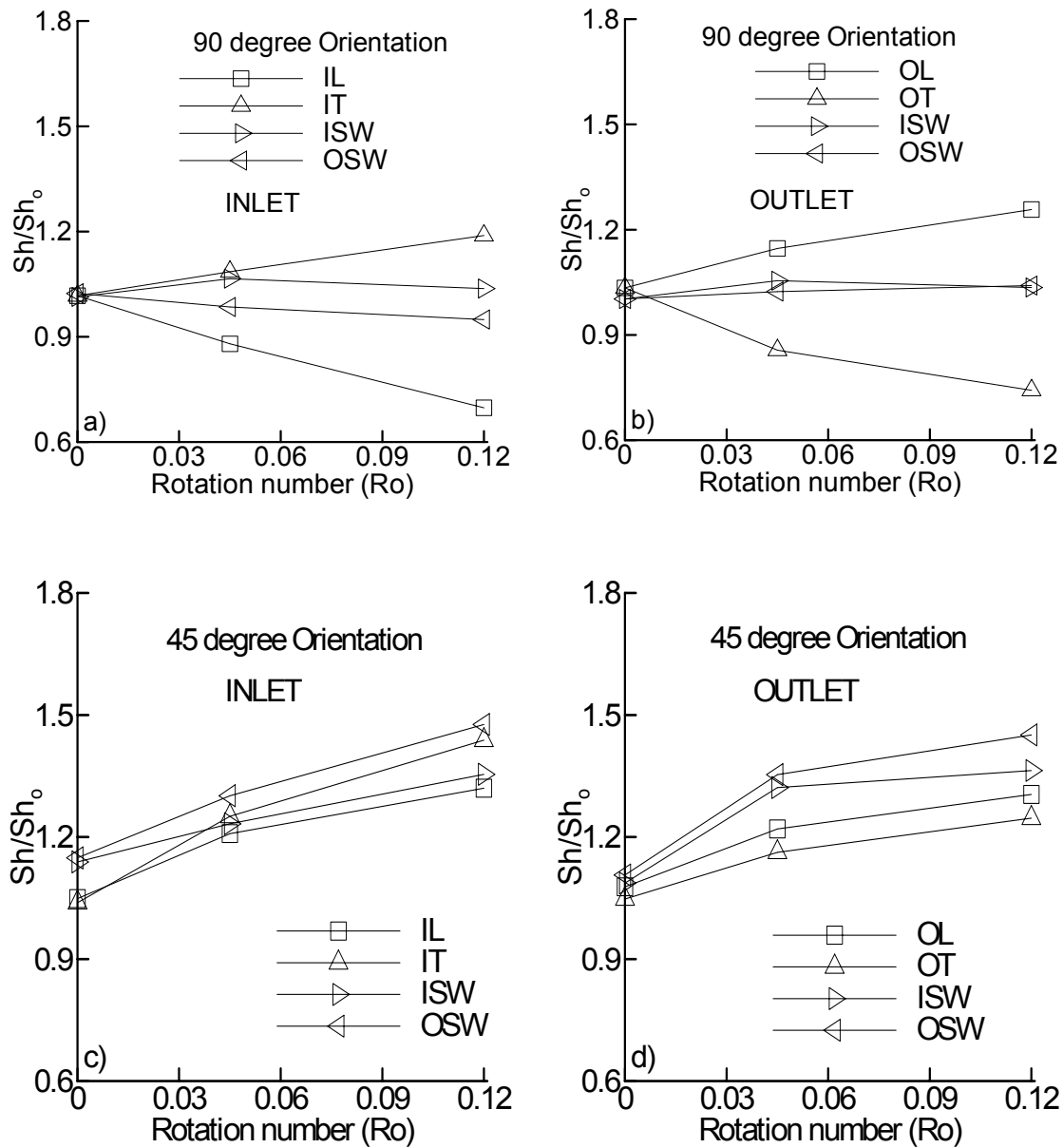


Figure 6.2.1: AR=1:4, Smooth Channel, Re=5,760, Fully developed Sherwood number ratio vs. Rotation number

For the 45-degree orientation, the mass transfer ratio increases on all the walls in the inclined orientation channel. Figure 6.2.1 (c) shows the same above effect for the 45-degree orientation in the inlet channel. The Leading edge increases by 12% while the trailing edge increases by 35% with respect to the stationary case. The inner sidewall

increases in an experimental uncertainty while the outer sidewall shows 28% increase. In the outlet channel, Figure 6.2.1 (d) shows an increase of 50% on the leading edge while the trailing and the inner sidewall does not show an appreciable increase. The outer sidewall shows an increase of 28%.

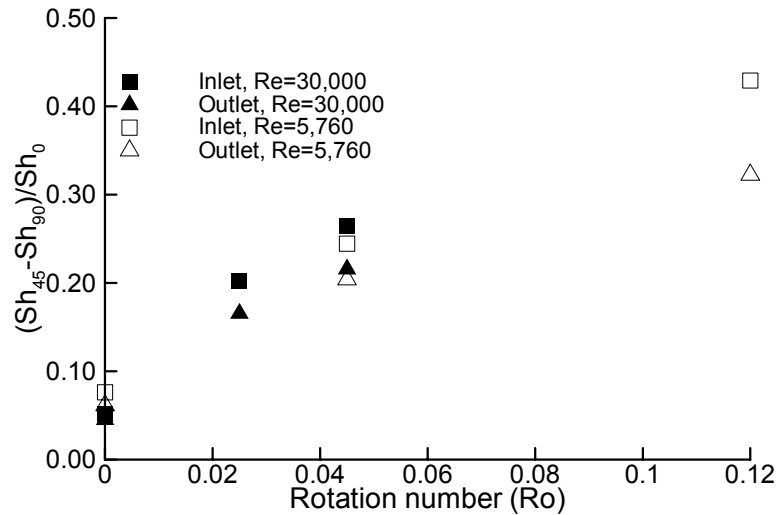


Figure 6.2.2: Overall effect of the orientation in 1:4 smooth ducts.

Figure 6.2.3 and Figure 6.2.4 shows the span-wise distributions for different rotation numbers in the fully developed region at Re=30,000 for AR=1:4 for 90-degree and 45-degree orientation smooth channel respectively. These distributions are a result of averaging in the stream wise direction in the fully developed region. Some level of asymmetry can be observed in the profiles and is indicative of the asymmetry in the flow induced by the bend and the asymmetry of the incoming flow. In smooth channels, these asymmetries do not wash out quickly, and persist well downstream. The cross-stream profiles follow the expected patterns of reduction and enhancement of mass transfer along leading and trailing walls.

For the destabilized surface in Figure 6.2.3, the peak heat transfer occurs close to the centerline where the Coriolis-induced secondary flows impinge, and decay outwards along the lateral direction. Along the stabilized surface in Figure 6.2.3, the minimum heat transfer occurs in the middle where the secondary flow lifts off the surface, and the peak heat transfer occurs close to the corners where the secondary flow moving down the sidewall impinges. Thus close to the corners, there is a cross-over of the profiles along the stabilized and destabilized surfaces, with heat transfer along the stabilized surface actually being greater than the heat transfer along the destabilized surface. Note that close to the centerline, the differences in the Sherwood number ratio between the stabilized and destabilized surface can be a factor of 1.5 different at  $Ro=0.045$  for 90-degree orientation. This is in contrast to the average Sherwood number ratio where the differences are much smaller and in the range of 10% to 20%. Along the sidewalls, enhancement is consistently noted with rotation, with the span-wise variation being relatively flat except close to the corners.

The asymmetry is more enhanced in the 45-degree channel (Figure 6.2.4) and apart from the reasons cited above, it could also be due to the flow entering the channel is at an angle to the channel and no efforts were being made to condition the flow normally. It is observed that the peak heat transfer does not occur at the centerline as observed for 90-degree channel on the stabilized and de-stabilized surface.

The mass transfer ratio profiles on all the surfaces in the radially inward and outward flow passages are clearly above the stationary channel although in the outlet channel, the differences are low. The peak mass transfer is inclined more towards the inner sidewall in the inlet channel and towards the outer sidewall in the outlet passage. The crossover of the profiles can be explained as before in Figure 6.2.3. It can be

concluded from Figure 6.2.4 that the inlet or the radially outward flow passage experiences more orientation effect than the outlet or the radially inward flow passage and is consistent with the finding of Wagner and Griffith.

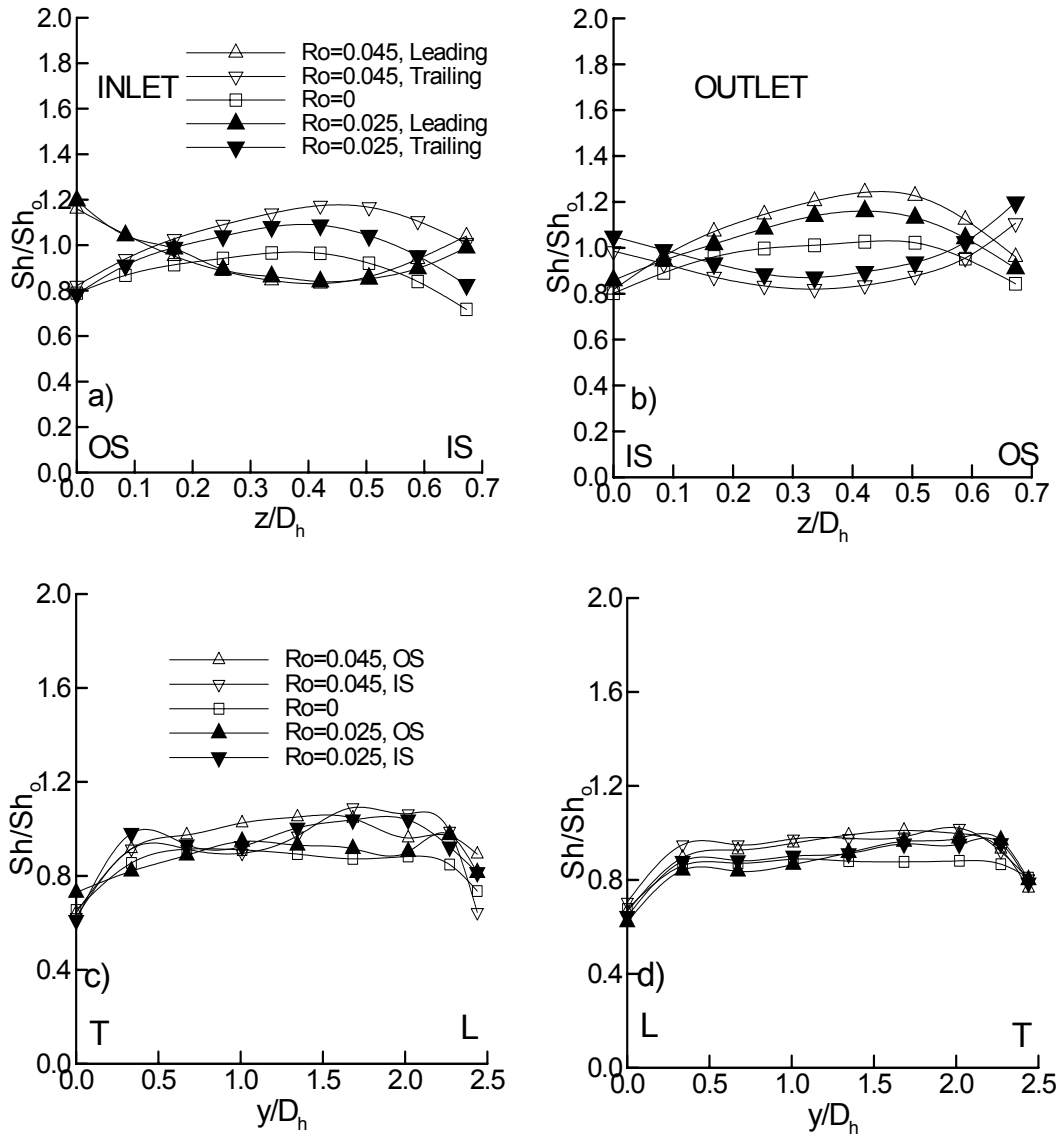


Figure 6.2.3: Span-wise distributions at different rotation numbers in the fully developed region at  $Re=30,000$  for  $AR=1:4$ , 90-degree Smooth channel (a) & (b) leading and trailing and (c)&(d) sidewalls.

For the 45-degree orientation, the span-wise profiles show enhancement along all walls due to the diagonal orientation of the secondary flows, and the span-wise variations

are asymmetric. Since the flow is directed from corner to corner, one can expect higher heat transfer along the outer trailing corner in the inlet duct and inner leading corner along the outlet duct.

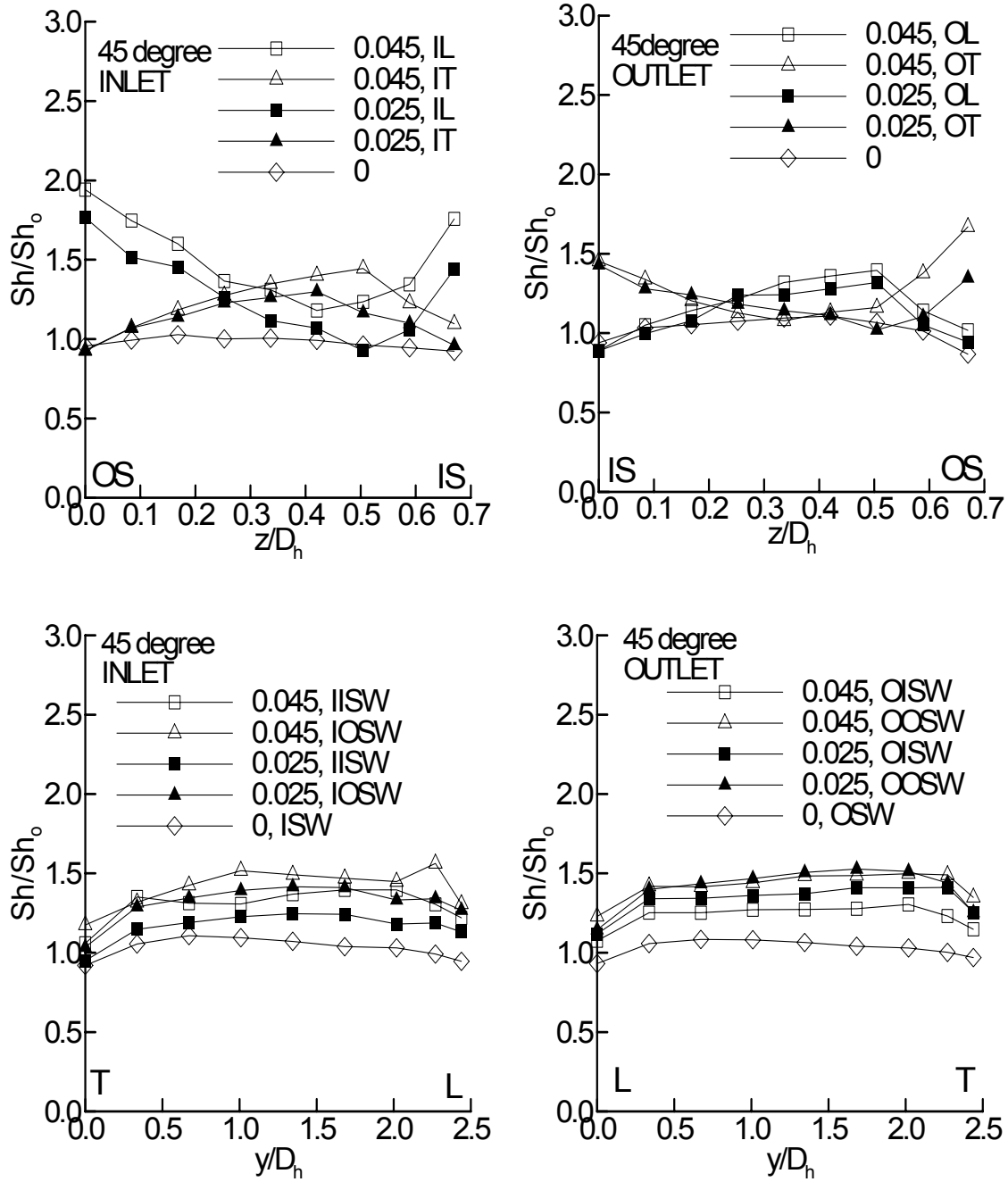


Figure 6.2.4: Span-wise distributions at different rotation numbers in the fully developed region at  $Re=30,000$  for  $AR=1:4$ , 45-degree in Smooth channel (a) & (b) leading and trailing and (c)&(d) sidewalls.

### 6.3 RESULTS FOR 1:4 RIBBED CHANNEL, ORIENTATION=90° AND 45°

Figure 6.3.1 (a&b) shows the effect of the rotation number at  $Re=5760$  for the ribbed channel for 90-degree orientation channel. In the inlet (radially outward flow) passage, the trailing wall shows an increase of 12.5% and leading wall decreases by 8.34% when the rotation number is increased to 0.12. Correspondingly, in the outlet (radially inward flow) passage, the mass transfer ratio on the leading edge increases by 14% and decreases by 9% on the trailing edge. The percentage change on the sidewalls is marginal. Figure 6.3.1 (c&d) shows the same for the 45-degree orientation channel in the inlet and the outlet channel. All the walls show the mass transfer ratio increasing with the leading and trailing wall showing an increase of approximately 10%-12% when the rotation number is increased to 0.12. The sidewalls show a rather modest increase with Rotation number in both the cases.

Figure 6.3.2 shows the bend effects in the 90-degree and 45-degree channel by comparing the stream-wise normalized Sherwood number ratio distribution in the inlet channel fully developed region and in the developing region of the outlet channel. In figure 6.3.2, the first peak corresponds to flow reattachment while the second peak corresponds to the corner vortex upstream of the rib. At  $Ro=0.045$  when the channel orientation is 45-degree, the difference between the leading edge and the trailing edge is not strong (about 3%-4%) while compared to the 90-degree orientation (approx. 20%).

The leading edge is more affected (increasing trend with the increase in Rotation number) with the 45-degree channel orientation. Figure 6.3.2(b&d) shows the corresponding profiles for the developing flow in the inter-rib module following the bend in the outlet channel. The interesting point is the behavior on the outlet sidewall, which shows an increasing trend in the stream-wise direction. This may be due to the reason that

the secondary flow hits the outer sidewall along with the trailing wall, thus increasing the mass transfer ratio. On the other side, inner sidewall does not see an appreciable increase in the Sherwood number ratio than with respect to the 90-degree orientation. In Figure 6.3.2(b), the first inter-rib module following the bend, there is an increase of (15%-20%)

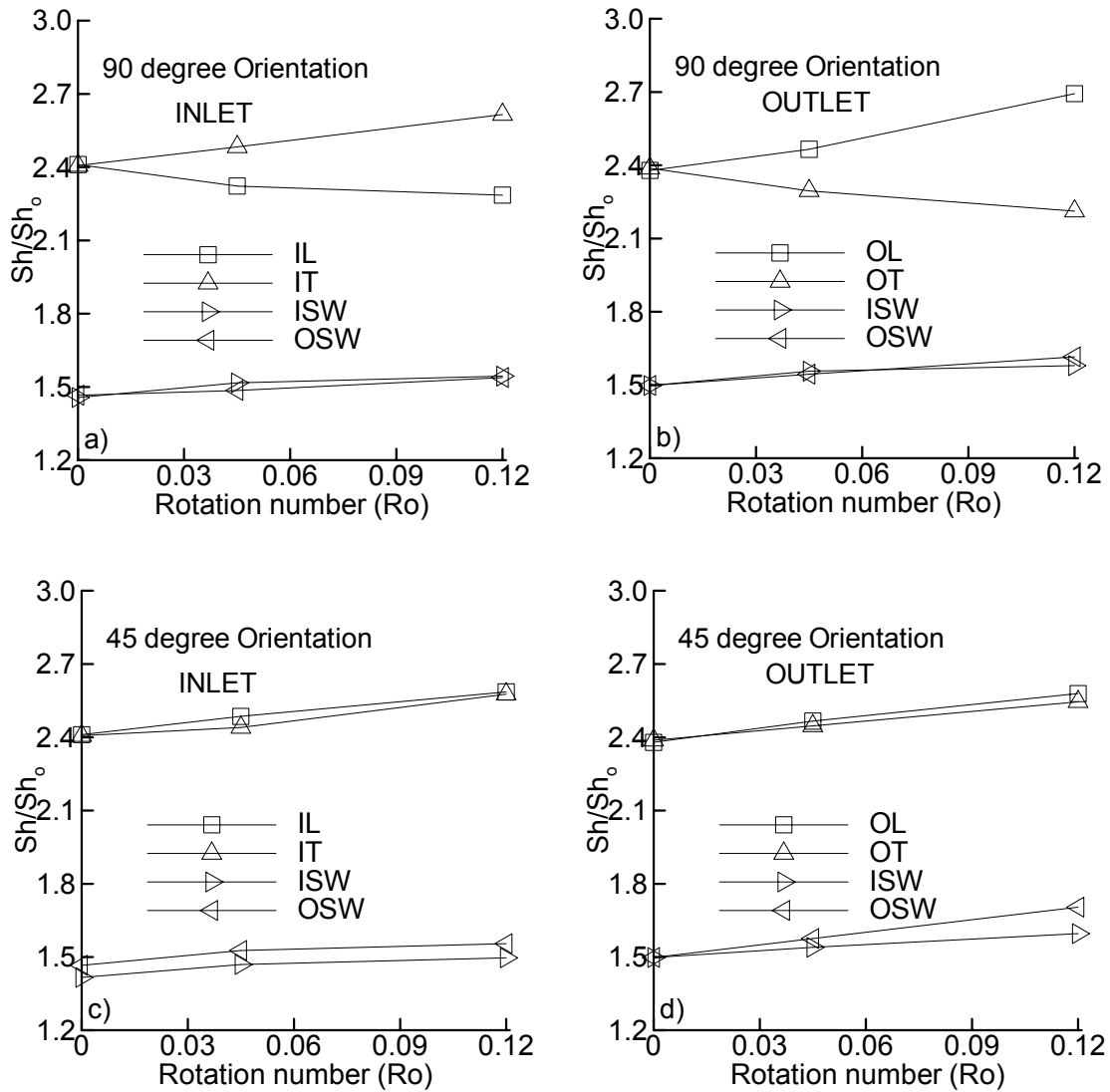


Figure 6.3.1: AR=1:4, Ribbed Channel, Re=5,760, Fully developed Sherwood number ratio vs. Rotation number.

sidewall immediately following the bend. This is to be expected, based on the fact that for the 1:1 channel the bend is effectively of a “shorter radius” compared to the 1:4

channel. This is also evidenced by the fact that for the 1:1 channel the Ito [33] curved-pipe similarity parameter ( $Re\{D_h/[2r]\}^2$ , where  $r$  is the bend radius) is larger by a factor of 3 compared to that of the 1:4 channel.

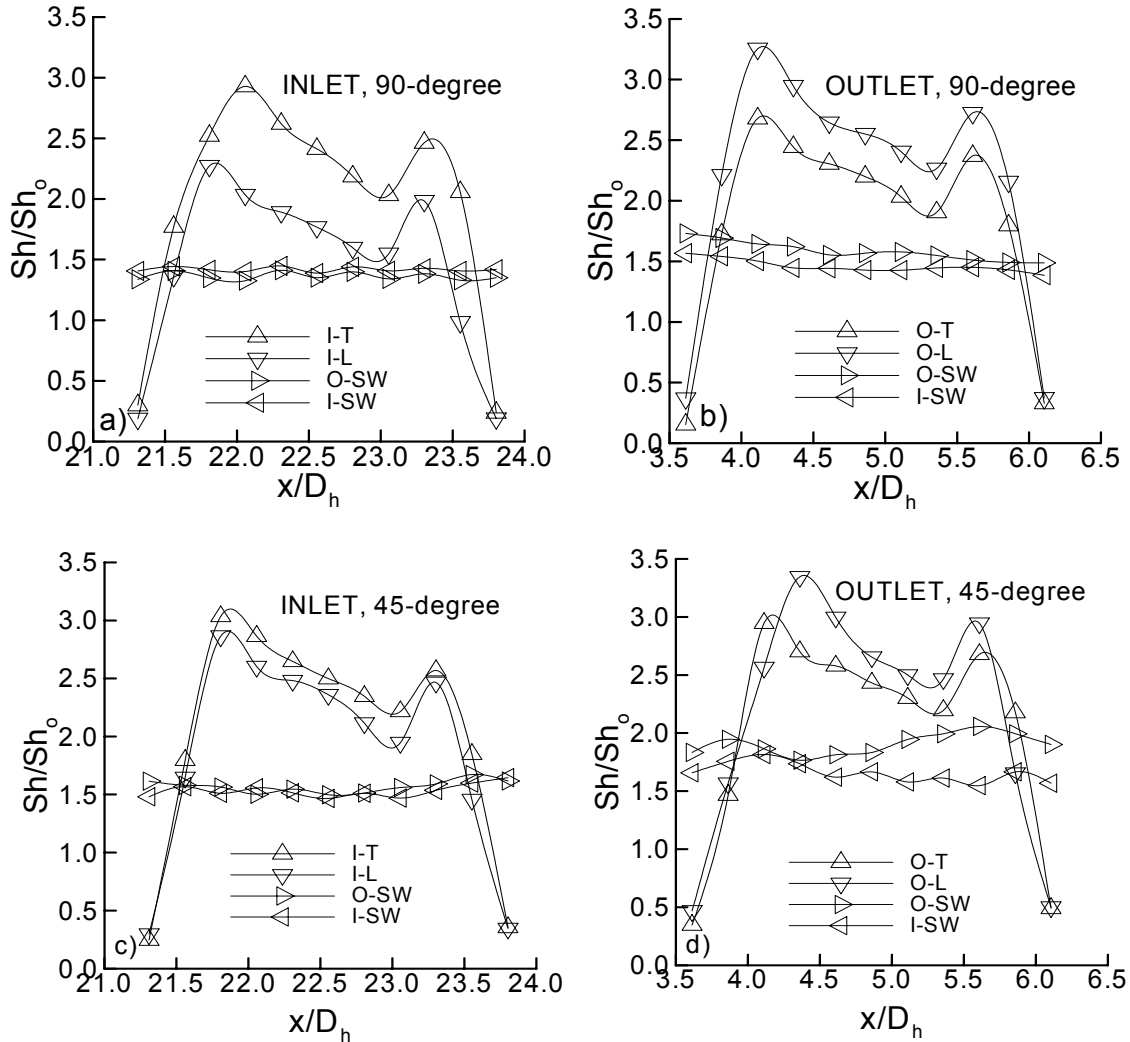


Figure 6.3.2: Centerline normalized Sherwood number distribution in the inter-rib region at  $Re=30,000$ ,  $Ro=0.045$  a) Inlet fully developed Region, orientation= $90^\circ$  b) Outlet developing flow region, orientation= $90^\circ$  c) Inlet fully developed Region, orientation= $45^\circ$  d) Outlet developing flow region, orientation= $45^\circ$

Figure 6.3.3 and Figure 6.3.4 shows the span-wise distribution along the ribbed trailing and leading surfaces and smooth inner and outer sidewalls for different rotation numbers in the fully developed region at  $Re=30,000$  for  $AR=1:4$  for  $90^\circ$  and  $45^\circ$  orientation ribbed channel respectively. These distributions are a result of

averaging in the stream wise direction between successive ribs. The profiles along the leading and trailing surfaces indicate a relatively uniform mass transfer distribution in the mid-span regions of the ribbed walls followed by a sharp drop-off toward the corners.

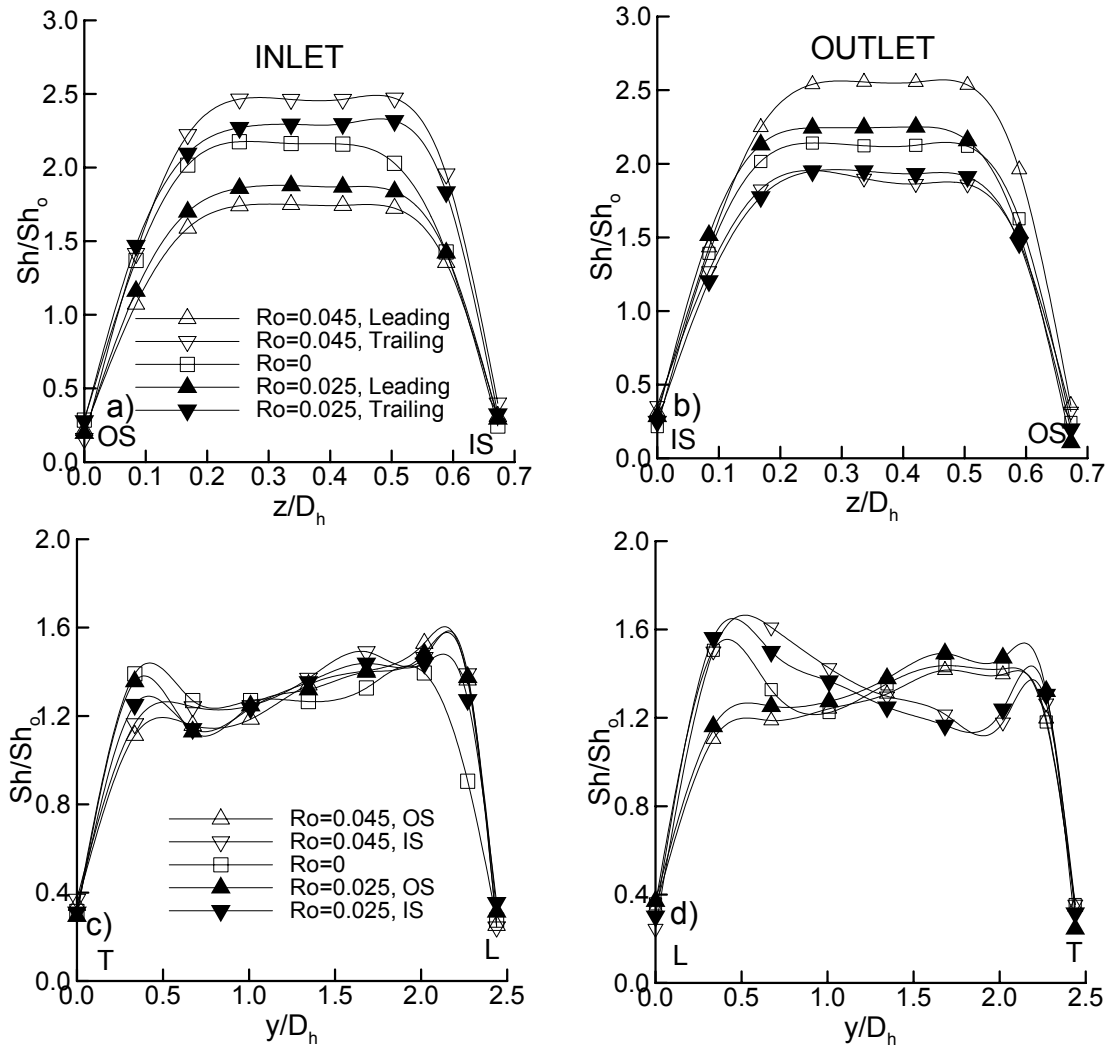


Figure 6.3.3: Span-wise distributions at different rotation numbers in the fully developed region at  $Re=30,000$  for AR=1:4, 90-degree Ribbed channel (a) & (b) leading and trailing and (c)&(d) sidewalls.

Note that this behavior is distinctly different than the smooth channel (Figure 6.2.3 and Figure 6.2.4) where an increase in the Sherwood number was observed toward the corners. Along the smooth sidewalls (Figure 6.3.3(c) and 6.3.3 (d)), no significant variation is observed with rotation in the inlet duct (Figure 6.3.3 (c)). Slightly higher

values (relative to the stationary case) are obtained close to the destabilized trailing-surface side where the rotation-induced secondary flows impinge, and correspondingly slightly lower values are obtained at the opposite end adjacent to the stabilized surface. In the outlet duct, larger differences are observed (Figure 6.3.3 (d)). Values are again higher closer to the destabilized surface (leading surface) and lower closer to the stabilized surface, but surprisingly this is only true along the inner wall. A plausible explanation for this is that the bend-induced acceleration along the outer wall skews the rotation induced secondary flow pattern toward the inner wall. Along the outer wall, a relatively uniform distribution is obtained with a mild increase toward the stabilized surface. With span-wise averaging however, the high and lows in the profiles average out, and the averaged values do not show a strong Rotation number dependence.

In figure 6.3.4, it is observed that in the radially outward flow duct (inlet duct), the stabilized surface is skewed towards the inner sidewall while the destabilized surfaces are more uniform in nature. In the radially inward flow duct (outlet duct).

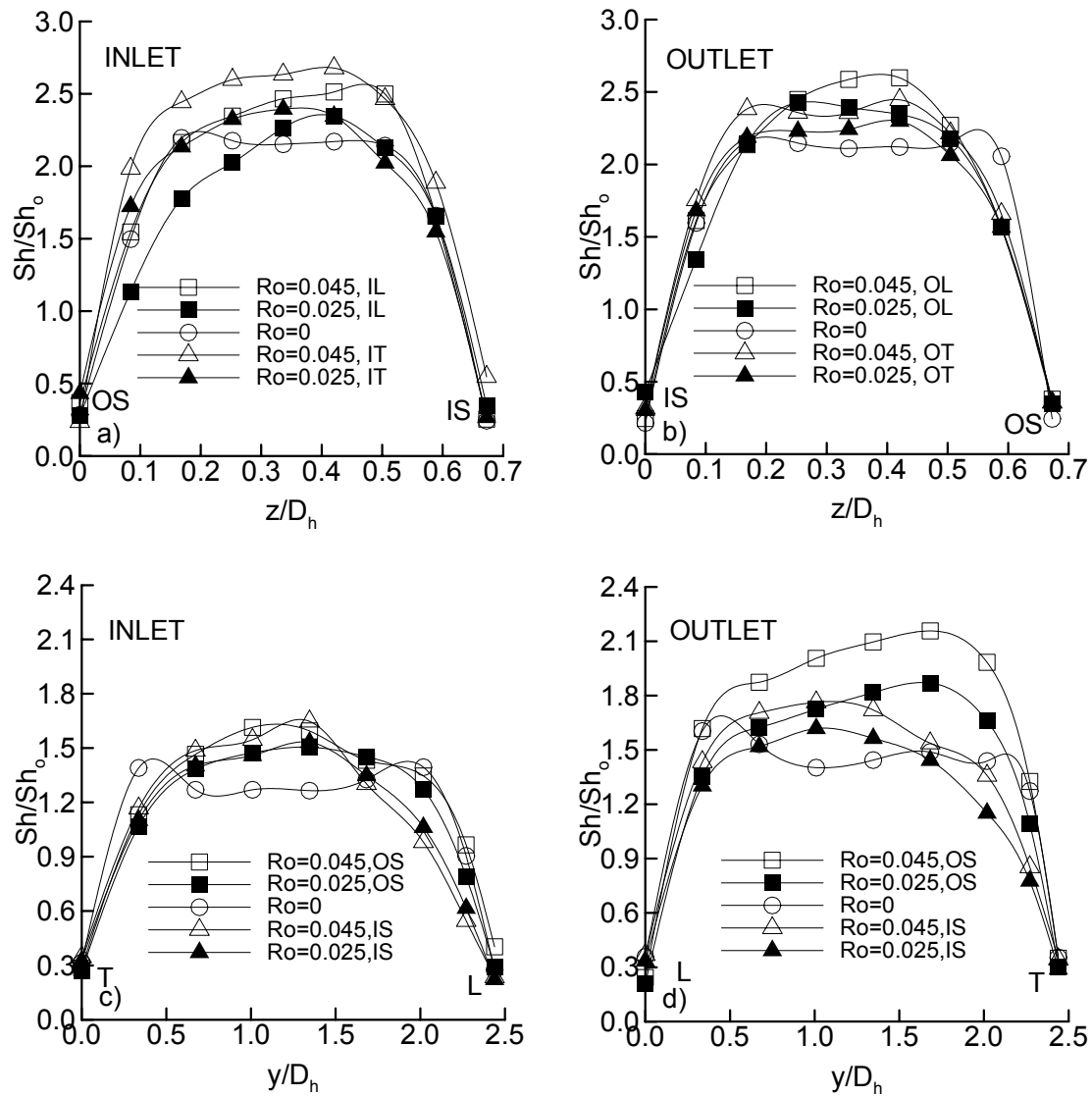


Figure 6.3.4: Span-wise distributions at different rotation numbers in the fully developed region at  $Re=30,000$  for AR=1:4, 45-degree Ribbed channel (a) & (b) leading and trailing and (c)&(d) sidewalls.

## BIBLIOGRAPHY

1. Park, C.W., Lau, S.C., and Kukreja, R.T., 1998, "Heat/Mass transfer in a rotating two-pass Channel with transverse ribs", *Journal of Thermophysics and heat transfer*, Vol. 12, No.1, pp. 80-86.
2. Myrum, T., Acharya, S., Sinha, S., and Qiu, X., 1996, "The effect of placing Vortex generators above ribs in ribbed ducts on the flow, flow temperature, and heat transfer behavior", *Journal of heat transfer*, Vol. 118, pp.294-300.
3. Eliades V., Nikitopoulos D. E., and Acharya S., "Mass Transfer Distribution in Rotating, Two-Pass Ribbed Channels with Vortex Generators", *AIAA Journal of Thermophysics and Heat Transfer*, 2001, Vol. 15, No. 3, pp 266-274.
4. Acharya S., Eliades V., and Nikitopoulos D. E., "Heat Transfer Enhancements in Rotating Two-Pass Coolant Channels with Profiled Ribs: Average Results", *ASME Journal of Turbomachinery*, 2001, Vol. 23, No. 1, pp 97-106.
5. Nikitopoulos D. E., Eliades V., and Acharya S., "Heat Transfer Enhancements in Rotating Two-Pass Coolant Channels with Profiled Ribs: Detailed Measurements", *ASME Journal of Turbomachinery*, 2001, Vol. 23, No. 1, pp 107-114.
6. Zhou, F., and Acharya, S., 2001, "Mass/heat transfer in dimpled turbine-blade Coolant Passages", *Heat transfer in Gas turbine systems*, Vol. 934, pp. 424-431.
7. Wagner, J.H., Johnson, B.V., and Kopper, F.C., 1991, "Heat transfer in rotating serpentine passages with Smooth walls", *Journal of Turbomachinery*, Vol. 113, pp. 321-330.
8. Johnson, B.V., Wagner, J.H., Steuber, G.D., and Yeh, F.C., 1994, "Heat transfer in rotating serpentine passages with trips skewed to the flow", *Journal of Turbomachinery*, Vol. 116, pp. 113-123.
9. Wagner, J.H., Johnson, B.V., Steuber, G.D., and Yeh, F.C., Oct.1992, "Heat transfer in rotating serpentine passages with trips normal to the flow", *Journal of Turbomachinery*, Vol. 114, pp. 847-857.
10. Kukreja, R.T., Park, C.W., and Lau, S.C., 1998, "Heat (Mass) transfer in a Rotating two pass Square Channel-Part-II: Local Transfer Coefficient, Smooth Channel", *International journal of rotating Machinery*, Vol. 4, No.1, pp. 1-15.
11. Han, J.C., 1988, "Heat transfer and friction characteristics in rectangular channels with rib turbulators", *Journal of heat transfer*, Vol. 110, pp. 321-328.
12. Han, J.C., Ou, S., Park, J.S., and Lei, C.K., 1989, "Augmented heat transfer in rectangular channels of narrow aspect ratios with rib turbulators", *International Journal of heat and mass transfer*, Vol. 32, No. 9, pp. 1699-1630.

13. Park, J.S., Han, J.C., Huang, Y., and Ou, S., 1992, "Heat transfer performance comparisons of five different rectangular channels with parallel angled ribs", *International Journal of heat and mass transfer*, Vol. 35, No. 11, pp. 2891-2903.
14. Sparrow, E., Cur, N., 1982, "Turbulent Heat transfer in a Symmetrically and Asymmetrically heated flat rectangular duct with flow separation at inlet", *Journal of heat transfer*, Vol. 104, pp.82-89.
15. Hart, J., 1971, "Instability and Secondary motion in a Rotating channel flow", *Journal of Fluid mechanics*, Vol. 45, part 2, pp. 341-351.
16. Johnston, J., Halleen, R., and Lezius, D., 1972, "Effects of Span-wise Rotation on the structure of two-dimensional fully developed turbulent channel flow", *Journal of fluid mechanics*, Vol. 56, part 3, pp. 533-557.
17. Hwang, G., and Jen, T., 1990, "Convective heat transfer in rotating isothermal ducts", *International journal of heat and mass transfer*, Vol. 33, No. 9, pp. 1817-1828.
18. Morris, W., and Ghavami-Nasr, G., 1991, "Heat transfer measurements in rectangular channels with orthogonal mode rotation", *Journal of Turbomachinery*, Vol. 113, pp. 339-345.
19. Harasgama, S., and Morris, W., 1988, "The influence of Rotation on the heat transfer characteristics of circular, triangular, and square sectioned coolant passages of gas turbine rotor blades", *Journal of Turbomachinery*, Vol. 110, pp. 44-50.
20. Metzger, D., and Sahn, M., 1986, "Heat transfer around sharp 180-degree turns in Smooth Rectangular channels", *Journal of Heat transfer*, Vol. 108, pp. 500-506.
21. Yang, W., Zhang, N., and Chiou, J., 1992, "Local heat transfer in a rotating Serpentine flow passage", *Journal of heat transfer*, Vol. 114, pp. 354-361.
22. Han, J., Zhang, Y., and Kalkuehler, K., 1993, "Uneven wall temperature effect on local heat transfer in a rotating two pass square channel with smooth walls", *Journal of heat transfer*, Vol. 115, pp. 912-920.
23. Durst, F., and Rastogi, A., 1979, "Theoretical and experimental investigation of turbulent flows with separation", *Turbulent Shear flows 1*, Berlin, Springer-Verlag, pp. 208-219.
24. Acharya, S., Myrum, T., and Baker, R., 1993, "Turbulent Flow and heat transfer past a surface mounted two dimensional rib. Part 1: Measurements", *Turbulent Enhanced heat transfer*, ASME HTD Vol. 239, pp. 27-34.
25. Acharya, S., Dutta, S., Myrum, T., and Baker, R., 1994, "Turbulent flow past a surface mounted rib", *Journal of fluid Engineering*, Vol. 116, No.2, pp. 238-246.

26. Humphrey, J., and Whitelaw, J., 1979, "Turbulent flow in a duct with roughness", *Turbulent Shear flows 2*, Berlin, Springer-Verlag, pp. 174-188.
27. Liou, T., and Hwang, J., 1992, "Turbulent heat transfer augmentation and friction in periodic fully developed channel flows", *Journal of heat transfer*, Vol. 114, pp. 56-64.
28. Hirota, M., Fujita, H., and Yokosawa, H., 1994, "Experimental study on convective heat transfer for turbulent flow in a square duct with a ribbed rough wall", *Journal of heat transfer*, Vol. 116, pp. 332-340.
29. Zhang, N., Chiou, J, Fann, S., and Yang, W., 1993, "Local heat transfer distribution in a rotating serpentine rib-roughened flow passage", *Journal of heat transfer*, Vol. 115, pp. 560-567.
30. Johnson, B., Wagner, J., Steuber, G., and Yeh, F., 1993, "Heat transfer in rotating serpentine passages with selected model orientation for smooth or skewed trip walls", NASA Tech. Memorandum 106126.
31. Hong, Y., and Heish, S., 1993, "Heat transfer and friction factor measurements in ducts with staggered and inline ribs", *Journal of heat transfer*, Vol. 115, pp. 58-65.
32. Taslim, M., Rahman, A., and Spring, S., 1991, "An experimental investigation of heat transfer coefficients in a span-wise rotating channel with two opposite rib-roughened walls", *Journal of Turbomachinery*, Vol. 113, pp. 75-82.
33. Ito, H., 1959, "Friction Factors for Turbulent Flow in Curved Pipes", *ASME J. of Basic Engineering*, Series D, Vol. 81, pp. 123-134.
34. Griffith, T.S., Hadrhrami, L.A., Han, J.C., 2002, "Heat transfer in Rotating Rectangular Cooling Channels (AR=4) with angled ribs", *J. of Heat transfer*, Vol. 124, pp. 1-9.
35. Kline, S. J., and McClintock, F. A., 1953, "Describing Uncertainties in Single-Sample Experiments", *Mechanical Engineering*, Vol. 75, pp. 3-8.
36. Souza Mendes, P.R., 1991, "The Naphthalene Sublimation Technique", *Experimental Thermal and Fluid Science*, Vol. 4, pp. 510-523.

## VITA

Peeyush Agarwal was born in Kanpur, an old business and historical town in Uttar Pradesh, India. He is the elder son of Mrs. Manju Agarwal and Mr. Ram Gopal Agarwal. He received his primary and secondary education in Kanpur. He received the degree of Bachelor of Technology in Mechanical Engineering from Indian Institute of Technology (IIT), Guwahati, in 2001. He then joined the graduate program at Louisiana State University, Baton Rouge (LSU) in spring, 2002. He worked in the field of experimental thermal/fluids during his graduate program in turbine innovation and energy research (TIER) center. He is a candidate for the degree of Master of Science in Mechanical Engineering to be awarded at the commencement of May, 2004.